

Destabilization and Aggregation Kinetics of Asphaltenes

by

Nasim Haji Akbari Balou

A dissertation submitted in partial fulfillment
of the requirements for the degree of
Doctor of Philosophy
(Chemical Engineering)
in The University of Michigan
2014

Doctoral Committee:

Professor H. Scott Fogler, Chair
Professor Massoud Kaviani
Professor Ronald G. Larson
Professor Phillip E. Savage

© Nasim Haji Akbari Balou 2014
All Rights Reserved

*To my loving parents, Zhila and Zakarya and my supportive siblings, Amir and
Nastaran*

ACKNOWLEDGEMENTS

This dissertation would not have been possible without the contribution, support and encouragement of many individuals in my life. I would first like to express my gratitude to my research advisor Professor Fogler for giving me the opportunity to join his research group and do my doctoral studies under his supervision. Professor Fogler has been a great advisor and a fabulous mentor and has been always supportive of new and creative ideas. He undoubtedly had great influence in my life and helped me to learn critical thinking and develop myself as an independent researcher. I am also very grateful for his trust and the unique mentorship opportunities that he provided me through my stay in his research group.

I would like to thank Professors Kaviani, Larson and Savage for accepting to serve as my doctoral committee members. Their valuable input and insightful questions are greatly appreciated and have been very helpful in improving the quality of my work. I am also thankful to Professor Ziff for providing me the opportunity to be admitted into PhD program of Chemical Engineering at Michigan and pursue my doctorate studies in one of the finest academic institutions in the world. I also wish to acknowledge my great appreciation to Department of Chemical Engineering staff: Harald Eberhart, Susan Hamlin, Laura Bracken, Michael Africa, Pamela Bogdanski, Shelly Fellers and Pablo Lavalle.

I am very thankful to all my current and previous colleagues in the Fogler research group for creating such a friendly and interactive environment. As my seniors in the

Fogler Group, Dr. Elizabeth Gorrepati, Dr. Michael Senra, Dr. Tabish Maqbool, Dr. Jason Huang and Dr. Michael Hoepfner were such great mentors and friends at the same time. I would specially like to thank Tabish for his help and advise in the early stages of my project. Michael Hoepfner and I overlapped for the most of my doctorate studies. I am grateful for our numerous discussions about asphaltenes which benefited me a lot and thank his continuous input on my project. I would also like to extend my thanks to Claudio Vilas Boas Favero, for enjoyable interactions not only about research topics but also about other areas of science in general. I have been also extremely lucky for having the opportunity to work with three amazing visiting master students from the Petroleum and Petrochemical College at Chulalongkorn University: Pennapa(Tai) Masirisuk, Thammaporn(Pearl) Somkhan and Phitsanu(Nu) Teeraphakul and I thank them for their help in performing experiments. I would like to extend my thanks to the rest of Fogler group: Nina Gasbarro, Sheng Zheng, Hela Marzouki, Pongkhun(Nhor) Siriprasurtsilp and all the previous visiting students. I would also like to acknowledge the financial assistance, provided by the University of Michigan Industrial Affiliates Program.

I would like to extend my thanks to my supportive friends in Chemical Engineering Department (Dr. Priyanka Pande, Dr. Tanawan Pinnarat, Lillian Hsiao, Dongil Kang, Dr. Andiappan Marimuthu, Dr. Shujauddin Changi, Vipawee(Yen) Limsakoune) that made my stay in University of Michigan an enjoyable and fun experience.

Finally I would like to express my deepest gratitude for my parents: Zhila and Zakarya for their unconditional love, support and encouragement throughout my entire life. I couldn't have asked for better parents and I wouldn't have reached this point without their help and support. I would also like to express my profound indebtedness for all the support and help that I have received throughout my life from my older brother, Amir. Amir has always been an exceptional mentor and a

role model in my life and has provided invaluable input both in my professional and personal life. Moreover, I would like to thank my dear sister Nastaran for her cheerful and supportive personality.

TABLE OF CONTENTS

DEDICATION	ii
ACKNOWLEDGEMENTS	iii
LIST OF FIGURES	viii
LIST OF TABLES	xii
LIST OF APPENDICES	xiii
ABSTRACT	xiv
CHAPTER	
I. Introduction	1
1.1 Background	1
1.2 Asphaltenes Properties	4
1.3 Asphaltenes Destabilization and Precipitation	9
1.4 Project Objectives	12
II. A Unified Model for Aggregation of Asphaltenes	22
2.1 Introduction	22
2.2 Experimental Section	26
2.3 Results and Discussion	29
2.4 Conclusions	51
III. The Effect of Asphaltene Concentration on the Aggregation and Precipitation Tendency of Asphaltenes	55
3.1 Introduction	55

3.2	Experimental Section	59
3.3	Results	61
3.4	Discussion	66
3.5	Conclusions	82
IV. Effect of <i>n</i>-Alkane Precipitants on Precipitation Kinetics of Asphaltenes		87
4.1	Introduction	87
4.2	Experimental Section	90
4.3	Results and Discussion	93
4.4	Conclusions	108
V. Polydispersity and Aggregation Tendency of Asphaltenes		112
5.1	Introduction	112
5.2	Experimental Section	114
5.3	Results and Discussion	118
5.4	Conclusions	129
VI. Conclusions		132
VII. Future Work		137
7.1	Studying Asphaltene Model Compounds	137
7.2	Further Investigating the Polydispersity of Asphaltenes	138
7.3	Precipitation Kinetics in Blend of Incompatible Crude Oils	139
7.4	Precipitation Kinetics in Live Oils	140
APPENDICES		144
A.1	Analytical Solution	145
A.2	Estimating Detection Time	148
A.3	Sensitivity Analysis of Asphaltenes Solubility Parameter	153
B.1	Accounting for the Polydispersity of Asphaltenes in Different Solvents	159
C.1	Aging of Asphaltenes	161
D.1	Effect of Sonication	165
E.1	Small-Angle X-ray Scattering for Different Asphaltene Concentrations	167

LIST OF FIGURES

Figure

1.1	Amount of asphaltenes precipitated as a function of precipitant’s carbon number (Image reproduced from [9])	3
1.2	(a) Archipelago and (b) Island molecular structures (Image (a) reproduced from [17] and Image (b) reproduced from [18])	5
1.3	Structural hierarchy of asphaltenes as a function of their concentration(Image reproduced from [43])	9
1.4	Time dependence of asphaltene precipitation for a single precipitant concentration (Image reproduced from [56])	11
2.1	Plot of detection time as a function of heptane concentration for five different crude oils.	30
2.2	Plot of detection time as a function of heptane concentration for different model oils.	31
2.3	Scattering intensity as a function of scattering vector for K1 asphaltenes.	34
2.4	Schematic of interactions between two asphaltenes as a function of their separation distance.	38
2.5	Plot of $\ln(t_{detection} \sqrt{C_1(0)}/\mu)$ vs. $(\delta_{asph} - \delta_{solution})^n$ for different values of n: $n = 1$ and 2	43
2.6	Plot of $\ln(t_{detection} \sqrt{C_1(0)}/\mu)$ vs. $(\delta_{asph} - \delta_{solution})^n$ for different values of n: $n = -1$ and -2	44
2.7	Plot of $\ln(t_{detection} \sqrt{C_1(0)}/\mu)$ vs. $(\delta_{asph} - \delta_{solution})^{-2}$ for crude oils.	45
2.8	$\ln(t_{detection} \sqrt{C_1(0)}/\mu)$ experiment vs. model prediction for crude oils and model oils mixed with n -heptane.	49
2.9	Detection times vs. heptane concentration measured experimentally (data points) and modeled (dashed lines).	50
2.10	Master curve for relation between $\ln(t_{detection} \sqrt{C_1(0)}/\mu)$ and $(\delta_{asph} - \delta_{solution})^{-2}$	50
3.1	Detection time as a function of heptane concentration for solutions with three different concentrations of K1 asphaltenes in toluene.	62

3.2	Detection time as a function of heptane concentration for solutions with four different concentrations of K1 asphaltenes in toluene. . . .	64
3.3	Detection time as a function of heptane concentration for solutions with four different concentrations of B1 asphaltenes in toluene. . . .	64
3.4	Detection time as a function of heptane concentration for solutions with three different concentrations of A1 asphaltenes in toluene. . .	65
3.5	Amount of asphaltenes precipitated per mass of toluene for 3 and 8 wt% asphaltenes as a function of heptane concentration, two months after heptane addition.	66
3.6	Fraction of asphaltenes precipitated two months after destabilization as a function of heptane concentration, 3 and 8 wt% asphaltenes in toluene.	73
3.7	Plot of $\ln(t_{detection}\sqrt{C_1(0)}/\mu)$ vs. $1/(\delta_{asph} - \delta_{solution})^2$ for 1 wt% of B1 and A1 asphaltenes in toluene using extrapolations E1 and E2 with respect to master curve.	74
3.8	Plot of $\ln(t_{detection}\sqrt{C_1(0)}/\mu)$ vs. $1/(\delta_{asph} - \delta_{solution})^2$ for 1, 3, 5 and 8 wt% B1 asphaltenes in toluene with respect to master curve. . . .	76
3.9	Plot of $\ln(t_{detection}\sqrt{C_1(0)}/\mu)$ vs. $1/(\delta_{asph} - \delta_{solution})^2$ for 1, 3 and 8 wt% A1 asphaltenes in toluene with respect to master curve.	77
3.10	Fraction of B1 and A1 asphaltenes precipitated as a function of $1/(\delta_{asph} - \delta_{solution})^2$	78
3.11	Plot of $\ln(t_{detection}\sqrt{C_1(0)}/\mu)$ vs. $1/(\delta_{asph} - \delta_{solution})^2$ for 0.1, 0.5, 1, 3, 5 and 8 wt% K1 asphaltenes in toluene with respect to master curve. . . .	81
4.1	Precipitation detection time vs. precipitant vol% for different n -alkanes mixed with GM2 crude oil(Image reproduced from [10]). . .	90
4.2	Precipitation detection time for different concentrations of hexane-octane blend mixed with GM2 crude oil (Images reproduced from [10]). . .	91
4.3	Detection time as a function of precipitant concentration for 1 wt% of K1 asphaltenes dissolved in toluene and then mixed with seven different precipitants ($C_6, C_7, C_8, C_9, C_{10}, C_{12}, C_{15}$).	94
4.4	Schematic of the solubility parameter distribution for asphaltenes precipitated using different n -alkanes.	96
4.5	Plot of $\ln(t_{detection}\sqrt{C_1(0)}/\mu)$ vs. $1/(\delta_{asph} - \delta_{solution})^2$ for seven different precipitants ($C_6, C_7, C_8, C_9, C_{10}, C_{12}, C_{15}$) mixed with 1wt% K1 asphaltenes in toluene and six different precipitants ($C_6, C_7, C_8, C_9, C_{10}, C_{15}$) mixed with GM2 crude oil.	98
4.6	Plot of asphaltenes solubility parameter vs. the precipitant carbon number (K1 and GM2).	100
4.7	Modeling results compared to experimental measurements of detection time for seven different precipitants mixed with 1wt% K1 asphaltenes in toluene.	101

4.8	Modeling results compared to experimental measurements of detection time for six different precipitants mixed with GM2 crude oil . . .	102
4.9	Detection times vs. precipitant concentration for blends of 0.5:0.5 C_7 - C_{12} , 0.3:0.3:0.4 C_7 - C_{10} - C_{12} and 0.2:0.2:0.2:0.2:0.2 C_6 - C_7 - C_{10} - C_{12} - C_{15} precipitants.	105
4.10	Model predictions compared to the experimental measurements of detection time for blends of precipitants mixed with 1wt% K1 model oil in toluene.	106
4.11	Plot of $\ln(t_{detection} \sqrt{C_1(0)}/\mu)$ vs. $1/(\delta_{asph} - \delta_{solution})^2$ (i.e. master curve) compared to the experimental measurements for ten different blends of precipitants (K1 model oil and GM2 crude oil).	107
5.1	Schematic of asphaltene fractionation from the crude oil and the model oil	117
5.2	Elemental composition for crude oil sub-fractions.	120
5.3	Scattering intensity as a function of scattering vector for crude oil sub-fractions	122
5.4	Scattering intensity as a function of scattering vector for the model oil sub-fractions	124
5.5	Detection time as a function of heptane concentration for crude oil sub-fractions	126
5.6	Detection time as a function of heptane concentration for model oil sub-fractions	127
5.7	Plot of $\ln(t_{detection} \sqrt{C_1(0)}/\mu)$ vs. $1/(\delta_{asph} - \delta_{solution})^2$ for crude oil and model oil sub-fractions compared to the master curve.	128
7.1	Detection time as a function of blend composition for blends of incompatible oils.	140
A.1	Plot of f' and g' as a function of $C_1(0)$	152
A.2	Plot of $\ln(t_{detection} \sqrt{C_M C_1(0) k_B T}/\mu)$ vs. $(\delta_{asph} - \delta_{solution})^2$ for crude oils and model oils presented in Chapter II.	154
A.3	Sensitivity of the model to the solubility parameter of asphaltenes in five different crude oils.	156
A.4	Sensitivity of the model to the solubility parameter of two types of asphaltenes (K1 and B1) in different model oils.	157
B.1	Accounting for the polydispersity of asphaltenes in different solvents.	160
C.1	Detection time as a function of heptane concentration for different batches of K1 asphaltenes in toluene.	163
C.2	Detection time as a function of heptane concentration for different batches of K1 asphaltenes in toluene (after shifting results).	164
D.1	Plot of detection time as a function of heptane concentration for different asphaltene concentrations.	166
E.1	Scattering results for supernatant of 3 and 8 wt% B1 asphaltenes at different heptane concentrations.	170

E.2	Scattering results for supernatant of 3 and 8 wt% A1 asphaltenes at different heptane concentrations.	171
-----	---	-----

LIST OF TABLES

Table

2.1	Physical properties of crude oils at room temperature.	27
2.2	Radius of gyration for samples shown in Figure 2.3.	33
2.3	Solubility parameter of crude oils and predicted solubility parameter of asphaltenes.	46
2.4	Solubility parameter of K1 and B1 asphaltenes.	46
3.1	Elemental analysis of A1, B1 and K1 asphaltenes.	59
4.1	Physical properties of compounds at room temperature.	92
4.2	Solubility parameter of asphaltenes destabilized with different <i>n</i> -alkanes (K1 asphaltenes in toluene).	99
4.3	Solubility parameter of asphaltenes destabilized with different <i>n</i> -alkanes (GM2 crude oil).	99
4.4	Calculated values of viscosities and solubility parameters used for predicting detection times in Figure 4.10	104
5.1	Elemental composition for crude oil sub-fractions.	118
5.2	Corrected elemental composition of <i>Cut_C1</i>	121
5.3	Radius of gyration of crude oil sub-fractions.	123
5.4	Radius of gyration of the model oil sub-fractions	125
5.5	Solubility parameter of crude oil sub-fractions obtained from Figure 5.7.	128
5.6	Solubility parameter of model oil sub-fractions obtained from Figure 5.7.	129
A.1	Analytical solution for results presented in Chapter II.	151
B.1	Solubility parameter of K1 and B1 asphaltenes.	160
E.1	Radius of gyration from scattering results of B1 asphaltenes shown in Figure E.1	172
E.2	Radius of gyration from scattering results of A1 asphaltenes shown in Figure E.2	172

LIST OF APPENDICES

Appendix

A.	Analytical Solution for Smoluchowski's Equation and Estimating De- tection Time	145
B.	Accounting for the Polydispersity of Asphaltenes in Different Solvents	159
C.	Aging of Asphaltenes	161
D.	Effect of Sonication	165
E.	Small-Angle X-ray Scattering for Different Asphaltene Concentrations	167

ABSTRACT

Destabilization and Aggregation Kinetics of Asphaltenes

by

Nasim Haji Akbari Balou

Chair: H. Scott Fogler

Asphaltenes are the heaviest fraction of crude oil and can precipitate due to changes in temperature, pressure or composition. It was previously shown that the precipitation and aggregation of asphaltenes is a kinetic phenomenon. In this thesis, it is demonstrated that the kinetics of aggregation is universal among many different crude oils, model oils and precipitants. The factors that can play a role in controlling this kinetic behavior are investigated in this study.

It is shown that the rate of asphaltene aggregation strongly depends on the type of solvent (i.e. crude oil) used for stabilizing asphaltenes. A new universal mathematical model relating the aggregation rate to the solution viscosity and the solubility parameters of the solution and asphaltenes is developed. With this model, all aggregation curves collapse onto a single master curve.

The asphaltene content and the chemical identity of the precipitant are also shown to play important roles in controlling the aggregation rates. The findings for the effect of asphaltene content challenge the intuitive expectation that higher asphaltene

concentration would lead to accelerated aggregation kinetics. Instead, two distinct regimes are identified for the effect of asphaltene concentration: 1) Below 1 wt%, the aggregation rate of asphaltenes increases, 2) Above 1 wt%, the aggregation rate decreases. The new universal model successfully predicts this behavior after accounting for the contribution of soluble asphaltenes to the solubility parameter of the solution.

In addition, the polydispersity of asphaltenes is shown to be important in dictating their kinetic behavior in different *n*-alkane precipitants. The universal model quantitatively accounts for the asphaltenes polydispersity using a solubility parameter distribution and can successfully predict the precipitation rate of asphaltenes in the blends of up to five different precipitants.

Finally, our findings reveal that asphaltenes with the highest solubility parameter precipitate first and have the tendency to form the largest nano-particles in toluene. The findings from this thesis leads to a better understanding of the factors that govern the kinetics and can in turn give rise to new predictive models to foresee precipitation and aggregation kinetics under different operational conditions.

CHAPTER I

Introduction

1.1 Background

Due to industrialization and globalization of the modern world, energy demands have been rising continuously since nineteenth century. To meet this demand, the world's desire for oil and other fossil fuels seems to be insatiable. Today more than 85% of total energy consumption in the United States relies on fossil fuels. Fossil fuels are expected to remain the major source of energy for decades to come. It is projected that they will constitute as high as 80% of global energy consumption in 2040 [1]. It is therefore important to invest in technologies aimed at optimizing the process of extracting and utilizing existing resources of fossil fuels.

Crude oil is one of the major forms of fossil fuels. It is a complex mixture of diverse hydrocarbons and organic compounds (composed of up to 10^5 - 10^6 distinct chemical species [2]). To simplify such a complex mixture, its components are often classified into four distinct groups, or solubility classes: saturates, aromatics, resins and asphaltenes (SARA). SARA fractionation of the crude oil is a separation technique based on differing solubility of each of these classes.

Changes in operational conditions such as temperature, pressure, or composi-

tion, can occur during production, transportation, and processing of crude oils, and can lead to precipitation and deposition of organic solids (i.e., waxes, hydrates and asphaltenes). Wax and hydrate deposits are more common than asphaltene deposits [3, 4], however due to difficult and costly remediation processes needed for asphaltenes, they are considered one of the most problematic fractions of crude oil [4]. Potential asphaltene-related problems have become more concerning in recent years due to an increase in the production of high-asphaltenic heavy oils [5]. Asphaltenic crudes are produced worldwide such as in oil fields in Venezuela, Persian Gulf, the Adriatic Sea and the U.S. Gulf of Mexico [6].

Asphaltenes are operationally defined as the collection of components precipitating out of the crude oil when mixed with precipitants such as *n*-pentane or *n*-heptane in a 1 : 40 volume ratio [7]. The definition of asphaltenes encompasses the heaviest and most polar fraction of the crude oil that are macroscopically soluble in aromatic solvents such as toluene or benzene [5]. According to this definition, asphaltenes are a class of molecules rather than one single component and their chemical structures, natural states and destabilization mechanisms are largely unknown and a subject of debate and speculation in the asphaltene research community. Asphaltenes are dark brown to black solids [5, 8]. The amount and properties (e.g., aromaticity, molecular weight and polarity) of precipitated asphaltenes depend on the chain length of the *n*-alkane precipitant used for their destabilization. Therefore, asphaltenes are typically named after the *n*-alkane precipitant used for their destabilization such as pentane asphaltenes or heptane asphaltenes (Figure 1.1 [7]).

Destabilized asphaltenes can easily adhere to the reservoir grains and downhole production equipment, transportation pipelines and also refining and storage facilities [4, 5, 8, 10, 11]. Moreover, asphaltenes can act as glues for the hardening of other organic deposits or act as nucleation sites for crystallization of wax molecules [11].

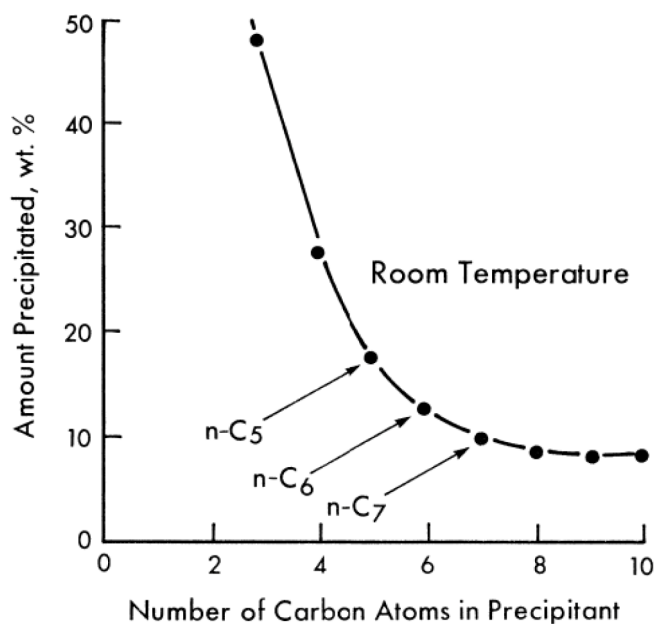


Figure 1.1: **Amount of asphaltenes precipitated as a function of precipitant's carbon number** (Image reproduced from [9])

Therefore, the economic impacts of asphaltene-related problems are enormous in the oil industry. For example, asphaltenes have led to complete blockage of some wells only few days after the start of their production with production rates up to 3000 barrels a day [12]. Remediation of deposited asphaltenes in the field may require well shutdown [8].

Different techniques such as solvent and dispersant treatments, and mechanical removal are currently used in the oil industry for cleaning up organic deposits [11]. However, the effectiveness of these techniques strongly depends on the characteristics of the crude oil and the deposit [11]. In some circumstances the costly remediation has been only partially effective [8, 11]. Therefore, the ability to predict and *prevent* deposit formation is preferred to their cleanup after they have already formed. In order to develop more effective predictive tools, it is necessary to obtain a funda-

mental knowledge about the factors that determine the tendency of asphaltenes for aggregation and phase separation.

1.2 Asphaltenes Properties

Typical asphaltenes molecules are composed of aromatic cores and aliphatic chains [13] with H/C ratio of $1.15 \pm 0.5\%$ [7]. Small quantities of heteroatoms such as oxygen (0.3% – 4.9%), sulfur (0.3% – 10.3%) and nitrogen (0.6% – 3.3%) [7] comprise various polar groups, such as aldehydes, carbonyls, carboxylic acids and amides in their molecular structure [13]. Asphaltenes also contain trace quantities of metals such as nickel, vanadium and iron in ppm levels (few parts per million to a few hundred parts per million) [14]. Nickel and vanadium could exist in porphyrin or non-porphyrin forms [14].

1.2.1 Molecular Structure

Due to extreme complexity of asphaltenes, their chemical structure has been the subject of heated debate in the research community. Two fundamentally different structural models have been proposed for asphaltenes: the archipelago model and the island model (Figure 1.2). According to the archipelago model, asphaltenes are typically composed of several aromatic cores linked with aliphatic chains. According to the island model however, asphaltene molecules are made up of a single aromatic core (made up of several interconnected aromatic rings) with aliphatic side chains surrounding this central core. The evidence for the archipelago model is heavily based on destructive techniques that result in decomposition of asphaltenes such as pyrolysis, oxidation and thermal degradation [15]. The products of such destructive reactions are small ringed aromatic molecules, a fact that is thought to be consistent

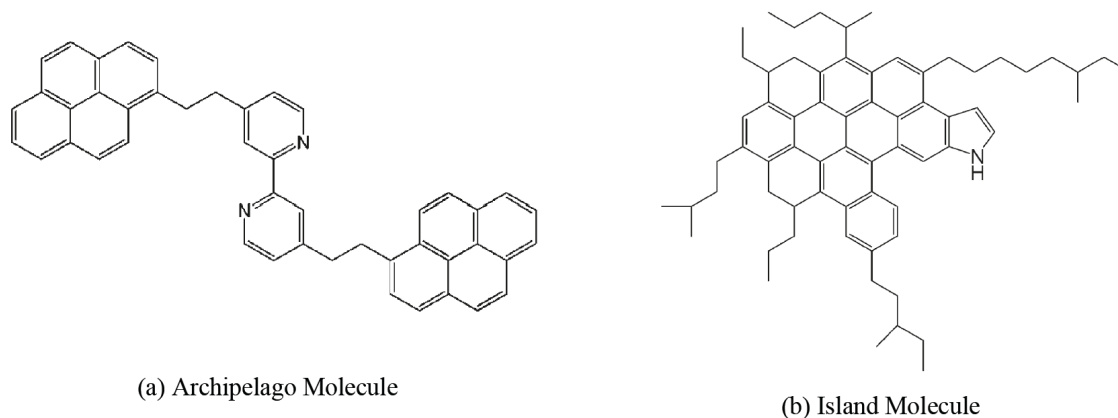


Figure 1.2: **(a) Archipelago and (b) Island molecular structures** (Image (a) reproduced from [17] and Image (b) reproduced from [18])

with the archipelago model [16]. However, recent experimental evidence shows that the decomposition of island model compounds with the same techniques can also result in the formation of small ringed aromatic molecules [16].

The experimental evidence for the island model can be obtained from a variety of experimental techniques. For example, optical techniques such as time-resolved fluorescence depolarization (TRFD) have shown that the rotational correlation time of asphaltenes can be better described by the Island structure [18–21]. In addition, two-step laser desorption laser ionization mass spectroscopy (L2MS) [17] has revealed that the fragmentation behavior of asphaltenes is identical to the fragmentation behavior of island model compounds and differs from that of archipelago compounds. Further evidence such as direct molecular imaging of asphaltene PAHs by scanning tunneling microscopy [22], high-resolution electron transmission microscopy [23] and Raman spectroscopy [24] along with lower stability of archipelago compounds [16] has resulted in the island structure being viewed the dominant structure for asphaltenes by the majority of researchers.

1.2.2 Molecular Weight

Different techniques such as small angle X-ray and neutron scattering (SANS and SAXS), vapor pressure osmometry (VPO), size-exclusion chromatography, mass spectroscopy and fluorescence depolarization have been utilized to measure the molecular weight of asphaltenes [5]. However, due to strong tendency of asphaltene molecules for self-association (even in strong solvents) (1.2.4), most of the reported values are the molecular weight of the aggregates of asphaltenes rather than individual molecules. More accurate estimates of their molecular weight (500-1000Da) using time-resolved fluorescence depolarization (TRFD) [19–21], fluorescence correlation spectroscopy (FCS) [25] and laser desorption ionization (LDI) MS [26] have been recently reported.

1.2.3 Solubility Parameter

Solubility parameter is a measure of the extent of interactions between molecules and is one of the main input parameters in the majority of thermodynamic models utilized for describing the phase behavior of asphaltenes [27–31]. Solubility parameter is defined as the square root of cohesive energy density:

$$\delta = \sqrt{E/V} \quad (1.1)$$

where δ is the solubility parameter, V is the molar volume of pure compound and E is its energy of vaporization [32]. For pure solvents, solubility parameter can be measured experimentally. However, measuring the solubility parameter of complex mixtures such as crude oils or asphaltenes is not experimentally feasible. Given the PVT data, solubility parameter of crude oils can be calculated using their equation of state. In the absence of PVT data, several empirical correlations have been used for estimating δ of crude oils. Among those are the correlations that relate δ and the

refractive index, or the density (one-third rule) [8, 30, 33]. However, extrapolation of such simple correlations to asphaltenes might be problematic. In addition, it is not straightforward to measure certain input quantities for asphaltenes, such as refractive index, that are needed in these correlations.

Solubility parameter of asphaltenes can be estimated by investigating their solubility in blends of different solvents with varying solubility parameters. However, as has been discussed in detail by Wang [8], this approach has significant limitations due to the ill-defined asphaltenes/solvent ratio, possibility of dissolution kinetics and also possible swelling of asphaltenes. Some other correlations such as the relationship between the H/C ratio and solubility parameter are also used in the literature [8]. Values ranging from 18.4-24.5 MPa^{0.5} have been typically reported as solubility parameter of asphaltenes [8]. However, values as high as 32 MPa^{0.5} has been also reported for the solubility parameter of asphaltenes [34]. Due to these technical complications, the solubility parameter of asphaltenes is generally treated as a fitting parameter in most existing models.

1.2.4 Natural State

The majority of researchers view asphaltenes as colloidal nano-sized particles immersed in the crude oil. Scattering techniques such as SANS and SAXS have been applied to crude oils and model oils and the measured scattering intensity is generally attributed to the existence of asphaltene nano-particles in the mixture [35–39]. On the other hand, it has been shown that scattering profiles can also be successfully explained by treating asphaltenes as fully dissolved and attributing their scattering to the concentration fluctuations in the solvent rather than the existence of solid particles [40]. Due to the chemical complexity of asphaltenes and the broad distribution of molecules characterized as asphaltenes, both liquid (dissolved) and solid (aggregated)

asphaltenes can coexist in the crude oil. However, ultra-centrifugation [41] and nano-filtration [42] of crude oils support the idea that the majority of asphaltenes exist as nano-sized colloidal particles. The average molecular weight of associated asphaltene molecules measured from vapor pressure osmometry (VPO) and size exclusion chromatography (SEC) has shown that their association tendencies strongly depend on the solvent and the asphaltene concentration and the association itself is a reversible process [7].

Aggregation of asphaltene molecules to nano-particles can be viewed as a dynamic equilibrium between the soluble molecules and the aggregates. The aggregation propensity is expected to increase as a result of an increase in the asphaltene concentration. Two different aggregated states have been proposed for describing the natural state of asphaltenes in a solvent or crude oil: nano-aggregates and clusters [18, 43]. Asphaltene nano-aggregates are believed to form from the stacking of individual molecules. Different techniques such as high-Q ultrasonic [44, 45], AC [18] and DC [46] conductivity and NMR [47] have been utilized for determining the asphaltene concentration at which nano-aggregates start to form in the solvent— known as the *critical nano-aggregate concentration (CNAC)*— by varying asphaltene concentration. CNAC values depend on the characteristics of the asphaltenes as well as the solvent used for their stabilization.

Asphaltene clusters are believed to form from further aggregation of nano-aggregates. Sudden changes in the properties of the solution such as surface tension [48] or heat of dissociation [49, 50] as a result of an increase in the asphaltene concentration have been attributed to the structural changes of asphaltenes due to the formation of asphaltene clusters. Figure 1.3 [43] shows the proposed model for structural hierarchy of asphaltenes [43]. In this model, asphaltene nano-aggregates are thought to be around 2 nm in size and to be composed of approximately 6 asphaltene molecules. Asphal-

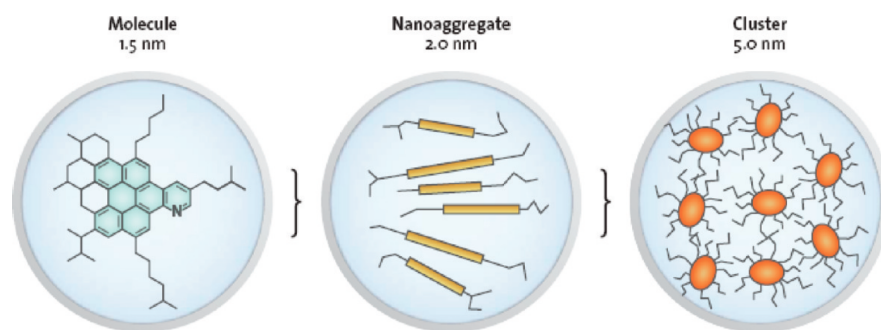


Figure 1.3: **Structural hierarchy of asphaltenes as a function of their concentration** (Image reproduced from [43])

tene clusters however, are thought to be around 5nm in size and to be composed of 8 nano-aggregates [18].

1.3 Asphaltenes Destabilization and Precipitation

The mechanism of asphaltene precipitation has been extensively investigated usually by titrating the crude oil with an n -alkane precipitant. Different techniques such as optical microscopy [8], refractive index measurements [5], viscosity measurements [51], UV- visible spectroscopy [52, 53] and NIR spectroscopy [54] have been utilized to detect asphaltenes instability. Most of these studies are performed based on the assumption that the solution equilibrates shortly after precipitant addition. In other words, according to this assumption, the crude oil-precipitant mixture is considered stable if asphaltenes do not become detectable *immediately* after destabilization. The concentration of n -alkane precipitant at which asphaltenes are detected for the first time is defined as the *onset volume*. Thermodynamic models generally have been developed using the data collected from the experiments performed according to the assumption of immediate equilibration [27–31].

Contrary to the immediate equilibration assumption, Angle *et al.* [55] showed that asphaltenes can become unstable below the pseudo onset concentration if enough time elapses. Angle *et al.* [55] made this observation for a mixture of crude oils diluted with toluene and subsequently mixed with heptane. Although their results clearly indicate that precipitation of asphaltenes at concentrations below onset is a slow process, it was not yet clear whether such a delayed destabilization was due to a delay in precipitation because of toluene addition or it was rather a more general phenomenon. Maqbool *et al.* [56] investigated kinetics by mixing a crude oil with heptane without dilution with toluene. Maqbool *et al.*'s [56], experiments revealed that the time required to detect asphaltene instability under optical microscope varies exponentially with the precipitant concentration, indicating that under certain circumstances, it can take up to several weeks and even months to detect asphaltene instability. It should be emphasized that the definition of *detection time* depends on the spatial resolution of the technique used for detecting asphaltene instability. Conventional techniques such as optical microscopy can only detect particles that are at least $0.5 \mu\text{m}$ in diameter.

Recent studies have demonstrated that when a precipitant is added to the crude oil, only a fraction of asphaltene nano-particles— known as *unstable asphaltenes*— undergo further aggregation and the rest— referred to as *stable asphaltenes*— remain in solution. [57]. The asphaltene particles that belong to these two different classes tend to have different fractal dimensions [57]. At asphaltene contents higher than clustering concentration(1.2.4), unstable asphaltene nano-particles experience a reaction-limited aggregation process [58, 59]. The slow precipitation kinetics below onset volume is attributed to the aggregation of sub-micron unstable asphaltene particles (i.e. nano-particles) to detectable sizes [60].

In order to explain the aggregation behavior of sub-micron and micron-sized unstable asphaltenes, several mathematical models have been proposed that are all based

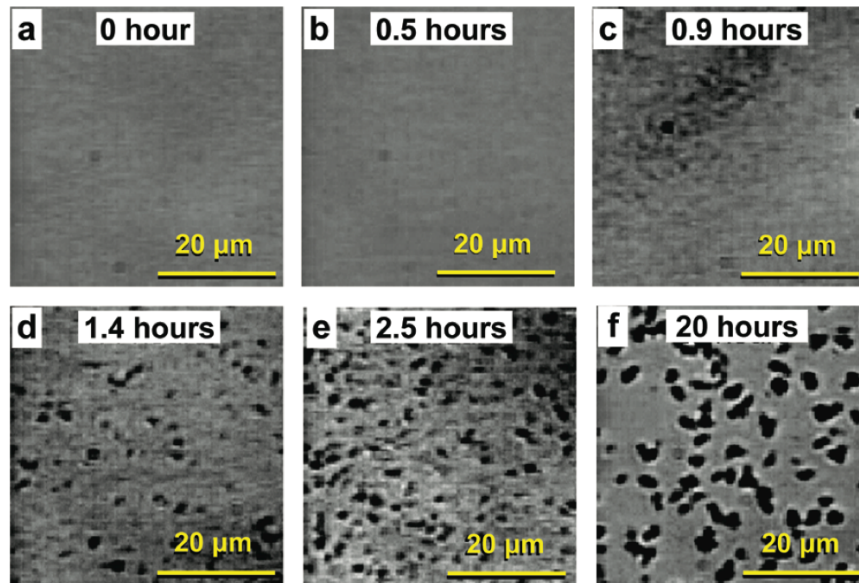


Figure 1.4: **Time dependence of asphaltene precipitation for a single precipitant concentration** (Image reproduced from [56])

on the the population balance equation developed by Smoluchowski [60–62]. Most of the existing models deal with asphaltenes growth at or above onset volume and are therefore valid only at those high precipitant concentrations [61, 62]. In order to study the precipitation of sub-micron particles, alternative models are needed for concentrations below the onset volume. One such model was proposed by Maqbool *et al.* [60], who studied aggregation kinetics at precipitant concentrations below the onset volume. Under such circumstances, the growth processes is extremely slow, and can be in the order of several hours, days or months. The main assumption in their model is that a certain fraction of asphaltenes become unstable immediately after precipitant addition. These unstable asphaltenes colloid with each other due to Brownian motion and aggregate to form larger particles. The initial destabilized asphaltene particles are assumed to be around 2 nm in size, which then grow to larger (micron) length

scales. Their model can only be used if the concentration of destabilized asphaltenes at each precipitant concentration is known; a quantity which can only be estimated if sufficient time is given for the mixture to reach equilibrium (at low concentrations, equilibration can take more than 500 hours). The aggregation of asphaltenes in their model is shown to be a reaction-limited process, therefore not all collisions are going to be successful and collision efficiencies are estimated by matching the experimental results with the model. Estimated collision efficiencies are not constant and depend on the precipitant concentration. Despite their model's success in reproducing experimental observations, this model is not predictive because both the input and fitting parameters depend on the precipitant concentration and cannot be estimated without performing actual experiments.

1.4 Project Objectives

The ability to predict asphaltenes phase behavior under various pressures, temperatures or compositions has been the major focus of asphaltene research community for decades. A wide variety of thermodynamic models with fundamentally different assumptions (i.e. regarding the interactions of asphaltenes with their surroundings) have been proposed in the literature [27–31, 63, 64]. Despite fundamental differences in these models, they are all developed based on the experimental data collected shortly after destabilization of asphaltenes. Therefore, any slow kinetics associated with detecting asphaltenes instability is generally overlooked in these models. As a result, these models can miss the correct equilibrium point by neglecting kinetic effects. This, in turn, can result in misleading predictions about the stability of asphaltenes. It is therefore important to obtain a systematic understanding of precipitation kinetics.

Slow kinetics of aggregation has been neglected for decades and is generally considered not to be important. The main reason for this misconception is the general belief that the life time of operational conditions are much smaller than the characteristic timescales of these slow kinetic processes. Due to this separation of timescales, the existence– or lack– of these kinetic effects is thought to be irrelevant to potential asphaltene-related problems in the oil industry. However, the existence of long term kinetics is an indicator for instability of asphaltenes in nano-scale which can potentially deposit further along the way. As will be presented in the upcoming chapters of this thesis, the asphaltenes that have been destabilized at earlier times, or at low driving forces, are the most unstable asphaltenes, and are expected to cause the most severe problems. The ability to understand, predict and prevent the destabilization of most unstable asphaltenes is therefore considered to be extremely important.

The main objective of this project is to improve our understanding of the asphaltenes precipitation kinetics and to investigate factors governing their aggregation process. Various key parameters such as the effect of solvent, the properties and the concentration of asphaltenes and the precipitant are explored in this investigation. Each chapter of the thesis focuses on a single factor and is organized independent of the other chapters, with its own introduction, experimental section, results/discussion, conclusion and references. Despite minor redundancy in some background information, this formatting allows each chapter to be self contained for easier access to relevant information. The chapters are organized as follows: In Chapter II the effect of solvent is investigated and the universality of kinetics is established for precipitation of asphaltenes from different crude oils and model oils. A mathematical model based on Smoluchowski’s aggregation model is then developed to describe the aggregation behavior of asphaltenes in different solvents (i.e., crude oils and model oils). The developed model correlates the aggregation rate of asphaltenes to the

changes in the viscosity and the solubility parameters and successfully explains the aggregation behavior of asphaltenes via a unified master curve.

In Chapter III, the effect of asphaltene concentration on their aggregation and precipitation tendencies is investigated for three different types of asphaltenes. It is intuitively expected that any increase in asphaltene concentration will accelerate the precipitation kinetics after heptane addition. For asphaltene concentrations below 1 wt% in toluene, this expected trend is indeed experimentally confirmed in microscopy experiments. However, for asphaltene concentrations above 1 wt%, an increase in concentration leads to slower aggregation instead. This counter-intuitive decline in the aggregation rate is attributed to the stabilizing effect of stable/soluble asphaltenes and has been overlooked in the existing aggregation models. Findings from Chapter III are incorporated to the model developed in Chapter II. The model successfully predicts the experimentally measured precipitation rates as a function of asphaltene concentration.

In Chapter IV the effect of chain length of the n -alkane precipitants on the precipitation kinetics of asphaltenes is investigated. Despite a monotonic change in the viscosity and the solubility parameter of n -alkanes as a function of change in their carbon number, the precipitation rate of asphaltenes does not vary monotonically. This behavior is explained by the polydispersity of asphaltenes and differences in the solubility parameter of asphaltenes precipitated using different n -alkanes. The solubility parameter distribution is obtained using the model developed in Chapter II and is then used to predict the precipitation rate of asphaltenes in blends of two, three, four and five different precipitants at different ratios.

In Chapter V the polydispersity of asphaltenes is further explored by fractionating asphaltenes into smaller sub-fractions precipitated at different times and heptane concentrations. It is shown that asphaltenes precipitating first are the most unsta-

ble ones with the fastest aggregation rate and the highest solubility parameter. In addition asphaltenes precipitating earlier have higher metal and heteroatom content compared to the other sub-fractions and form the largest nano-particles in toluene. The presented results reveal that polydispersity of asphaltenes has a crucial role in controlling their kinetic behavior and understanding this polydispersity is important in predicting and preventing potential asphaltene problems.

Concluding remarks and directions for future research are presented in Chapters [VI](#) and [VII](#) respectively.

Bibliography

- [1] U.S. Energy Information Administration. International energy outlook 2013.
- [2] I. A. Wiehe and K. S. Liang. Asphaltenes, resins, and other petroleum macromolecules. *Fluid Phase Equilibria*, 117, 1996.
- [3] B. T. Ellison, C. T. Gallagher, L. M. Frostman, and S. E. Lorimer. The physical chemistry of wax, hydrates, and asphaltene. *The Physical Chemistry of Wax, Hydrates, and Asphaltene*, 2000.
- [4] A. Hammami and J. Ratulowski. Precipitation and deposition of asphaltenes in production systems: A flow assurance overview. In O. C. Mullins, A. Hammami E. Y. Sheu, and A. G. Marshall, editors, *Heavy Oils, and Petroleomics*, pages 617–660. Springer New York, 2007.
- [5] P. Wattana. *Precipitation and Characterization of Petroleum Asphaltenes*. PhD thesis, University of Michigan, 2004.
- [6] L. Cenegy. Survey of successful world-wide asphaltene inhibitor treatments in oil production fields. Society of Petroleum Engineers, 2001.
- [7] James G. Speight. *The Chemistry and Technology of Petroleum*. CRC Press, fourth edition, 2006.
- [8] Jianxin Wang. *Predicting Asphaltene Flocculation in Crude Oils*. PhD thesis, New Mexico Institute of Mining and Technology, 2000.
- [9] D.L. Mitchell and J.G. Speight. The solubility of asphaltenes in hydrocarbon solvents. *Fuel*, 52:149–152, 1973.
- [10] K. Akbarzadeh, A. Hammani and A. Kharrat, D. Zhang, S. Allenson, J. Creek, A. Jamaluddin, A. Marshal, R. Rogers, O. Mullins, and T. Solbakken. Asphaltenes-problematic but rich in potential. *Oilfield Rev*, 19(2):22–43, 2007.
- [11] G. A. Mansoori. Remediation of asphaltene and other heavy organic deposits in oil wells and in pipelines. *ELMI Sarlar J Reserv. Pet. Eng. SOCAR*, pages 12–21, 2010.

- [12] K. J. Leontaritis and G. Ali Mansoori. Asphaltene deposition: a survey of field experiences and research approaches. *J. Pet. Sci. Eng.*, 1(3):229–239, 1988.
- [13] Chia-Lu Chang. *Formation of Silica Particles and Stabilization of Asphaltene Colloids in Apolar Media Using Anphiphiles and Polymers*. PhD thesis, University of Michigan, 1995.
- [14] Teh Fu Yen. Asphaltenes. In O. C. Mullins and E. Y. Sheu, editors, *Structure and Dynamics of Asphaltenes*. Plenum Press, 1998.
- [15] Jeff M. Sheremata, Murray R. Gray, Heather D. Dettman, and William C. McCaffrey. Quantitative molecular representation and sequential optimization of athabasca asphaltenes. *Energy & Fuels*, 18(5):1377–1384, 2004.
- [16] Fernando Alvarez-Ramírez and Yosadara Ruiz-Morales. Island versus archipelago architecture for asphaltenes: Polycyclic aromatic hydrocarbon dimer theoretical studies. *Energy & Fuels*, 27:1791–1808, 2013.
- [17] Hassan Sabbah, Amy L. Morrow, Andrew E. Pomerantz, and Richard N. Zare. Evidence for island structures as the dominant architecture of asphaltenes. *Energy & Fuels*, 25(4):1597–1604, 2011.
- [18] Oliver C. Mullins. The modified yen model. *Energy & Fuels*, 24(4):2179–2207, 2010.
- [19] H. H. Groenzin and O. C. Mullins. Asphaltene molecular size and structure. *J. Phys. Chem. A*, 103(11237–11245), 1999.
- [20] E. Buenrostro-Gonzalez, H. Groenzin, C. Lira-Galeana, and O. C. Mullins. The overriding chemical principles that define asphaltenes. *Energy & Fuels*, 15:972–978, 2001.
- [21] H. Groenzin and O. C. Mullins. Asphaltene molecular size and weight by time-resolved fluorescence depolarization. In O. C. Mullins., E. Y. Sheu, A. Hammami, and A. G. Marshall, editors, *Asphaltenes, Heavy Oils and Petroleomics*, chapter 2, pages 17–62. Springer New York, 2007.
- [22] G. W. Zajac, N. K. Sethi, and J. T. Joseph. Molecular imaging of asphaltenes by scanning tunneling microscopy: Verification of structure from ^{13}C and proton nmr data. *Scanning Microsc.*, 8:463, 1994.
- [23] A. Sharma, H. Groenzin, A. Tomita, and O. C. Mullins. Probing order in asphaltenes and aromatic ring systems by hrtem. *Energy & Fuels*, 16(490–496), 2002.

- [24] Y. Bouhadda, D. Bormann, E. Y. Sheu, D. Bendedouch, A. Krallafa, and M. Daaou. Characterization of algerian hassi-messaoud asphaltene structure using raman spectrometry and x-ray diffraction. *Fuel*, 86:1855–1864, 2007.
- [25] A. B. Andrews, R. E. Guerra, O. C. Mullins, and P. N. Sen. Diffusivity of asphaltene molecules by fluorescence correlation spectroscopy. *Physical Chemistry A*, 110(26):8093–8097, 2006.
- [26] O. C. Mullins, B. Martínez-Haya, and A. G. Marshall. Contrasting perspective on asphaltene molecular weight. this comment vs the overview of a. a. herod, k. d. bartle, and r. kandiyoti. *Energy & Fuels*, 22(3):1765–1773, 2008.
- [27] A. Hirschberg, L. N. J. deJong, B. A. Schipper, and J. G. Meijer. Influence of temperature and pressure on asphaltene flocculation. *Society of Petroleum Engineers Journal*, 24(3), 1984.
- [28] R. Cimino, S. Correra, A. Del Bianco, and T. P. Lockhart. Solubility and phase behavior of asphaltenes in hydrocarbon media. In E. Y. Sheu and O. C. Mullins, editors, *Asphaltenes: Fundamentals and Applications*, pages pp 97–130. Plenum Press, 1995.
- [29] K. D. Mannistu, H. W. Yarranton, and J. H. Masliyah. Solubility modeling of asphaltenes in organic solvents. *Energy Fuels*, 11:615–622, 1997.
- [30] J. X. Wang and J. S. Buckley. A two-component solubility model of the onset of asphaltene flocculation in crude oils. *Energy Fuels*, 15(5):1004—1012, 2001.
- [31] Hussein Alboudwarej, Kamran Akbarzadeh, James Beck, William Y. Svrcek, and Harvey W. Yarranton. Regular solution model for asphaltene precipitation from bitumens and solvents. *AIChE Journal*, 49(11):2948–2956, 2003.
- [32] Charles M. Hansen. *Hansen Solubility Parameters*. CRC Press, 2nd edition, 2007.
- [33] Francisco M. Vargas and Walter G. Chapman. Application of the one-third rule in hydrocarbon and crude oil systems. *Fluid Phase Equilibria*, 290, 2010.
- [34] F. Mutelet, G. Ekulu, R. Solimando, and M. Rogalski. Solubility parameters of crude oils and asphaltenes. *Energy Fuels*, 2004.
- [35] C. W. Dwiggin Jr. A small angle x-ray scattering study of the colloidal nature of petroleum. *The Journal of Physical Chemistry*, 69:3500–3506, 1965.
- [36] D. A. Storm, E. Y. Sheu, and M. M. DeTar. Macrostructure of asphaltenes in vacuum residue by small-angle x-ray scattering. *Fuel*, 72:977–981, 1993.

- [37] J.-N. Roux, D. Broseta, and B. Demé. Sans study of asphaltene aggregation: concentration and solvent quality effects. *Langmuir*, 17(16):5085–5092, 2001.
- [38] T. F. Headen, E. S. Boek, J. Stellbrink, and U. M. Scheven. Small angle neutron scattering (sans and v-sans) study of asphaltene aggregates in crude oil. *Langmuir*, 25(1):422–428, 2009.
- [39] J. Eyssautier, P. Levitz, D. Espinat, J. Jestin, J. Gummel, I. Grillo, and L. Barré. Insight into asphaltene nanoaggregate structure inferred by small angle neutron and x-ray scattering. *J. Phys. Chem. B*, 115(21):6827–6837, 2011.
- [40] E. B. Sirota. Physical structure of asphaltenes. *Energy and Fuels*, 19(4):1290–1296, 2005.
- [41] F. Mostowfi, K. Indo, O. C. Mullins, and R. McFarlane. Asphaltene nanoaggregates studied by centrifugation. *Energy Fuels*, 23(3):1194–1200, 2009.
- [42] B. Zhao and J. M. Shaw. Composition and size distribution of coherent nanostructures in athabasca bitumen and maya crude oil. *Energy Fuels*, 21(5):2795–2804, 2007.
- [43] O. C. Mullins, Hassan Sabbah, Joëlle Eyssautier, Andrew E. Pomerantz, Loïc Barré, A. Ballard Andrews, Yosadara Ruiz-Morales, Farshid Mostowfi, Richard McFarlane, Lamia Goual, Richard Lepkowitz, Thomas Cooper, Jhony Orbulescu, Roger M. Leblanc, John Edwards, and Richard N. Zare. Advances in asphaltene science and the yen–mullins model. *Energy Fuels*, 26(7):3986–4003, 2012.
- [44] Gaëlle Andreatta, Neil Bostrom, and O. C. Mullins. High-q ultrasonic determination of the critical nanoaggregate concentration of asphaltenes and the critical micelle concentration of standard surfactants. *Langmuir*, 21(7):2728–2736, 2005.
- [45] Gaëlle Andreatta, Cristiane Carla Goncalves, Gabriel Buffin, Neil Bostrom, Cristina M. Quintella, Fabricio Arteaga-Larios, Elías Pérez, and O. C. Mullins. Nanoaggregates and structurefunction relations in asphaltenes. *Energy Fuels*, 19(4):1282–1289, 2005.
- [46] Huang Zeng, Yi-Qiao Song, David L. Johnson, and O. C. Mullins. Critical nanoaggregate concentration of asphaltenes by direct-current (dc) electrical conductivity. *Energy Fuels*, 23(3):1201–1208, 2009.
- [47] N. V. Lisitza, D. E. Freed, P. N. Sen, and Y.-Q. Song. Study of asphaltene nanoaggregation by nuclear magnetic resonance (nmr). *Energy Fuels*, 23(3):1189–1193, 2009.
- [48] E. Rogel, G. Torres O. León, and J. Espidel. Aggregation of asphaltenes in organic solvents using surface tension measurements. *Fuel*, 79(11):1389–1394, 2000.

- [49] S. I. Andersen and K. S. Birdi. Aggregation of asphaltenes as determined by calorimetry. *J. Colloid Interface Sci.*, 142(2):497–502, 1991.
- [50] S. I. Andersen and S. D. Christensen. The critical micelle concentration of asphaltenes as measured by calorimetry. *Energy Fuels*, 14(1):38–42, 2000.
- [51] J. Escobedo and G.A. Mansoori. Viscosimetric determination of the onset of asphaltene flocculation: a novel method. *SPE Production and Facilities*, 1995.
- [52] Kriangkrai Kraiwattanawong, H. Scott Fogler, Samir G. Gharfeh, Probjot Singh, William H. Thomason, and Sumaeth Chavadej. Thermodynamic solubility models to predict asphaltene instability in live crude oils. *Energy Fuels*, 21(3), 2007.
- [53] Kriangkrai Kraiwattanawong, H. Scott Fogler, Samir G. Gharfeh, Probjot Singh, William H. Thomason, and Sumaeth Chavadej. Effect of asphaltene dispersants on aggregate size distribution and growth. *Energy Fuels*, 23(3), 2009.
- [54] K. Oh, T. A. Ring, and M. D. Deo. Asphaltene aggregation in organic solvents. *J. Colloid Interface Sci.*, 271(1), 2004.
- [55] C. W. Angle, Y. Long, H. Hamza, and L. Lue. Precipitation of asphaltenes from solvent-diluted heavy oil and thermodynamic properties of solvent-diluted heavy oil solutions. *Fuel*, 85(4), 2006.
- [56] Tabish Maqbool, Arjames T. Balgoa, and H. Scott Fogler. Revisiting asphaltene precipitation from crude oils: A case of neglected kinetic effects. *Energy Fuels*, 23:3681–3686, 2009.
- [57] M. P. Hoepfner, C. Vilas Bôas Fávero, N. Haji-Akbari, and H. S. Fogler. The fractal aggregation of asphaltenes. *Langmuir*, 29, 2013.
- [58] I. Yudin, G. Nikolaenko, E. Gorodetskii, E. Markhashov, V. Agayan, M. Anisimov, and J. Sengers. Crossover kinetics of asphaltene aggregation in hydrocarbon solutions,” *physica a: Statistical mechanics and its applications. Physica A: Statistical Mechanics and its Applications*, 251, 1998.
- [59] Y. G. Burya, I. K. Yudin, V. A. Dechabo, V. I. Kosov, and M. A. Anisimov. Light-scattering study of petroleum asphaltene aggregation. *Appl. Opt.*, 40, 2001.
- [60] Tabish Maqbool, Sasanka Raha, Michael P. Hoepfner, and H. Scott Fogler. Modeling the aggregation of asphaltene nanoaggregates in crude oilprecipitant systems. *Energy Fuels*, 25, 2011.
- [61] H. Rassamdana and M. Sahimi. Asphalt flocculation and deposition: Ii. formation and growth of fractal aggregates. *AIChE Journal*, 42, 1996.

- [62] K. Rastegari, W.Y. Svrcek, and H.W. Yarranton. Kinetics of asphaltene flocculation. *Industrial Engineering Chemistry Research*, 43, 2004.
- [63] K.J. Leontaritis and G.A. Mansoori. Asphaltene flocculation during oil production and processing: A thermodynamic colloidal model. *SPE International Symposium on Oilfield Chemistry*, 1987.
- [64] Huanquan Pan and Abbas Firoozabadi. Thermodynamic micellization model for asphaltene precipitation from reservoir crudes at high pressures and temperatures. *SPE Production and Facilities*, 15, 2000.

CHAPTER II

A Unified Model for Aggregation of Asphaltenes ¹

2.1 Introduction

Crude oil is a complex mixture of diverse hydrocarbons and organic components with different chemical properties [2]. Asphaltenes are defined as the collection of components precipitating out of crude oil when mixed with *n*-alkanes such as *n*-heptane and are soluble in aromatic solvents such as toluene [3]. This definition encompasses the heaviest and most polar fraction of crude oil [4]. Asphaltenes can precipitate due to changes in temperature, pressure or composition. These changes might occur at any point during oil production, transportation or processing. Precipitated asphaltenes can plug pipelines and production facilities, reduce storage capacity and cause equipment fouling and catalyst deactivation [5, 6]. Due to chemical complexity of asphaltenes, their structure and natural state is still unknown and therefore subject to debate and speculation [7, 8]. While a few researchers view phase behavior of asphaltenes as a liquid-liquid concentration fluctuations [7], the majority of researchers postulate asphaltenes as small solid nano-sized colloidal particles [8–13]. Regardless of what the stable form of asphaltenes is, their precipitation occurs when a fraction of

¹This chapter is partly based on the following manuscript: Nasim Haji-Akbari, Pennapa Masirisuk, Michael P. Hoepfner and H. Scott Fogler *EnergyFuels* **27**: 2497-2505 (2013) [1].

them are destabilized. Destabilization refers to both the phase separation or increase in aggregation tendency of nano-particles and the subsequent collision and eventual aggregation of asphaltene nano-particles into aggregates that are detectable under optical microscopy (precipitation) [14].

In order to unravel the factors that govern the asphaltene precipitation, numerous studies [15–19] have explored the behavior of destabilized asphaltenes. Destabilization is usually induced by adding a precipitant rather than changing the temperature or the pressure. Detection techniques such as optical microscopy [18], light scattering [15], UV-visible spectrophotometry [16] and refractive index [19] have been used to detect the precipitated micron-sized particles for different precipitants and precipitant concentrations. The majority of these studies assume that destabilized nano-sized asphaltene aggregates instantaneously grow into sizes detectable via conventional techniques. Such an assumption is only valid for the experimental conditions that produce strong attractive forces between aggregating asphaltenes and where the only rate-limiting step is the diffusion of asphaltene particles. However, at low precipitant concentrations, weaker attractions between asphaltene particles could lead to a reaction-limited process where slow kinetics become significant [20, 21]. For example Maqbool *et al.* [21] showed that the time it takes to detect asphaltene instability at low precipitant concentrations can be in the order of weeks, months or even years. Even in the case of higher precipitant concentrations where instabilities can be detected immediately, it can still take up to several weeks for the measured solubility of asphaltenes to reach to their final values [21]. Therefore the existing thermodynamic models [22–24] that are developed based on the assumption that the experiments conducted attained immediate solubility equilibration can lead to misleading predictions about the asphaltene behavior under different conditions.

The rate of asphaltene aggregation is controlled by two important factors: (1) the

frequency of the collisions between sub-micron sized particles and (2) the strength of interactions between aggregating asphaltenes [14]. In a pure solvent or crude oil, repulsive forces overcome attractions, therefore the asphaltenes remain stable [25, 26]. The nature of these repulsions is believed to be steric effects exerted by alkyl chains surrounding the aromatic cores [8]. Wang *et al.* [26] showed that long-range steric repulsions between two asphaltene surfaces in toluene-heptane mixtures can be modeled with the scaling theory of polymer brushes. Their model was successful in fitting interaction force measurements from atomic force microscopy (AFM) with three fitting parameters. Although their model provides a good insight into the nature of repulsive forces between asphaltene particles, it was only applied to one type of asphaltenes immobilized on silica surfaces and their fitting parameters are functions of the solution composition (i.e. the heptane to toluene ratio). The proposed model thus lacks predictive power and there is no known procedure for extracting model parameters for other types of asphaltenes, solvents or precipitants. In addition the model parameters obtained for immobilized asphaltene surfaces might not be applicable to nano-sized asphaltenes involved in the aggregation process. For example the thickness of the immobilized asphaltene layers in pure toluene was found to be around 50 nm [26] while the, size of asphaltene nano-particles in a pure solvent or a crude oil has been estimated to be less than 10 nm [9, 12, 13]. Therefore the thickness of steric layers cannot exceed a few nanometers. Since the magnitude of steric repulsions strongly depends on the thickness of the steric layer, model parameters used to describe steric repulsion at layers as thick as 50 nm are not likely to be applicable to nano-sized asphaltenes dispersed in crude oils. The magnitude of repulsive forces exerted by steric layers in aggregating asphaltenes is expected to be smaller than values measured in the aforementioned AFM study [26].

The fitting parameters from the scaling theory of polymer brushes used by Wang

et al. [26] showed that the asphaltene layers become more compact upon precipitant addition and this leads to a reduction in repulsive forces. In addition, it is believed that precipitant addition increases the magnitude of attractive forces between asphaltenes. Several types of interactions such as dispersion forces, polar interactions and hydrogen bonding have been proposed as possible contributors to such attractions. In order to formulate all these forces, a vast knowledge of the chemical structure of asphaltene molecules is required. Most researchers [18, 27, 28] believe that London dispersion forces are the dominant type of interactions between asphaltenes during their aggregation and precipitation. On the other hand, it has been argued that the impact of other types of forces such as hydrogen bonding, acidic/basic interactions and metal coordination complexes should not be overlooked [29]. In addition to dispersion forces, other types of interactions such as depletion attraction [30] can also increase the strength of attractive forces experienced by aggregating asphaltenes. In the case of depletion attractions, stable nano-sized asphaltenes can act as depletants for aggregating unstable asphaltenes.

Irrespective of the types of the interactions between asphaltenes, any increase in attractive forces- or any decrease in repulsive forces- will make collisions between aggregating particles more efficient and will therefore increase the rate of aggregation. The extent to which such interactions can change is not only a function of destabilization conditions (e.g. type of precipitant) but also depends on the properties of the crude oil. For instance, it is widely accepted that asphaltenes self-associate even in a good solvent [31]. Molecular weight (MW) measurements of associated asphaltenes from vapor pressure osmometry (VPO) have shown a solvent dependency indicating that the degree of association varies from one solvent to another [31]. Differences in association tendency of asphaltenes in different solvents are also observed in surface tension measurements [32]. In addition, both the association tendencies and the ag-

gregation rates between associated asphaltenes differ for different crude oils even if the same precipitant is used [21].

The aforementioned studies highlight the importance of the solvent or the crude oil on the type and strength of interactions between asphaltenes and therefore the kinetics of precipitation. However, predicting the effect of such changes on the aggregation rate requires a thorough understanding of the diffusion and reaction rates of asphaltene particles as a function of crude oil properties. Further studies are therefore necessary to identify the properties of crude oils and asphaltenes responsible for differences in their aggregation rates. In this paper, we focus on investigating the impact of changes in asphaltenes, solvent and crude oil properties on their aggregation behavior. In order to have the flexibility of studying the effect of solvent and asphaltenes independently, model mixtures are used in some of the experiments. A new predictive method has been then developed and will be discussed in detail. In this new method of analysis, it is established that precipitation rates can be predicted if certain physical properties of the asphaltenes and the solution surrounding them (e.g., viscosity and solubility parameter) are known.

2.2 Experimental Section

2.2.1 Materials

Five different crude oils and five different model oils were used in our study. Two additional crude oils (K1 and B1) were used to extract asphaltenes for the model mixture preparations. HPLC-grade toluene from Fisher and 97% purity 1-methylnaphthalene from Acros Organics were used as solvents for model oil preparation. HPLC-grade heptane from Fisher was used as precipitant to induce asphaltene instability for all our experiments. Table 2.1 summarizes certain physical properties

of the crude oils investigated in this study. The viscosities of the crude oils were measured by a rotational cone and plate rheometer (TA AR 1000). The refractive indices of crude oils were measured using a Schmidt and Haensch DUR-HT refractometer. All experiments were conducted at room temperature (20°C).

Table 2.1: Physical properties of crude oils at room temperature.

Sample Name	Oil A	Oil B	Oil C	Oil D	Oil E
Heptane Asphaltene Content (wt%)	3.25±0.01	0.74±0.03	1.44±0.03	1.45±0.05	0.78±0.04
Viscosity × 10 ³ (20°C, Pa · s)	27.52±0.6	19.99±0.5	165.78±5.4	12.23±0.3	5.82±0.1
Density (20°C, kg/m ³)	869.6±0.1	870.0±0.2	921.5±0.7	852.3±0.1	831.9±0.3
Refractive Index (20°C) (all±0.0002)	1.4964	1.4905	1.5204	1.4845	1.4720

2.2.2 Methods

All crude oils were centrifuged at 10,000 rpm for 3 hours to separate water, sand or any other solid particulates. To extract asphaltenes, K1 and B1 crude oils were mixed with heptane in 1:25 volume ratio. The solutions were kept well mixed for 24 hours and then were centrifuged at 3,500 rpm for an hour to separate precipitated asphaltenes. The asphaltenes were Soxhlet washed with heptane for 24 hours to wash any oil trapped in the cake. The asphaltenes were then dried in oven at 75°C to evaporate any heptane left in the cake from Soxhlet wash. Dried asphaltenes were grinded and stored. To prepare model mixtures, 2.55 vol% of dried asphaltenes were dissolved in the desired solvent. The density of asphaltenes was assumed to be 1200 kg/m³. The solutions were then sonicated until the proper dissolution was achieved. In each case, optical microscopy was used to confirm that dissolution is complete.

Microscopy experiments: A total of ten different oils (five crude oils, five model oils) were studied. Asphaltene precipitation was induced by adding different concentrations of heptane to each oil. A known volume of oil was placed in a 4mL vial. Heptane was then added slowly to the mixture using a syringe pump at a rate of 20 mL/hr. During the precipitant addition, all solutions were kept well mixed using magnetic stirrers in order to minimize localized high precipitant concentrations. To increase experimental accuracy, all samples were prepared on a mass basis and final volume fractions of heptane were calculated using the final densities. After sample preparation, a droplet of well-stirred sample was placed under the microscope at different times in order to detect asphaltene particles. An optical microscope from Nikon (model: Eclipse E600) with 50x objective lens and 10x eyepiece was used for detecting asphaltene particles and a CCD camera from Sony (model: AVC-D7) was used for shooting images off the microscope. The smallest particles detectable under the microscope are approximately $0.5 \mu\text{m}$ in diameter. The earliest time when particles were observed is defined as the *detection time*.

Small Angle X-ray Scattering (SAXS): Asphaltenes are believed to form nano-sized particles both in crude oil and in a solvent [8–13]. Small angle X-ray scattering is a powerful technique that can provide information about the size and structure of asphaltene nano-aggregates. To better understand the behavior of asphaltenes in different solvents SAXS was applied to monitor change in size of asphaltene nanoparticles as a function of time and the solvent. Bruker Nanostar SAXS Equipment at University of Michigan was used to perform scattering measurements. The X-ray generator was set at 40 kV and 35 mA with 0.5 second per frame and 900 second per sample. Guinier approximation was then used to get an average shape-independent size, radius of gyration, for asphaltenes:

$$I(q) = I_0 \exp\left(-\frac{(qR_g)^2}{3}\right) \quad (2.1)$$

where I is the scattering intensity, I_0 is the zero angle intensity, $q(1/\text{\AA})$ is the scattering vector and $R_g(\text{\AA})$ is the Guinier radius of gyration.

2.3 Results and Discussion

Optical microscopy is used for detecting the time at which asphaltenes reach a certain size ($0.5 \mu\text{m}$). It can therefore be conveniently used to characterize precipitation by measuring the time required for asphaltenes to reach a size detectable after precipitant addition. The lag time between asphaltenes detection and the precipitant addition is because the growth of asphaltene aggregates is not instantaneous, but instead is a kinetically controlled process. In this paper, detection times obtained from microscopy experiments provide an estimate for initial aggregation rates.

Figure 2.1 shows detection times as a function of heptane concentration for five different crude oils. The asphaltene precipitation detection time is a function of heptane concentration in all samples indicating the universality of kinetic growth phenomena among different crude oils. The aggregation rates however strongly depend on the properties of individual crude oils. One can clearly observe different slopes and offsets for the fitted lines, something that will be analyzed in the next section on modeling of the asphaltene aggregation process. As discussed earlier, the aggregation rate depends on both the frequency and the efficiency of collisions between unstable particles. Due to differences in viscosity and total asphaltene content, the diffusivities and collision frequencies of asphaltenes are expected to be different in each crude oil. However, as

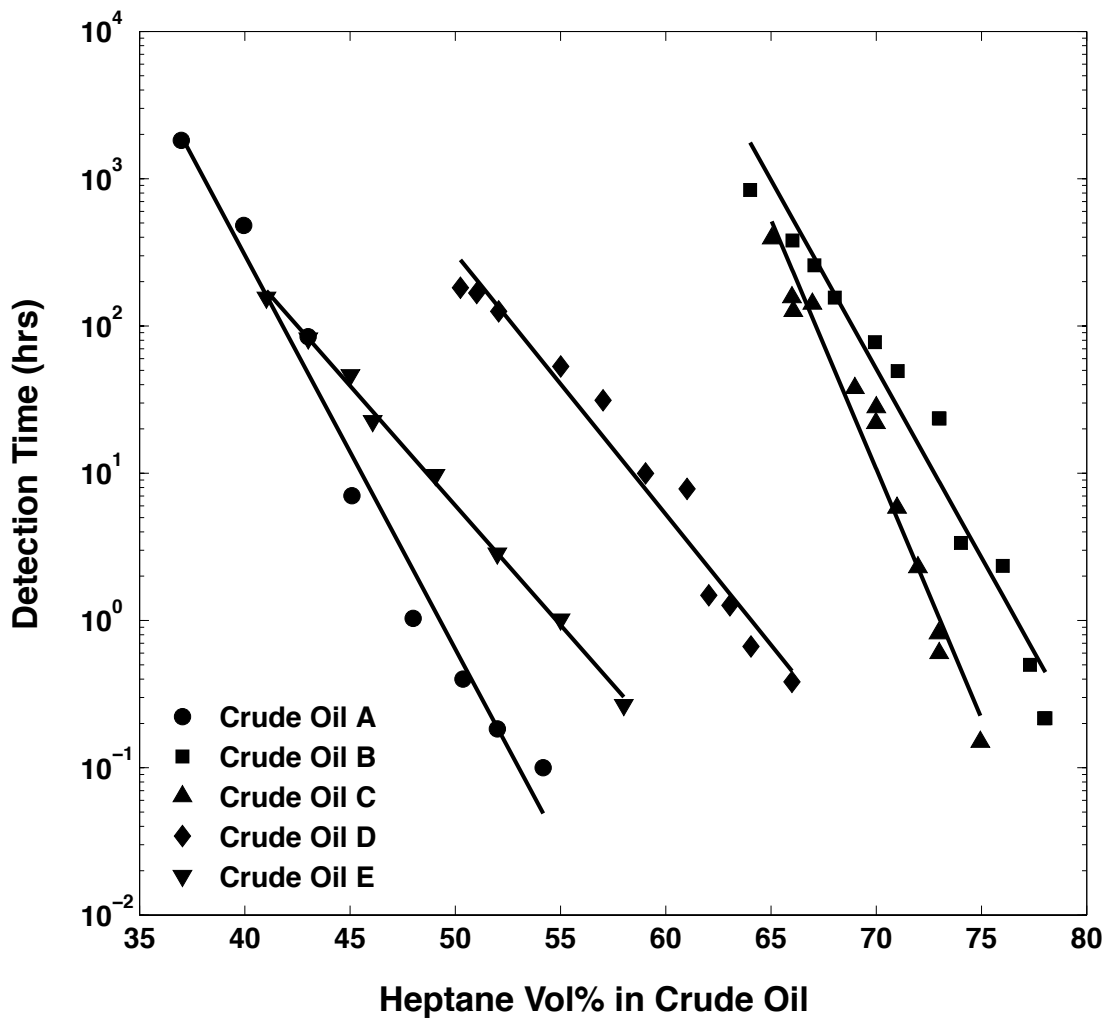


Figure 2.1: Detection time as a function of heptane concentration for five different crude oils (Crude oil A (●), crude oil B (■), crude oil C (▲), crude oil D (◆) and crude oil E (▼)).

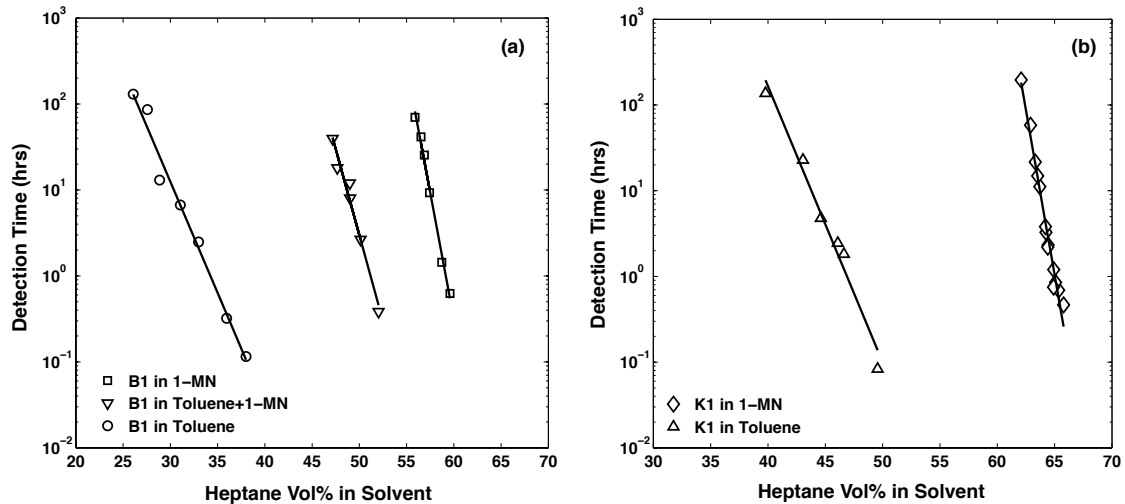


Figure 2.2: **Detection time as a function of heptane concentration for model oils:** (a) 2.55 vol% B1 asphaltenes in: toluene (\circ), mixture of 50:50 (vol%) toluene–1-methylnaphthalene (∇) and 1-methylnaphthalene (\square) (b) 2.55 vol% K1 asphaltenes in: toluene (\triangle) and 1-methylnaphthalene (\diamond).

can be seen in Figure 2.1, no consistent trends can be observed among the aggregation rates and viscosity or asphaltene content. Therefore it is believed that differences in coagulation efficiencies have a larger impact on controlling the aggregation rate of asphaltenes compared to their diffusivities. Consequently it is necessary to understand why and how coagulation efficiencies change from one crude to another. It is an objective of our model to understand changes in coagulation efficiencies as a result of changes in solution properties.

Figure 2.2 shows the detection times measured from microscopy as a function of heptane concentration for different types of asphaltenes dissolved in toluene, in 1-methylnaphthalene and in a mixture of these two solvents (50 vol% toluene+50 vol% 1-methylnaphthalene). For the same type of asphaltenes, precipitation rate strongly depends on the solvent used for their stabilization. Once again, one can observe different slopes and offsets. The aggregation rate of asphaltenes in different solvents

can be compared in two different ways: (1) identical detection times, (2) identical heptane concentrations.

These findings reveal that larger amounts of heptane are required to induce identical detection times (similar aggregation rates) in 1-methylnaphthalen compared to toluene. This result is not surprising because the larger viscosity of 1-methylnaphthalene decreases the diffusion rate of particles at the same heptane concentration. Furthermore, asphaltenes are believed to be composed of several aromatic rings surrounded by alkyl chains [8]. 1-methylnaphthalene has one more aromatic ring than toluene and is therefore more polarizable. The interaction between 1-methylnaphthalene and asphaltenes, which is of a van der Waals nature, will thus be stronger than the interaction between toluene and asphaltenes. Stronger interactions between asphaltenes and the solvent will decrease the aggregation tendency of destabilized asphaltenes. As a result, higher concentrations of precipitant are needed in 1-methylnaphthalene in order to obtain similar aggregation rates.

At identical heptane concentrations, differences in aggregation rates of asphaltenes in different solvents cannot be directly compared because there is no overlapping range of heptane concentrations at which kinetic effects are observed for both solvents (e.g., K1 asphaltenes in toluene and 1-methylnaphthalene). This lack of overlap can be either due to thermodynamic stability of asphaltenes at low precipitant concentrations for solutions with higher 1-methylnaphthalene content or it can just be a result of very slow agglomeration kinetics. In the former case, there will be no change in sizes and natural states of asphaltene particles as a function of time after precipitant addition. However, in the later case, asphaltenes will slowly grow to larger sizes as time progresses. As discussed earlier, both the collision frequency and the collision efficiencies will produce slower kinetics in 1-methylnaphthalene at identical heptane concentrations. To shed light on the actual behavior of asphaltenes at low precipitant

concentrations, it was decided to monitor the change in the scattering behavior of K1 asphaltenes as a function of time using small angle X-ray scattering. Figure 2.3 shows the scattering results for K1 asphaltenes in toluene and 1-methylnaphthalene mixed with 30 vol% heptane.

Table 2.2 shows radius of gyrations estimated from the Guinier analysis for asphaltenes in each mixture as a function of time. It is clear that asphaltenes immediately grow in size when heptane is added to the toluene-asphaltene solution and the growth continues as time progresses. However, for 1-methylnaphthane no change in scattering is observed neither as a function of heptane concentration nor as a function of time. These findings indicate that asphaltenes are not growing in 1-methylnaphthalene at 30 vol% heptane (i.e. they are thermodynamically stable) while they grow in size in toluene. Therefore the observed discrepancies in asphaltene aggregation rates in these two solvents at such low precipitant concentrations are due to the thermodynamic stability of asphaltenes in 1-methylnaphthalene.

Table 2.2: Radius of gyration for samples shown in Figure 2.3.

Sample Name	R_g (nm)
Toluene	5.0 ± 0.09
Toluene + C_7 (day 1)	7.1 ± 0.18
Toluene + C_7 (day 40)	9.6 ± 0.40
1-MN	3.7 ± 0.09
1-MN + C_7 (day 1)	3.6 ± 0.05
1-MN + C_7 (day 40)	3.6 ± 0.07

A simple model is proposed to determine the aggregation rate of asphaltenes at precipitant concentrations where the kinetics are slow. This model accounts for the factors that control the aggregation rate as a function of changes in solution properties at every heptane concentration.

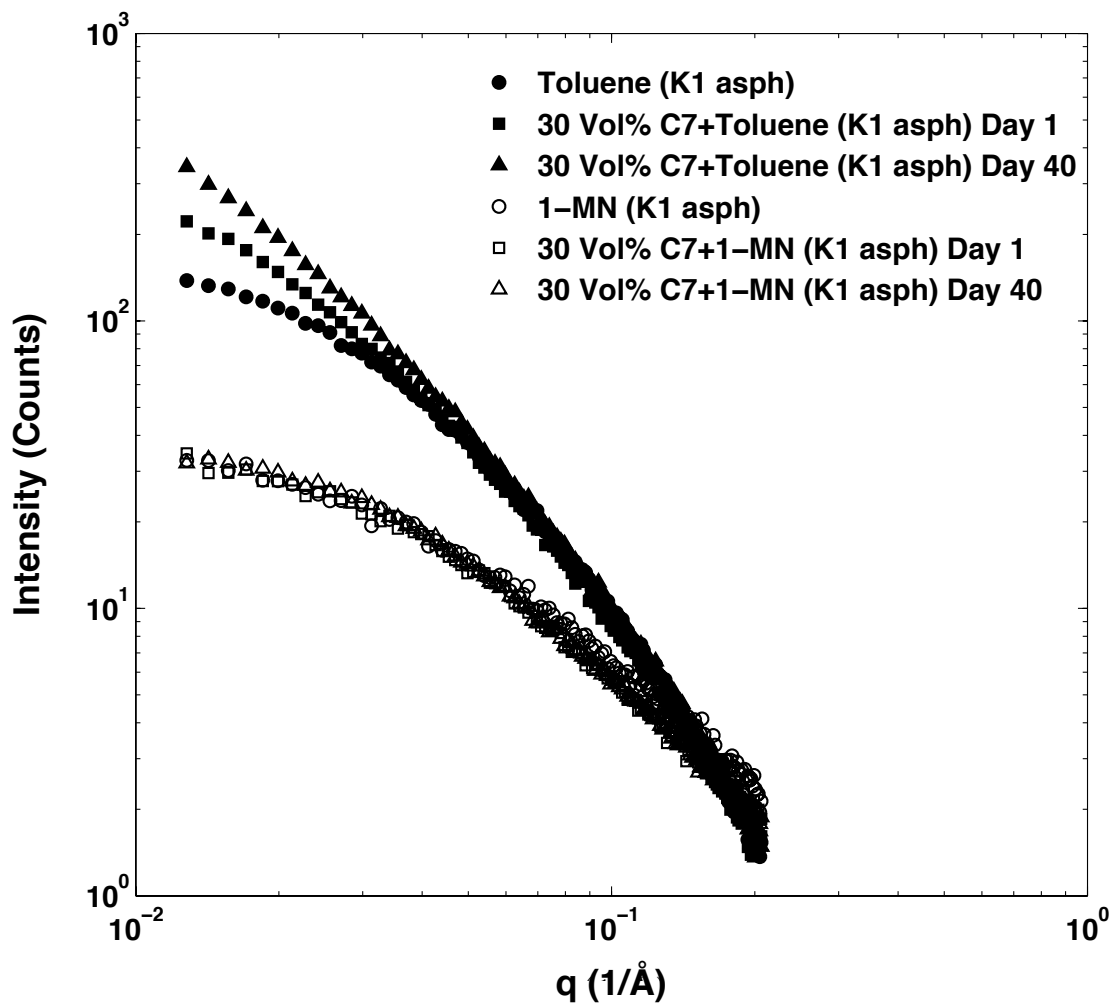


Figure 2.3: **Scattering intensity as a function of scattering vector for K1 asphaltenes:** in toluene (\bullet), 1-methylnaphthalene (\circ), 30 vol% heptane in: toluene day 1 (\blacksquare), day 40 (\blacktriangle) and 30 vol% heptane in 1-methylnaphthalene day 1(\square) and day 40(\triangle).

2.3.1 Asphaltene Aggregation Modeling

The aggregation behavior of asphaltenes can be predicted by the widely accepted Smoluchowski's aggregation model [33, 34]. The key parameters in this model are the frequency of collisions between aggregating particles and the fraction of successful collisions that lead to aggregation. The rate of formation of each particle in the Smoluchowski's model is given by [33]:

$$\frac{dC_k}{dt} = \frac{1}{2} \sum_{i+j=k} K_{ij} C_i C_j - C_k \sum_{i \geq k} K_{ik} C_i \quad (2.2)$$

where C_i is the number concentration of particles of size i (# particles/m³), and K_{ij} is the collision kernel for aggregation (m³/s). Asphaltenes exist as nano-sized particles in the solution and at these length scales the major transport mechanism for their movement is the Brownian motion. For collision of approximately equal sized particles during a diffusion-limited process, the rate constant for Brownian diffusion can be estimated using following equation [34]:

$$K_{ij} = \frac{8k_B T}{3\mu} = K \quad (2.3)$$

where T is the temperature (K), k_B is the Boltzmann constant (m² kg/s²K) and μ is the viscosity (Pa · s).

During the reaction-limited aggregation, only a fraction of Brownian collisions can lead to the formation of larger particles. In order to account for unsuccessful collisions, the rate constant will be given by:

$$K = \frac{8k_B T}{3\mu} \beta \quad (2.4)$$

where β is the collision efficiency:

$$\beta = \frac{\text{Number of successful collisions}}{\text{Total number of collisions}} \quad (2.5)$$

Using the exponential Ansatz procedure [33] the above set of differential equations shown in Equation (2) can be solved analytically (See Appendix A):

$$\frac{C_K(t)}{C_1(0)} = \frac{4}{(\alpha t + 2)^2} \left[\frac{\alpha t}{\alpha t + 2} \right]^{k-1} \quad (2.6)$$

where $\alpha = \frac{8k_B T}{3\mu} \beta C_1(0)$, and $C_1(0)$ is the initial number concentration of aggregating asphaltenes.

The analytical solution provided in Equation 2.6 predicts the change in the concentration of each particle as a function of time. The particle size continues to increase until a number concentration with a size around $0.5 \mu\text{m}$ is reached where they can be detected under microscopy. Equation 2.6 can be simplified (See Appendix A) to estimate detection times from viscosity, collision efficiency and initial concentration of asphaltene nano-particles:

$$t_{\text{detection}} \propto \frac{1}{\sqrt{C_1(0)}} \frac{\mu}{\beta} \quad (2.7)$$

In order to predict initial aggregation rates (detection times) of asphaltenes when their stability changes either as a result of precipitant addition or due to pressure depletion, it is necessary to estimate the subsequent change in viscosity or collision efficiency. Changes in the viscosity as a function of precipitant concentration can be easily estimated by knowing the viscosity of the crude oil and precipitant. On the other hand, due to the complexity of asphaltenes, their chemical structure is not well understood even after several decades of research. Therefore, predicting the changes in collision efficiency (i.e. aggregation tendency of asphaltenes) after changing the solvent or crude oil is not an easy task to achieve.

As discussed earlier, the aggregation tendency of asphaltenes is controlled by the strength of interaction forces between aggregating asphaltenes. The magnitude of repulsive forces compared to attractive forces dictates the success of attachment of two colliding particles. In the case of larger attractive forces compared to repulsive forces, every collision will be successful. However, at the separation distances where the steric layers start to overlap, the magnitude of repulsion force becomes larger than attractions. Large repulsions generate a local maximum on the potential energy landscape (repulsion barrier) as illustrated in Figure 2.4. Colliding asphaltene particles need to have enough thermal energy during collision to overcome this repulsive barrier. Therefore not all collisions lead to an aggregation event and the collision efficiency will be less than one. The larger the repulsive energy, the higher the repulsive barrier will be and as a result a smaller fraction of collisions will have adequate thermal energy to overcome the barrier. To predict the collision efficiency between two aggregating particles, one needs to know how attractive and repulsive forces change as a function of separation distance. Fuch's stability ratio (W) between colliding particles of equal size is extensively used in the colloids literature to estimate the collision efficiency from the interparticle potential U_t [34]:

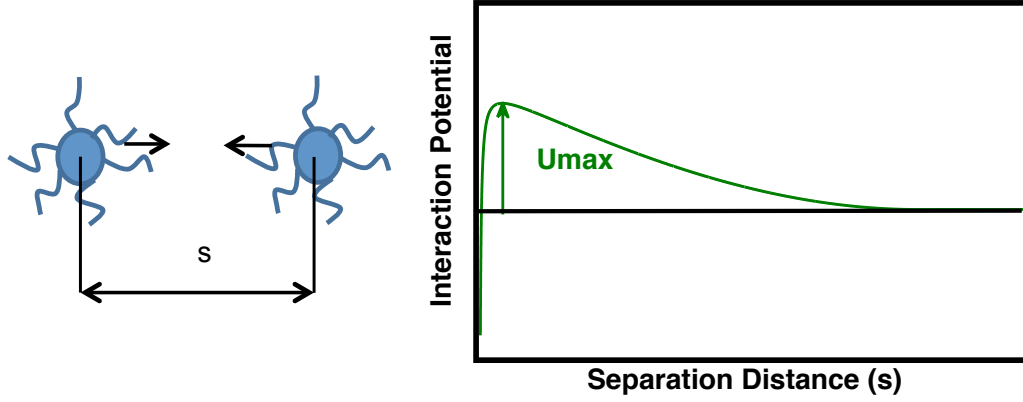


Figure 2.4: Schematic of interactions between two asphaltenes as a function of their separation distance.

$$\frac{1}{\beta} = W = 2r_0 \int_{2r_0}^{\infty} \frac{\exp\left(\frac{U_t}{k_B T}\right)}{s^2} ds \quad (2.8)$$

where r_0 is radius of primary particles (m), U_t is the total energy of interaction between two primary particles (J), s is the distance between the particles center (m), k_B is Boltzman's constant ($\text{m}^2\text{kg}/\text{s}^2\text{K}$) and T is the temperature (K).

Because of the exponential term in Equation 2.8, the major contribution to the stability ratio is from the separation distances close to U_{max} , therefore the collision efficiency defined in Equation 2.5 can be estimated using following correlation:

$$\beta = \exp\left(-\frac{U_{max}}{k_B T}\right) \quad (2.9)$$

Asphaltene are stable in their natural state in crude oils or model mixtures, indicating that the magnitudes of the repulsive forces are larger than the attractive

forces. Therefore in a pure solvent repulsive barrier is the largest. When asphaltenes are destabilized- e.g. as a result of heptane addition- the steric layers become more compact [26]. This compaction in turn leads to a decrease in the magnitude of repulsive forces that are no longer as effective as in a pure solvent. In addition, attractive forces between asphaltene particles become larger upon heptane addition. Therefore, the repulsive barriers become smaller as more heptane is added. On the other hand, adding more heptane to the solution results in a decrease of its solubility parameter. Hence, the difference between the solubility parameters of asphaltenes and the surrounding solution will become larger upon destabilization. The maximum potential barrier in our analysis depends on the overall interaction energy between asphaltenes. Motivated by the experimental observations that the change in the solubility parameter difference and the change in the maximum potential barrier are correlated when a precipitant is added, it is postulated that the repulsion barrier is related to the difference in solubility parameter of asphaltenes and the solution as follows:

$$U_{max} \propto (\delta_{asph} - \delta_{solution})^n \quad (2.10)$$

where δ_{asph} and $\delta_{solution}$ stand for the Hildebrand solubility parameter ($\text{Pa}^{0.5}$) of the asphaltenes and the solution respectively and n is a constant. Equation 2.10 can be used to predict changes in the collision efficiency under different experimental conditions. Combining Equations 2.9 and 2.10 we get at constant temperature:

$$-\ln(\beta) \propto (\delta_{asph} - \delta_{solution})^n \quad (2.11)$$

Another alternative approach is considering the collision efficiency a function of the activation energy needed for the coagulation between two colliding asphaltene particles (i.e. Arrhenius activation energy):

$$\beta \propto \exp\left(-\frac{E_a}{RT}\right) \quad (2.12)$$

where E_a is the activation energy and R is the universal gas constant. Inspired by dependency of the activity coefficients (regular solution theory or Flory-Huggins theory) on $(\delta_{asph} - \delta_{solution})$, one can assume that E_a is proportional to the $(\delta_{asph} - \delta_{solution})$:

$$E_a \propto (\delta_{asph} - \delta_{solution})^n \quad (2.13)$$

In addition it is known from Equation 2.7 that:

$$\ln\left(\frac{t_{detection}\sqrt{C_1(0)}}{\mu}\right) \propto -\ln(\beta) \quad (2.14)$$

Assuming that Equations 2.10 or 2.13 are successful in capturing changes in repulsive barriers or activation energy as a function of solution solubility parameter, the experimentally measured detection times will be related to changes in the solubility parameters at a given temperature by:

$$\ln \left(\frac{t_{detection} \sqrt{C_1(0)}}{\mu} \right) \propto (\delta_{asph} - \delta_{solution})^n \quad (2.15)$$

2.3.2 Model Application

Equation 2.15 can be applied to our experimental measurements of detection times of different mixtures with different values of n . The viscosity of the solution is calculated based on the modified logarithmic average mixing rule for mixtures of heptane in the oils [35]. The solubility parameter of each mixture is estimated using the volumetric average of solubility parameters of its components. Solubility parameters of different crude oils are estimated by measuring their refractive indices and using the correlation proposed by Wang and Buckley [24]. The solubility parameters of toluene, 1-methylnaphthalene and heptane are 18300, 20300 and 15200 Pa^{0.5} respectively [36]. The viscosities and densities of toluene, 1-methylnaphthalene and heptane at room temperature are 0.000604, 0.00346 and 0.000415 Pa · s and 868, 1020 and 679 kg/m³ respectively. Initial nano-particle concentration² at the precipitation point for each oil is assumed to be proportional to the total asphaltene content in each crude oil or model oil after average dilution effects with heptane has been taken into account. Asphaltenes are solid and complex compounds and it is experimentally difficult to measure their solubility parameters (See section 1.2.3). A wide range of values have been proposed for the solubility parameter of asphaltenes in the literature [37]. Consequently solubility parameters of asphaltenes within the acceptable range are adjusted to get the best fit that matches all experimental findings of 10 different systems (5 crude oils and 5 model mixtures) investigated in this work. Our analysis shows that the quality of the fit is not sensitive to the absolute value of the asphaltenes solubil-

² $C_1(0)$ Calculated using Equation A.22

ity parameter for different asphaltenes and the most important factor is the relative difference between the solubility parameter of different asphaltenes. The solubility parameters of asphaltenes reported in this chapter for each asphaltene type are obtained by searching for the global minimum of error squared between predicted and measured value of $\ln(t_{\text{detection}}\sqrt{C_1(0)}/\mu)$ in the range of asphaltenes solubility parameters reported in literature (18400-24500 Pa^{0.5} [37]). In the model mixtures, a single value is used for the solubility parameter of each asphaltene type regardless of the solvent under investigation.

Figure 2.5 and 2.6 show the plot of $\ln(t_{\text{detection}}\sqrt{C_1(0)}/\mu)$ vs. $(\delta_{\text{asph}} - \delta_{\text{solution}})^n$ for different values of n ($n = 1, 2$ and $n = -1, -2$). Our findings show that $(\delta_{\text{asph}} - \delta_{\text{solution}})^n$ and $\ln(t_{\text{detection}}\sqrt{C_1(0)}/\mu)$ are linearly correlated; suggesting that correlation proposed for changes in the repulsive barrier or activation energy can successfully capture changes in aggregation rates for the crude oils and model oils. All the curves shown in Figures 2.5 and 2.6 fall onto a single master curve for each n with a simple form that we propose to predict the change in collision efficiency as a function of heptane concentration. Our results also show that the quality of fits are independent of the value chosen for n . The quality of fits for model oils are not as good as crude oils. Figure 2.7 shows the analysis only for the crude oils with $n = -2$. The inaccuracy of analysis for model oils is probably due to the polydispersity of asphaltenes and will be discussed in further detail later (See Appendix B).

Table 2.3 shows the measured values of solubility parameter for crude oils and the estimated values for solubility parameter of asphaltenes in each crude oil and Table 2.4 shows the solubility parameters of K1 and B1 asphaltenes. The estimated values for solubility parameter of asphaltenes are close to the upper limit of values proposed in the literature. This is not surprising because the analysis approach presented here is based on microscopy experiments, which detect asphaltenes aggregating immediately

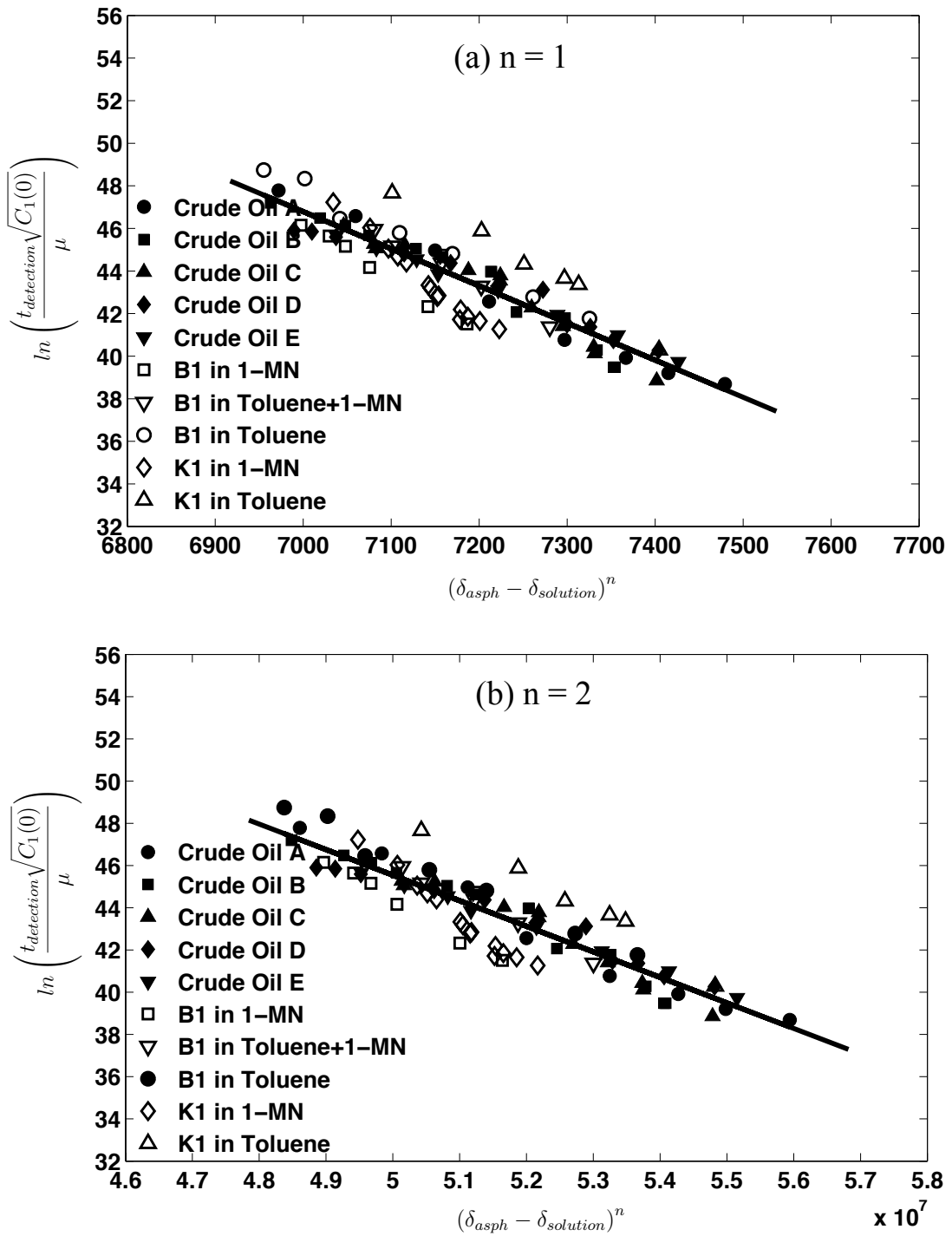


Figure 2.5: Plot of $\ln(t_{\text{detection}} \sqrt{C_1(0)} / \mu)$ vs. $(\delta_{\text{asph}} - \delta_{\text{solution}})^n$ for different values of n : (a) $n = 1$ and (b) $n = 2$.

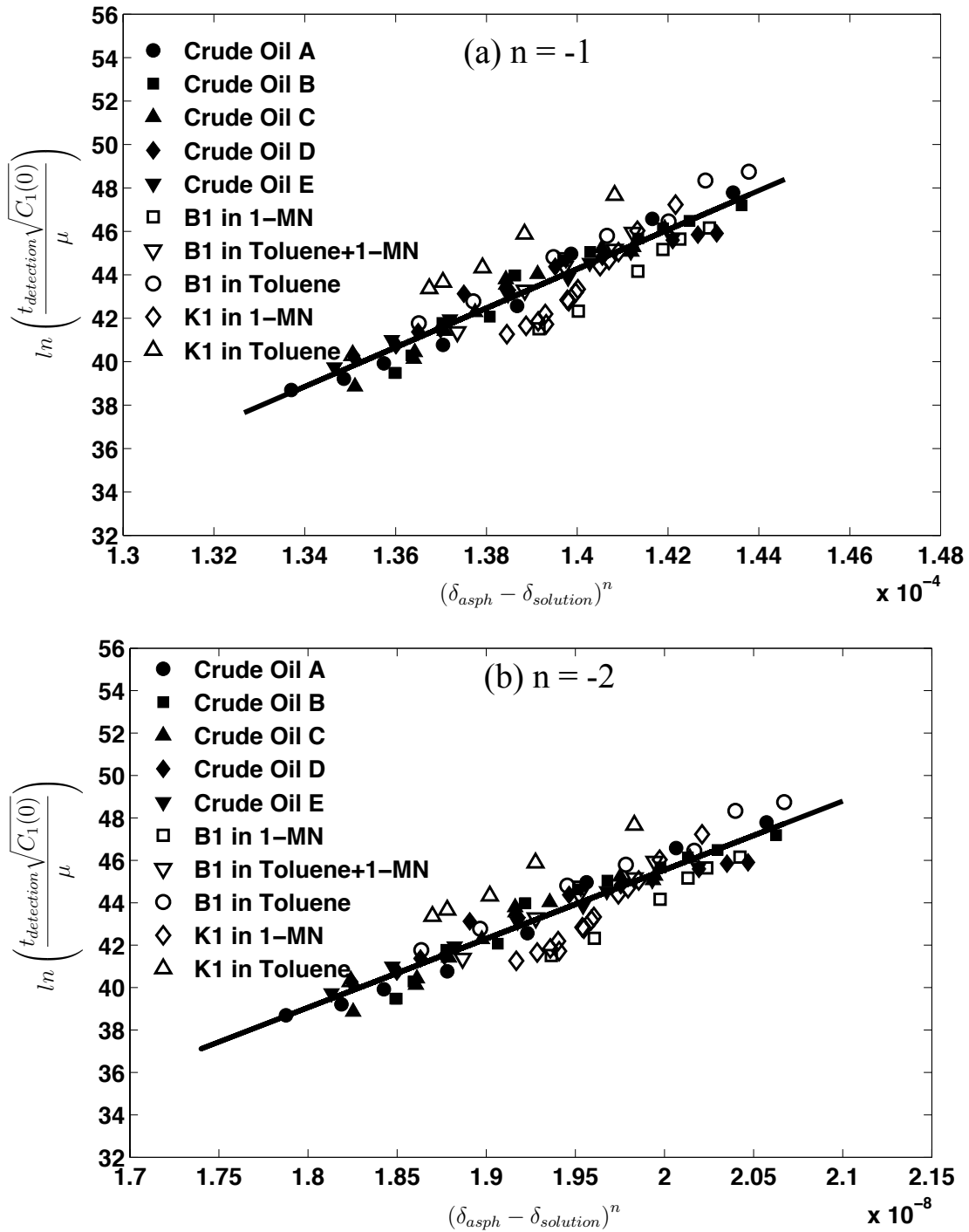


Figure 2.6: Plot of $\ln\left(\frac{t_{\text{detection}} \sqrt{C_1(0)}}{\mu}\right)$ vs. $(\delta_{\text{asph}} - \delta_{\text{solution}})^n$ for different values of n : (a) $n = -1$ and (b) $n = -2$.

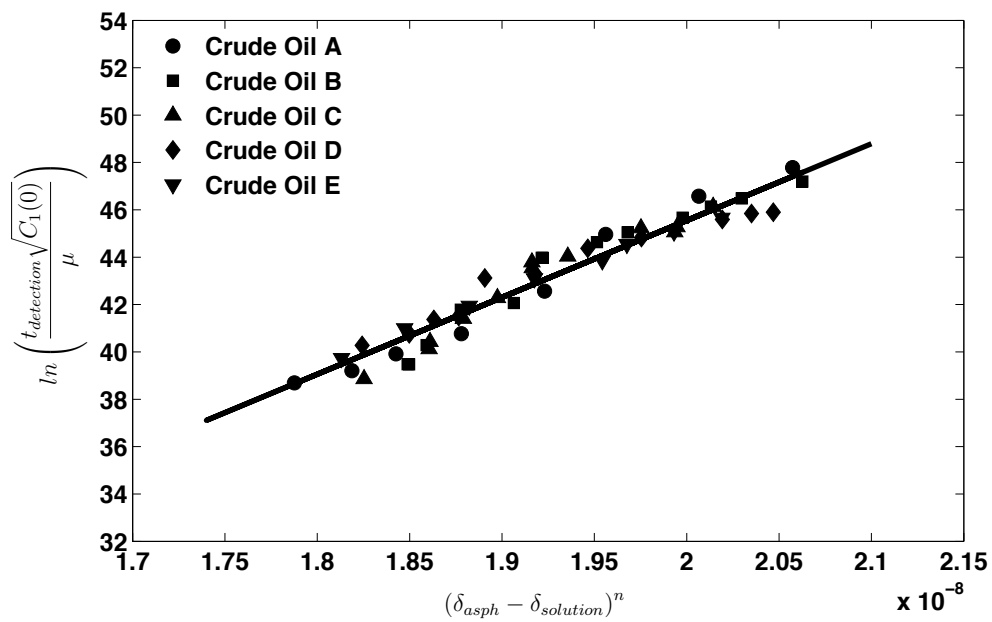


Figure 2.7: Plot of $\ln(t_{\text{detection}} \sqrt{C_1(0)} / \mu)$ vs. $(\delta_{\text{asph}} - \delta_{\text{solution}})^n$ for crude oils ($n = -2$).

after precipitant addition. These asphaltenes are probably the most unstable fraction of asphaltenes and therefore are expected to have the largest solubility parameters among all the asphaltenes in the crude oil. A simple estimate for the solubility parameter of asphaltenes is proposed by Wang [37] by estimating their refractive index in a solvent and using the correlation between the refractive index function and solubility parameter [24]. We applied this approach for B1 asphaltenes diluted in toluene and obtained a solubility parameter of around 24400 Pa^{0.5}. It can be seen from Table 2.4 that the measured value is in good agreement with the values used in our model.

Table 2.3: Solubility parameter of crude oils and predicted solubility parameter of asphaltenes.

Sample Name	Solubility Parameter Crude Oil (Pa ^{0.5})	Solubility Parameter Asphaltenes (Pa ^{0.5})
Crude Oil A	18150	24031
Crude Oil B	17990	23167
Crude Oil C	18790	23501
Crude Oil D	17830	23498
Crude Oil E	17490	23588

Table 2.4: Solubility parameter of K1 and B1 asphaltenes.

Sample Name	Solubility Parameter Asphaltenes (Pa ^{0.5})
K1 Asphaltenes	24168
B1 Asphaltenes	24447

The correlation from each master curve can be used to evaluate the accuracy of the model in fitting individual data points. Figure 2.8 shows the modeling results compared to the experimental measurements of detection times and Figure 2.9 compares the predicted detection times with the measured times as a function of heptane

concentration for each experiment separately. Model fits are in excellent agreement with experimental results for the crude oils (Figure 2.9(a)). In the case of model mixtures the fits are in reasonable agreement with experiments. The inaccuracy in some fits for model mixtures (e.g. K1 asphaltenes in toluene) can be explained by polydispersity of asphaltenes as the asphaltenes dispersed in a single crude oil are not a single entity with a single solubility parameter but a mixture of different components with a distribution of solubility parameters. The kinetics of destabilization is governed by the difference between the solubility parameters of asphaltenes and the solution, with larger differences leading to faster destabilization and aggregation. At low precipitant concentrations, the asphaltenes whose mean solubility parameter is the furthest from the solubility parameter of the solution will thus aggregate, while the remaining asphaltenes will either not phase separate at all, or will do that at a much smaller rate. The solubility parameter of the fraction of asphaltenes that precipitate first could depend on the solvent or the precipitant (Chapter IV), and in different solvents (e.g., toluene and 1-methylnaphthalene) different fractions of asphaltenes might get involved in the aggregation process. As a result a single solubility parameter might not accurately describe the behavior of asphaltenes in different solvents (See Appendix B). The effect of polydispersity is less dominant for a narrow range of precipitant concentrations mixed with the same solvent (i.e. crude oils mixed with heptane in Figure 2.7). The influence of asphaltenes polydispersity on their aggregation rates is further discussed in Chapters IV and V.

One of the important parameters in the Flory-Huggins theory of polymer-solution thermodynamics is the difference between the solubility parameters of the solute and the solvent [38]. In this theory, the Flory-Huggins interaction parameter (χ) is used to account for the intermolecular forces between the polymers and the solvent and to describe the effect of solvent quality on the polymer solubility. The interaction

parameter (χ) depends on the square of difference in the solubility parameters of the polymers and the solution. Some researchers have applied this theory to predict the phase behavior of asphaltenes [22–24]. Due to the appearance of power two in Flory-Huggins theory and due to insensitivity of our analyses to the power chosen, for the rest of this thesis all the analyses are done using $n = -2$. Power of -2 means that the maximum potential barrier is inversely proportional to the difference in solubility parameters squared, which physically is in agreement with the reduction of U_{max} as $(\delta_{asph} - \delta_{solution})^2$ increases. This model cannot explain the behavior of asphaltenes at $\delta_{asph} = \delta_{solution}$ and is only valid when the asphaltenes are destabilized and their solubility parameter is different from the solubility parameter of solution.

Despite differences in aggregation behaviors of asphaltenes in different model oils or crude oils, the proposed model captures and predicts the aggregation behavior of asphaltenes and was tested for aggregation rates of ten different samples at room temperature. The solubility parameter of asphaltenes can be estimated by a single detection time measurement at a fixed precipitant concentration using the correlation between $\ln(t_{detection} \sqrt{C_1(0)}/\mu)$ and $(\delta_{asph} - \delta_{solution})^2$ from the master curve shown in Figure 2.10 (2.6 (b)). This new method is expected to be valid for asphaltene precipitation under other operational conditions. For example Maqbool *et al.* [39] investigated precipitation kinetics for different temperatures and showed that the discrepancies in the aggregation rates at 20°C and 50°C can be explained by accounting for the change in viscosity. This observation is not surprising because the difference in the solubility parameter of mixture and asphaltenes does not significantly change with temperature [37]. Therefore the major contribution to the change in aggregation rate is from the changes in viscosity as temperature increases from 20°C to 50°C. The proposed approach can be also used to estimate the degree of asphaltenes instability and their tendency for aggregation and deposition during the pressure depletion.

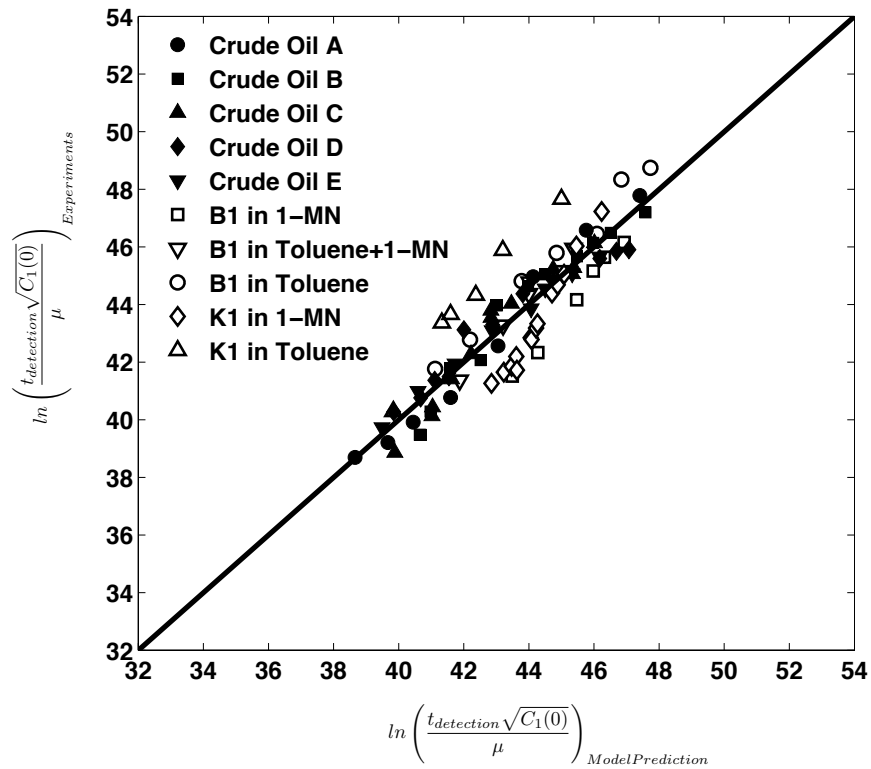


Figure 2.8: $\ln(t_{\text{detection}} \sqrt{C_1(0)} / \mu)$ experiment vs. model prediction for crude oils and model oils mixed with *n*-heptane.

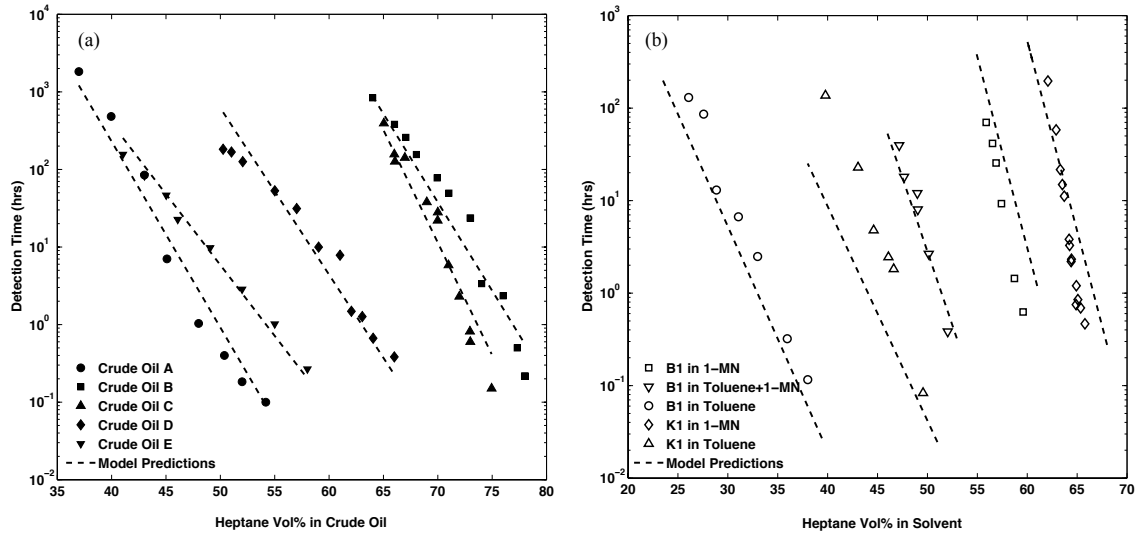


Figure 2.9: Detection times vs. heptane concentration measured experimentally (data points) and modeled (dashed lines):(a) crude oils, (b) model mixtures.

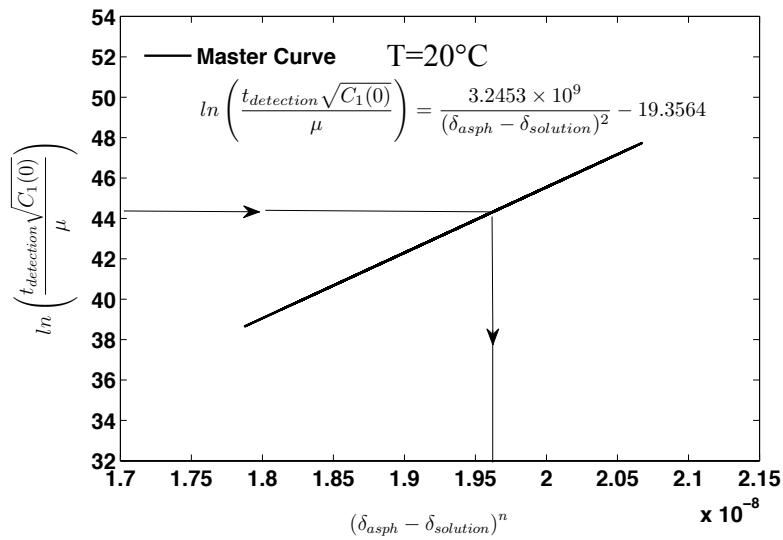


Figure 2.10: Master curve for relation between $\ln(t_{\text{detection}}\sqrt{C_1(0)}/\mu)$ and $(\delta_{\text{asph}} - \delta_{\text{solution}})^n$, $n = -2$.

2.4 Conclusions

This study provides new avenues for predicting destabilization and aggregation rates of asphaltenes. Kinetic experiments highlight the importance of crude oil or solvent properties on precipitation of asphaltenes. Such predictive models will be extremely useful in foreseeing the precipitation kinetics. Changing the crude oils or the model mixture changes the collision frequency and the efficiency of collisions between aggregating particles. Smoluchowski's aggregation model has been used to account for any change in collision frequency by accounting for properties such as mixture viscosity. A new model has also been proposed to account for the changes in interaction forces of asphaltene particles during aggregation process. The model correlates the change in collision efficiency to the change in the difference between the asphaltenes and the mixture's solubility parameters. Despite the differences in properties of crude oil and model mixtures the proposed approach is shown to be effective in modeling the detection times measured from microscopy experiments for ten different systems. The results show that all the differences for different types of asphaltenes and crude oils can be explained reasonably well by this new model and their aggregation rates collapse onto a single master curve.

Bibliography

- [1] N. Haji-Akbari, P. Masirisuk, M. P. Hoepfner, and H. S. Fogler. A unified model for aggregation of asphaltenes. *Energy Fuels*, 27, 2013.
- [2] K. H. Altgelt and M. M. Boduszynski. *Composition Analysis of Heavy Petroleum Fractions*. CRC Press, 1994.
- [3] T.F. Yen and G.V. Chilingarian. *Asphaltenes and Asphalts*, volume 1. Elsevier Science, 1994.
- [4] P. Wattana and H.S. Fogler. Characterization of polarity-based asphaltene sub-fractions. *Energy Fuels*, 2005.
- [5] P. Wattana. *Precipitation and Characterization of Petroleum Asphaltenes*. PhD thesis, University of Michigan, 2004.
- [6] A. Hammami and J. Ratulowski. Precipitation and deposition of asphaltenes in production systems: A flow assurance overview. In O. C. Mullins, A. Hammami E. Y. Sheu, and A. G. Marshall, editors, *Heavy Oils, and Petroleomics*, pages 617–660. Springer New York, 2007.
- [7] E. B. Sirota. Physical structure of asphaltenes. *Energy and Fuels*, 19(4):1290–1296, 2005.
- [8] Oliver C. Mullins. The modified yen model. *Energy & Fuels*, 24(4):2179–2207, 2010.
- [9] J.-N. Roux, D. Broseta, and B. Demé. Sans study of asphaltene aggregation: concentration and solvent quality effects. *Langmuir*, 17(16):5085–5092, 2001.
- [10] B. Zhao and J. M. Shaw. Composition and size distribution of coherent nanostructures in athabasca bitumen and maya crude oil. *Energy Fuels*, 21(5):2795–2804, 2007.
- [11] J. Eyssautier, P. Levitz, D. Espinat, J. Jestin, J. Gummel, I. Grillo, and L. Barré. Insight into asphaltene nanoaggregate structure inferred by small angle neutron and x-ray scattering. *J. Phys. Chem. B*, 115(21):6827–6837, 2011.

- [12] T. F. Headen, E. S. Boek, J. Stellbrink, and U. M. Scheven. Small angle neutron scattering (sans and v-sans) study of asphaltene aggregates in crude oil. *Langmuir*, 25(1):422–428, 2009.
- [13] F. Mostowfi, K. Indo, O. C. Mullins, and R. McFarlane. Asphaltene nanoaggregates studied by centrifugation. *Energy Fuels*, 23(3):1194–1200, 2009.
- [14] Tabish Maqbool, Sasanka Raha, Michael P. Hoepfner, and H. Scott Fogler. Modeling the aggregation of asphaltene nanoaggregates in crude oilprecipitant systems. *Energy Fuels*, 25, 2011.
- [15] Y. G. Burya, I. K. Yudin, V. A. Dechabo, V. I. Kosov, and M. A. Anisimov. Light-scattering study of petroleum asphaltene aggregation. *Appl. Opt.*, 40, 2001.
- [16] Kriangkrai Kraiwattanawong, H. Scott Fogler, Samir G. Gharfeh, Probjot Singh, William H. Thomason, and Sumaeth Chavadej. Thermodynamic solubility models to predict asphaltene instability in live crude oils. *Energy Fuels*, 21(3), 2007.
- [17] J. S. Buckley. Predicting the onset of asphaltene precipitation from refractive index measurements. *Energy Fuels*, 13, 1999.
- [18] J. Wang and J.S. Buckley. Asphaltene stability in crude oil and aromatic solvents—the influence of oil composition. *Energy Fuels*, 17, 2003.
- [19] P. Wattana, D. J. Wojciechowski, G. Bolaños, and H. S. Fogler. Study of asphaltene precipitation using refractive index measurement. *Petroleum Science and Technology*, 21, 2003.
- [20] C. W. Angle, Y. Long, H. Hamza, and L. Lue. Precipitation of asphaltenes from solvent-diluted heavy oil and thermodynamic properties of solvent-diluted heavy oil solutions. *Fuel*, 85(4), 2006.
- [21] Tabish Maqbool, Arjames T. Balgoa, and H. Scott Fogler. Revisiting asphaltene precipitation from crude oils: A case of neglected kinetic effects. *Energy Fuels*, 23:3681–3686, 2009.
- [22] A. Hirschberg, L. N. J. deJong, B. A. Schipper, and J. G. Meijer. Influence of temperature and pressure on asphaltene flocculation. *Society of Petroleum Engineers Journal*, 24(3), 1984.
- [23] R. Cimino, S. Correr, A. Del Bianco, and T. P. Lockhart. Solubility and phase behavior of asphaltenes in hydrocarbon media. In E. Y. Sheu and O. C. Mullins, editors, *Asphaltenes: Fundamentals and Applications*, pages pp 97–130. Plenum Press, 1995.
- [24] J. X. Wang and J. S. Buckley. A two-component solubility model of the onset of asphaltene flocculation in crude oils. *Energy Fuels*, 15(5):1004—1012, 2001.

- [25] S. Wang, J. Liu, L. Zhang, Z. Xu, and J. Masliyah. Colloidal interactions between asphaltene surfaces in toluene. *Energy Fuels*, 23, 2009.
- [26] Shengqun Wang, Jianjun Liu, Liyan Zhang, Jacob Masliyah, and Zhenghe Xu. Interaction forces between asphaltene surfaces in organic solvents. *Langmuir*, 26, 2010.
- [27] G. Porte, H. Zhou, and V. Lazzeri. Reversible description of asphaltene colloidal association and precipitation. *Langmuir*, 19, 2003.
- [28] Irwin A. Wiehe. *Process Chemistry of Petroleum Macromolecules*. CRC Press, 2008.
- [29] M. R. Gray, R. R. Tykwinski, J. M. Stryker, and X. Tan. Supramolecular assembly model for aggregation of petroleum asphaltenes. *Energy Fuels*, 25, 2011.
- [30] H. N. W. Lekkerkerker and R. Tuinier. *Colloids and the Depletion Interaction*. Springer, 2011.
- [31] James G. Speight. *The Chemistry and Technology of Petroleum*. CRC Press, fourth edition, 2006.
- [32] E. Rogel, G. Torres O. León, and J. Espidel. Aggregation of asphaltenes in organic solvents using surface tension measurements. *Fuel*, 79(11):1389–1394, 2000.
- [33] P. L. Krapivsky, S. Redner, and E. Ben-Naim. *A Kinetic View of Statistical Physics*. Cambridge University Press, 2010.
- [34] M. Elimelech, X. Jia, J. Gregory, and R. Williams. *Particle Deposition and Aggregation: Measurement, Modelling and Simulation*. Butterworth-Heinemann, 1998.
- [35] C. C. Enweremadu, H. L. Rutto, and J. T. Oladeji. Investigation of the relationship between some basic flow properties of shea butter biodiesel and their blends with diesel fuel. *International Journal of Physical Sciences*, 6, 2011.
- [36] A. F. M. Barton. *Barton, Handbook of Solubility Parameters and Other Cohesion Parameters*. CRC Press, 1991.
- [37] Jianxin Wang. *Predicting Asphaltene Flocculation in Crude Oils*. PhD thesis, New Mexico Institute of Mining and Technology, 2000.
- [38] J. M. Prausnitz, R. N. Lichtenthaler, and E. G. de Azevedo. *Molecular Thermodynamics of Fluid-Phase Equilibria*. Pearson Education, 1998.
- [39] T. Maqbool, P. Srikiratiwong, and H. S. Fogler. Effect of temperature on the precipitation kinetics of asphaltenes. *Energy Fuels*, 25, 2011.

CHAPTER III

The Effect of Asphaltene Concentration on the Aggregation and Precipitation Tendency of Asphaltenes¹

3.1 Introduction

Asphaltenes have strong tendency for self-association and the vast majority of researchers view them as colloidal nano-sized particles immersed in the crude oil [2–11]. The aggregation tendency of asphaltene molecules in a pure solvent has been shown to be a strong function of their concentration [12, 13]. At low concentrations (e.g., less than 50 mg/L) in a solvent such as toluene, asphaltenes are believed to exist either as molecularly dispersed entities or as oligomers of asphaltene molecules [13]. The aggregation propensity, increases with an increase in the asphaltene concentration. At concentrations close to the *critical nano-aggregate concentration* (CNAC \sim 50 mg/L), asphaltenes form structures with larger aggregation numbers called nano-aggregates [13–15]. It is also postulated that as asphaltene concentrations exceed the CNAC, further clustering of the existing nano-aggregates can also occur. Sud-

¹This chapter is partly based on the following manuscript: Nasim Haji-Akbari, Phitsanu Teeraphakul and H. Scott Fogler *EnergyFuels*(2014) [1].

den changes in the properties of the solution such as surface tension [16] or heat of dissociation [17, 18] resulting from a change in asphaltene concentration have been attributed to asphaltene clustering.

Upon destabilization mediated by changes in solution thermodynamics (e.g. precipitant addition), destabilized asphaltene nano-particles (i.e., nano-aggregates and clusters) have a strong tendency to further aggregate and form micron-size particles and eventually to phase separate. The aggregation rate of destabilized nano-particles is controlled by their collision frequency and the efficiency of those collisions, which is determined by the strength of the interactions between aggregating asphaltenes [19–21]. The strength of the interaction forces depends on the degree of attraction and repulsion experienced by the asphaltenes in the solution. Attractive forces have been attributed to several types of interactions such as van der Waals forces [22–24] (i.e., London dispersion, polar interactions and hydrogen bonding), acidic/basic interactions [25] and metal coordination complexes [25]. Repulsion forces, on the other hand, are generally believed to be of a steric origin [26, 27] caused by alky side chains surrounding the aromatic cores of asphaltene molecules [13]. In a strong solvent, the repulsive forces overcome the attractive forces and asphaltenes remain in solution as stable nano-particles. By adding a precipitant, the effectiveness of repulsion forces decreases due to the collapse of steric layers [26] and asphaltenes start aggregating and growing into micron-sized particles.

As discussed earlier, asphaltene particles can undergo structural changes when their concentration increases in a solvent [13]. Such structural transformations can alter the relative strength of attractive and repulsive forces, which can in turn affect their rate of aggregation after destabilization. For instance, Yudin et al. [28, 29] measured the aggregation rates for different concentrations of asphaltene dissolved in toluene and then destabilized by heptane. Dynamic light scattering (DLS) was used

to monitor the changes in size as a function of time at heptane concentrations close to the instantaneous onset point (i.e. the amount of precipitant needed for immediate detection of asphaltene instability). It was shown that for asphaltene concentrations less than 5 g/L (0.57 wt%) in toluene, the precipitation process proceeds through a diffusion-limited aggregation (DLA). At concentrations above 5 g/L however, asphaltene experience a reaction-limited aggregation (RLA). The authors attributed this change in the aggregation mechanism from DLA to RLA to the changes in the structure of asphaltene nano-particles from elementary nano-aggregates to associated nano-aggregates (clustering) [29]. Kyeongeok et al. [30] refer to the clustering concentration as the *critical aggregation concentration (CAC)* and measured the change in surface tension as a function of asphaltene concentration for asphaltene dispersed in different solvents. The asphaltene-solvent mixtures used in their experiments were also titrated with heptane to obtain the instantaneous onset concentration using near-infrared (NIR) spectroscopy. For both sets of experiments (surface tension and NIR), a break point in the measured property as a function of asphaltene concentration was observed and was defined as CAC [30].

The aforementioned studies highlight the importance of asphaltene concentration on the structure of the aggregates and therefore their aggregation tendencies. However, the majority of the studies dedicated to this subject used only pure solvents or used precipitant concentrations around the instantaneous onset point. At such high precipitant concentrations, asphaltene experience strong attractive forces and grow to micron sizes and phase separate immediately after destabilization. However, weak attractions between aggregating particles can result in slow aggregation process [19, 21]. The aggregation behavior of asphaltene at low precipitant concentrations could have different characteristics compared to that at higher precipitant concentrations.

In the previous chapter, it was demonstrated that crude oil plays an important role in controlling the kinetics of precipitation at low precipitant concentrations [21]. Aggregation kinetics also depend on the rate of collision between asphaltene particles [20, 21] and therefore the asphaltene concentration is also expected to have an influence on the kinetics of precipitation. As a result further studies are necessary to investigate the effect of asphaltene concentration on their aggregation rate for conditions where the precipitation kinetics are significant. In addition, all previous studies [28–31] cover a very limited range of low asphaltene concentrations (less than 1.5 wt% asphaltenes in solvent) and as such do not accurately represent the asphaltene content of conventional or heavy crude oils. The few studies that have investigated the effect of higher asphaltene concentrations in pure toluene, found that the diffusivities of asphaltenes are no longer constant but instead a strong function of asphaltene concentration [32–35]. This effect on diffusion could influence asphaltenes' aggregation rates after destabilization. In this chapter, we focus on investigating the effect of asphaltene concentration for a wide range of asphaltene and precipitant concentrations and also for three different types of asphaltenes. Due to the compositional complexity of crude oils, model mixtures were used to vary asphaltene content. A counterintuitive reduction in aggregation rate is observed for an increase in asphaltene concentration. Hypotheses to explain this reduction are then utilized to predict the aggregation rate of asphaltenes as a function of their concentration using Smoluchowski's aggregation model.

3.2 Experimental Section

3.2.1 Materials

Asphaltenes were extracted from three different crude oils (K1, B1 and A1) to be used for model mixture preparation. High performance liquid chromatography (HPLC)-grade toluene and heptane from Fisher were used as the solvent and the precipitant respectively. All crude oils were mixed with heptane in 1:25 volume ratio and were kept well mixed for 24 hours. The solutions were then centrifuged with a Sorvall Legend X1R at 3500 rpm for 1 hour to separate precipitated asphaltenes. The asphaltenes were Soxhlet-washed with heptane for 24 hours to wash any non-asphaltenic material trapped in the cake. The asphaltenes were then dried in the oven at 75°C (K1 asphaltenes were dried in a vacuum oven and A1 and B1 asphaltenes were dried in presence of air). Table 3.1 shows the elemental analysis for these asphaltenes.

Table 3.1: Elemental analysis of A1, B1 and K1 asphaltenes.

Sample Name	wt%					H/C	ppm	
	C	H	N	O	S		Ni	V
A1	81.5	7.79	1.05	2.21	7.2	1.15	152	479
B1	77.32	7.54	0.93	2.41	8.99	1.17	197	574
K1	84.25	6.36	1.29	1.91	4.5	0.91	185	571

To prepare model mixtures, different concentrations of dried asphaltenes were dissolved in toluene and sonicated (See Appendix D for the effect of sonication) until the proper dissolution was achieved. In each case, optical microscopy was used to confirm that the dissolution is complete and any insoluble particles were centrifuged before conducting the experiments. The weight percent (wt%) of asphaltenes reported in this chapter refer to their concentration in toluene before heptane addition.

3.2.2 Methods

Microscopy experiments: A known volume of model oil (asphaltene in toluene) was placed in a 4mL vial. The asphaltene-toluene solutions were then destabilized by adding heptane at concentrations below the instantaneous onset point. Heptane was added slowly to the mixture using a syringe pump at 20 mL/h flow rate. All solutions were kept well mixed using magnetic stirrers during precipitant addition to minimize localized regions of high precipitant concentrations. All samples were prepared on a mass basis and final volume fractions of heptane were calculated using the corresponding densities. After sample preparation, a droplet of well-stirred sample was placed under the microscope at different times to detect asphaltene particles. An optical microscope from Nikon (model: Eclipse E600) with 40x objective lens and 10x eyepiece was used for detecting asphaltene particles and a CCD camera from Sony (AVC-D7) and a Nikon camera (DS-Fi2) were used for shooting images off the microscope. The smallest particles detectable under the microscope are approximately $0.5 \mu\text{m}$ in diameter. The earliest time at which the particles were observed under the microscope is defined as the *detection time*. Sampling frequency varied depending on the expected detection time and was done less frequently for samples with longer detection times to minimize evaporation. The values reported for the detection time are the average of two limits: lower limit with no precipitation and upper bond with unequivocal precipitation. Error bars correspond to the standard deviations of these two averages.

Centrifugation experiments: To quantify the amount of precipitated asphaltenes, 10 mL of the asphaltene-toluene-heptane mixtures were prepared at desired asphaltene and heptane concentrations (See sample preparation for microscopy experiments). Centrifugation experiments were performed at heptane concentrations close

to or above the instantaneous onset point. Two samples of 1.5 mL were withdrawn from each sample after one month and were centrifuged using an Eppendorf 5418 centrifuge at 14000 rpm for ten minutes. To ensure that these samples have reached the thermodynamic equilibrium, the samples were also centrifuged two months after destabilization with heptane. The asphaltene cake was separated from supernatant after centrifugation, dried in the oven at 75°C and weighed. In addition, the asphaltene content of the supernatant was also measured by evaporating toluene and heptane in the oven. To have a more accurate estimate of the mass precipitated, values reported in this work are the averages of values obtained from the mass balance between the mass of collected cake and the mass of the asphaltenes that remains in the supernatant.

3.3 Results

3.3.1 Microscopy Experiments

Microscopy results presented below identify two distinct regions for the effect of asphaltene concentration on their aggregation rate: 1) concentrations below 1wt% and 2) concentrations above 1 wt%.

Figure 3.1 shows detection time measurements for K1 asphaltenes in toluene at concentrations equal to or below 1wt% (0.1, 0.5 and 1 wt%), after being destabilized with heptane. It is experimentally difficult to obtain accurate estimates of detection times for 0.1 wt% samples because those samples have low asphaltene content, resulting in relatively large error bars. Figure 3.1 demonstrates that for identical heptane concentrations, the aggregation rate of asphaltenes increases with increasing asphaltene concentration (aggregation rate 1 wt% > 0.5 wt% > 0.1 wt%).

The aggregation rate of asphaltenes is controlled by the frequency of the colli-

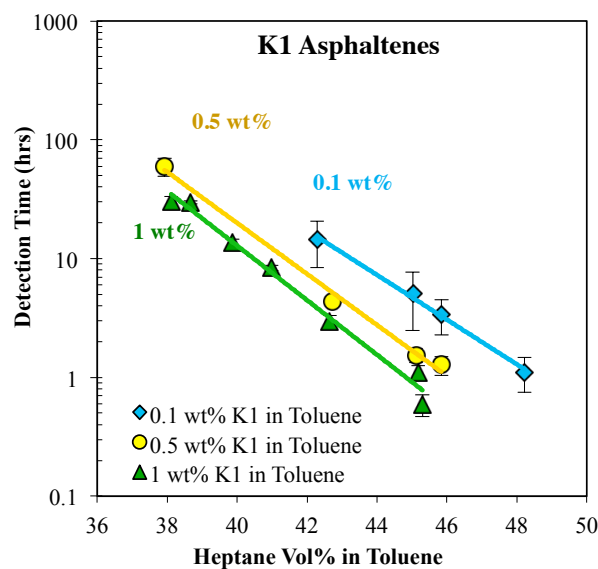


Figure 3.1: **Detection time as a function of heptane concentration for solutions with three different concentrations of K1 asphaltenes in toluene (0.11 wt%, 0.52 wt% and 1 wt%).**

sions between sub-micron sized particles and their coagulation efficiency (i.e. collision efficiency). The frequency of collisions depends on the diffusivity and the number density of the aggregating asphaltenes. Therefore, the number of collisions is expected to increase as a result of increased asphaltene concentration. The coagulation efficiency however is controlled by the type and strength of interparticle forces between aggregating asphaltenes and can be assumed to be independent of asphaltene concentration at identical heptane/toluene ratios. As a result, the aggregation rate of asphaltenes is expected to increase when their concentration increases. For asphaltene concentrations below 1 wt%, the expected increase in the aggregation rate of asphaltenes at identical heptane concentrations is confirmed experimentally (Figure 3.1). Kyeongseok et al. [30] also observed a reduction in the instantaneous onset point as a result of increase in asphaltene concentration up to 1.6 wt% asphaltenes in

toluene, which was the highest asphaltene concentration investigated in their work. Their results are in agreement with our microscopy results for asphaltene concentrations below 1 wt%.

Figure 3.2 shows detection time measurements for K1 asphaltenes in toluene at concentrations above 1 wt%. The time required for detecting asphaltene instability increases as their concentration increases. In other words, the aggregation rates are slower at higher asphaltene concentrations (aggregation rate 1wt% >3wt% >5wt% >8wt%). This trend is contrary to the expected increase in aggregation rates with increasing asphaltene concentrations discussed in the previous paragraph. An explanation for this behavior can be the contribution of stable asphaltenes to the solution properties and will be discussed in further detail later. In addition, a clear change in slopes and offsets of the detection lines is observed. These findings demonstrate that solutions with higher asphaltene contents are more sensitive to changes in heptane concentration (i.e. higher slope). Moreover, the differences between aggregation rates become less noticeable as precipitant concentration approaches the instantaneous onset point.

Similar trends are also observed for B1 and A1 asphaltenes dispersed in toluene at asphaltene concentrations above 1 wt% as shown in Figures 3.3 and 3.4. For A1 asphaltenes, the differences between 3 wt% and 8 wt% are much smaller when compared to B1 and K1 asphaltenes. It was generally more difficult to obtain the detection time in the 8 wt% samples compared to the samples with lower asphaltene concentrations. Indeed, the transition from a clear microscopic background to distinguishable precipitated particles occurs in short time spans at low concentrations. However, for the 8 wt% samples the transition occurs more slowly which makes defining detection time somewhat more difficult. This behavior was particularly problematic for asphaltenes extracted from A1 crude oil.

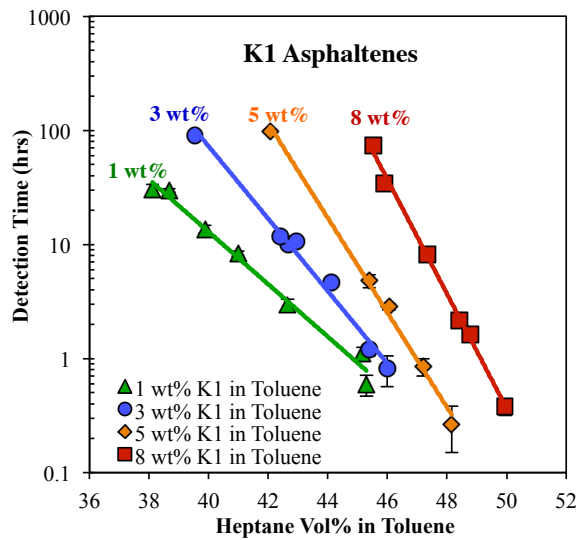


Figure 3.2: Detection time as a function of heptane concentration for solutions with four different concentrations of K1 asphaltenes in toluene (1, 3, 5 and 8.2 wt%).

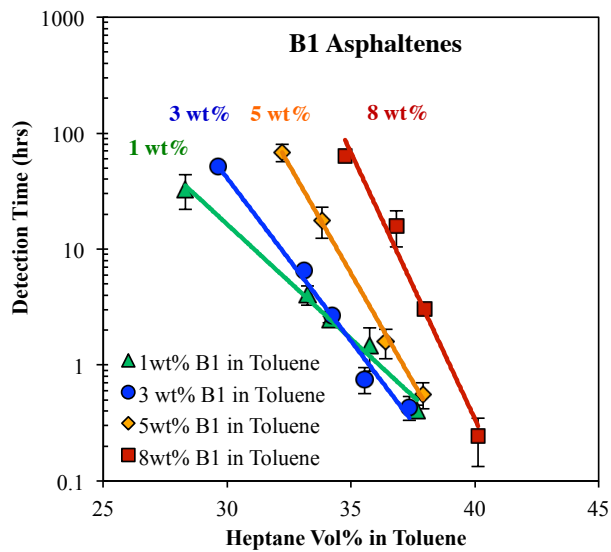


Figure 3.3: Detection time as a function of heptane concentration for solutions with four different concentrations of B1 asphaltenes in toluene (1, 3, 5 and 8 wt%).

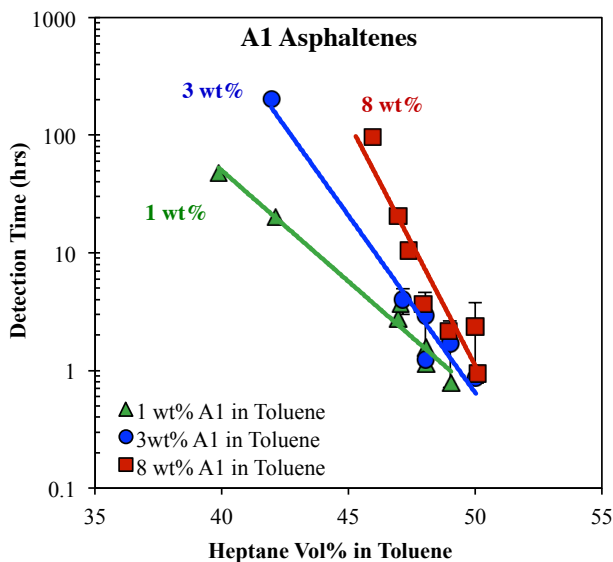


Figure 3.4: **Detection time as a function of heptane concentration for solutions with three different concentrations of A1 asphaltenes in toluene (1, 3 and 8 wt%).**

3.3.2 Centrifugation Experiments

The mass of asphaltenes precipitated per mass of toluene was quantified using centrifugation experiments for samples of 3 wt% and 8 wt% B1 and A1 asphaltenes dispersed in toluene and then destabilized by heptane at different heptane concentrations. The mass precipitated was measured one and two months after destabilization. Figure 3.5 shows the amount precipitated two months after destabilization for B1 and A1 asphaltenes. No difference was observed for the mass precipitated between the first and the second month for A1 asphaltenes within the experimental uncertainty suggesting that the samples had reached thermodynamic equilibrium by the end of the first month. For B1 asphaltenes however, there was a slight increase in the mass precipitated after two months due to aggregation kinetics.

As expected, the amount precipitated increases with increasing heptane concen-

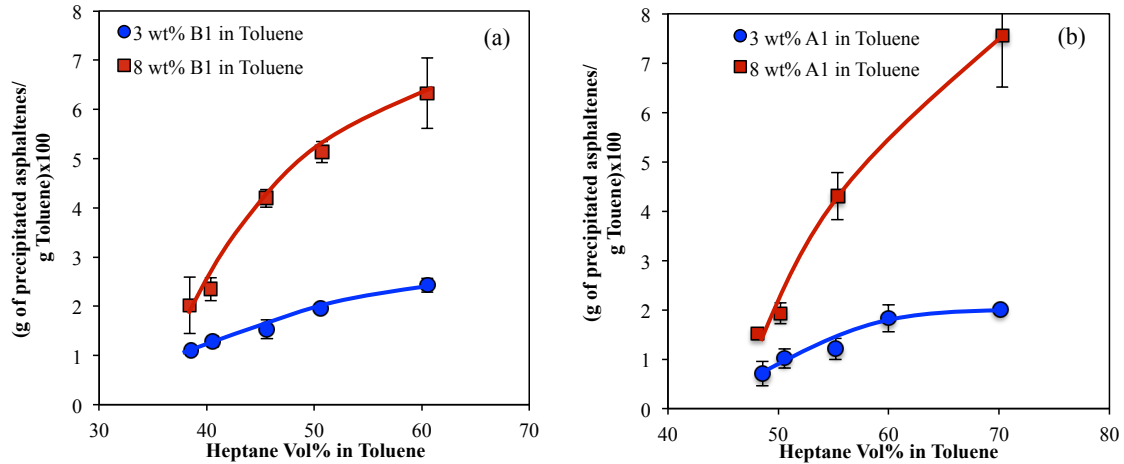


Figure 3.5: Amount of asphaltene precipitated per mass of toluene for 3 and 8 wt% asphaltene as a function of heptane concentration, two months after heptane addition: (a) B1 asphaltene and (b) A1 asphaltene (actual asphaltene concentrations for 3 and 8 wt% of A1 samples were 2.7 and 7.9 wt% respectively).

tration for all the samples. In addition, at identical heptane concentrations, more asphaltene precipitate in 8 wt% samples than in 3 wt% samples. Larger quantities of unstable particles are typically associated with faster aggregation rates and are consequently expected to decrease the time needed for detecting any instability. However this expected decrease is not the case for asphaltene concentrations greater than 1 wt%.

3.4 Discussion

The apparent inconsistency between the precipitation rates measured from microscopy experiments and the total amount of asphaltene participating in the aggregation process for concentrations above 1 wt%, indicates that a competing effect is in play. This effect can arise from a change in the thermodynamic driving force (despite

identical heptane/toluene ratios) or from kinetic limitations (e.g., due to reduction in diffusivities or an increase in viscosities). At asphaltene concentrations below 1 wt%, this competing effect is either nonexistent or is insignificant.

We believe that the competing effect acting against the increase in number of unstable asphaltenes, is related to the stabilizing role of stable asphaltenes. For moderate heptane concentrations (e.g. 40 vol% heptane in toluene), not all asphaltenes precipitate and a fraction of them remain as nano-sized particles in the solution (i.e. stable/soluble asphaltenes). Because asphaltenes are aromatic compounds, they are structurally more similar to aromatic solvents such as toluene than aliphatic precipitants such as *n*-heptane. Stable asphaltenes can therefore be considered to act as a solvent that increases the overall solvency power of the solution for unstable ones. Spiecker et al. [38] have investigated the role of more stable asphaltenes on the behavior of unstable asphaltenes and have shown that the abundance of the soluble fraction of asphaltenes increases the stability of the insoluble fraction. Their results are in agreement with our hypothesis for the increase in the solvency power of the solution and the self-stabilizing effect of asphaltenes. However, the actual mechanism through which insoluble asphaltenes are stabilized by soluble ones is unknown at this time.

The amounts of soluble and insoluble asphaltenes depend on the composition of the solution (e.g. heptane/toluene ratio). As the heptane concentration increases, the fraction of asphaltenes characterized as soluble decreases and at high heptane concentrations eventually all the asphaltenes become insoluble and precipitate. Therefore, the effect of stable asphaltenes on modifying the solvency power of the solution is expected to diminish with increasing heptane concentration. As seen in Figures 3.2-3.4, at high precipitant concentrations (close to instantaneous onset point), the differences in detection times are small and for some samples are not distinguishable between

the 1wt% and the 3 wt%. However, as the precipitant concentration decreases, the differences between the detection times increase and detection lines from microscopy experiments diverge.

A change in the solution's solvency power in the presence of stable asphaltenes could be attributed to the change in the solubility parameter of the solution. The solubility parameter is a measure of the extent of the interactions between asphaltenes and accounts for the intermolecular forces. Large differences between the solubility parameters of asphaltenes and the solution provides the driving force required for the aggregation and the phase separation. It has been previously shown that the phase behavior of asphaltenes strongly depends on the solubility parameter of the solution surrounding them [39]. In addition it has been shown in Chapter II that the aggregation tendencies and the effectiveness of collisions between aggregating asphaltenes is controlled by the differences between the solubility parameters of the asphaltenes and the solution [21]. Increasing the total asphaltene concentration increases the quantity of both the stable and the unstable asphaltenes. Therefore, for the identical heptane/toluene ratios, the solubility parameter of the solution for samples with higher asphaltene concentrations is expected to be larger than samples with lower asphaltene contents. Thus, the effectiveness of collisions between aggregating asphaltenes is expected to decrease as their concentration increases.

In summary on this point, upon an increase in asphaltene content of the solution, the collision frequency and coagulation efficiency change in two opposite directions. The existence of these two competing effects complicates the efforts to obtain a thorough understanding of how a change in asphaltene concentration affects the kinetics of the aggregation process. Our results suggest that for asphaltene concentrations above 1 wt%, the quantity of stable asphaltenes is large enough to significantly alter the solvency power and the solubility parameter of the solution and therefore offset

the competing increase in the collision frequency. However, for asphaltene concentrations below 1 wt% (i.e., 0.1 and 0.5 wt% K1 asphaltenes) any change in the solubility parameter is at best negligible due to small quantity of soluble asphaltenes. Therefore, the increase in the number of aggregating particles overcomes the reduction in the coagulation efficiency and the aggregation rate increases upon an increase in asphaltene concentration.

Clustering concentrations (i.e. CAC values) reported for asphaltenes-toluene mixtures in the literature are in the range of 3–22.9 g/L (0.34–2.6 wt%) [16, 17, 30] and 1 wt% in our experiments falls within this range. However, we believe that the concept of critical aggregation concentration (CAC) does not explain our experimental observations. Because referring to CAC as *critical concentration* implies that the structure of asphaltenes would not change upon further increase in their concentration. In such circumstances (i.e. beyond CAC), the degree of interactions between asphaltenes at identical heptane concentrations is expected to be identical regardless of asphaltene concentration. Therefore, the aggregation rate is expected to increase by increasing asphaltene concentration due to an increase in number density. However, our experimental trends above 1 wt% are opposite to this expected trend and suggest that coagulation efficiency (and possibly structure of asphaltenes) gradually varies from 1 wt% to 8 wt%. In addition, experimentally CAC is defined as a break point in the measured property (e.g., surface tension [16, 30], heat of dissociation [17] or instantaneous onset point [30]) as a function of asphaltene concentration. The experimental trend for the measured property is preserved above and below CAC and the only change is a change in the slopes (i.e. break point at CAC) [17, 30]. However, in our investigation, opposite trends are observed below and above 1 wt% and it is therefore difficult to directly link/compare it to the CAC values reported in the literature.

Previous studies [28, 30, 31, 40] of the effect of asphaltene concentration on their

aggregation and precipitation tendency have focused on asphaltene concentrations around or below 1 wt% and precipitant concentrations at or above instantaneous onset point. At such low asphaltene concentrations and high precipitant concentrations, the effect of soluble asphaltenes in modifying the solution composition is negligible, and the competing effects discussed earlier act in favor of faster aggregation rate. Therefore, solely focusing on high precipitant concentrations (at or above instantaneous onset) or low asphaltene concentrations (~ 1 wt%) is not appropriate to draw general conclusions about the aggregation behavior of asphaltenes as a function of their concentration. For example, Yudin et al. [28, 29] investigated the effect of asphaltene concentration in concentrations ranging from 1–10 g/L (0.11–1.14 wt% in toluene). They reported a change in the aggregation mechanism from DLA to RLA at 5 g/L (0.57 wt% in toluene). Most of our experiments (except 0.1 and 0.5 wt%) are above 5 g/L. However, Yudin et al. [28, 29] have only studied asphaltene concentrations up to 10 g/L (1.14 wt%) and did not detect any changes in coagulation efficiencies in the RLA regime. We have shown that the coagulation efficiency decreases by increasing asphaltene concentration and it will be shown that this change can be explained by accounting for the change in the solubility parameter of the solution. In the next section, the aggregation model developed in our earlier study [21] is adapted to the current findings and is used to accurately predict the aggregation rate of asphaltenes in solutions with different asphaltene concentrations.

In addition to the change in the solvency power of the solution, the diffusion coefficient of unstable asphaltenes and therefore their collision frequency also depends on the total concentration of asphaltenes. It has been shown that the average motion of each particle in the concentrated samples depends on the direct interactions between particles and their concentration. For example DOSY-NMR experiments performed over a wide range of asphaltene concentrations showed that the self-diffusivity of

asphaltenes in a solvent (e.g. toluene) decreased with increasing asphaltene concentration [32–35]. The reduction in the diffusion coefficient is believed to be negligible for our samples due to relatively low initial asphaltene concentrations in toluene and also further dilution of the samples with heptane.

3.4.1 Asphaltene Aggregation Modeling

A unified aggregation model was developed in Chapter II using Smoluchowski’s aggregation equation. In this model the experimentally measured detection time is related to the solution properties with the following relationship [21]:

$$\ln \left(\frac{t_{detection} \sqrt{C_1(0)}}{\mu} \right) \propto \frac{1}{(\delta_{asph} - \delta_{solution})^2} \quad (3.1)$$

where δ_{asph} and $\delta_{solution}$ are the solubility parameters ($\text{Pa}^{0.5}$) of the asphaltenes and the solution respectively and μ is the local viscosity ($\text{Pa} \cdot \text{s}$) experienced by asphaltene particles. $C_1(0)$ ($\#$ particles/ m^3) represents the number concentration of aggregating asphaltenes (i.e. unstable asphaltenes). By increasing the heptane concentration, the number of the unstable asphaltenes increases. However due to dilution effect resulting from heptane addition, the change in number concentration of the unstable asphaltenes (i.e. $C_1(0)$) could be insignificant. Therefore, in Chapter II, $C_1(0)$ was assumed to be a constant and independent of heptane concentration and was calculated using the total asphaltene content of each crude oil after accounting for average dilution with heptane. However in this chapter, $C_1(0)$ is calculated using experimental centrifugation results for B1 and A1 asphaltenes. The amount of asphaltenes precipitated per total mass of asphaltenes can be easily calculated from the centrifugation results shown in Figure 3.5. These calculated values are shown in Fig-

ure 3.6. The fraction precipitated appears to be independent of asphaltene content and linearly depends on the heptane concentration. Consequently, Figure 3.6 can be used to calculate the fraction precipitated at different asphaltene and precipitant concentrations. The heptane concentrations used for the centrifugation experiments were all close to or greater than the instantaneous onset point. Smaller heptane concentrations were not investigated due to the long times required for equilibration (in the order of months) and also because of the small mass of precipitated asphaltenes that would have increased experimental uncertainty. To obtain the fraction precipitated at smaller heptane concentrations, the results from larger concentrations can be extrapolated. Two extremes for extrapolation exist, E1 and E2: E1) represents the lower limit and is the extrapolation of the linear correlation from high heptane concentrations to the point where asphaltenes would be completely soluble and E2) represents the extrapolation of the last experimental data point to pure toluene (i.e. 0 vol% heptane). Extrapolations E1 and E2 likely represent the lower and upper limits for the fraction precipitated, and the actual values are expected to fall between these two extremes.

The plot of $\ln(t_{detection} \sqrt{C_1(0)}/\mu)$ vs. $1/(\delta_{asph} - \delta_{solution})^2$ has previously shown to follow a linear master curve for ten different crude oils and model oils [21]. In order to apply and compare the aggregation model for the samples with different asphaltene concentrations, $C_1(0)$ and δ_{asph} need to be determined. By obtaining the fraction of B1 and A1 asphaltenes precipitated at different heptane concentrations (Figure 3.6), $C_1(0)$ can be calculated for each experimental run (See Equation A.22). The solubility parameter of asphaltenes can be easily obtained by fitting the experimental measurements of detection time to the master curve [21]. The solubility parameter of each asphaltene type in this study was calculated using detection time measurements of the samples with lowest asphaltene concentrations (i.e. 1 wt% asphaltenes in toluene

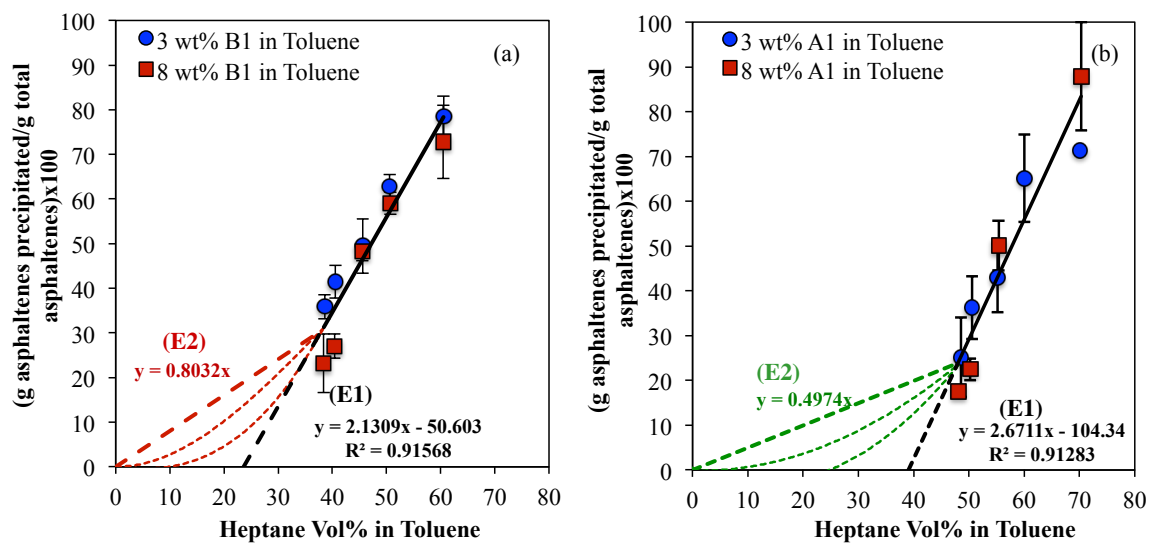


Figure 3.6: **Fraction of asphaltenes precipitated two months after destabilization as a function of heptane concentration, 3 and 8 wt% asphaltenes in toluene:** (a) B1 asphaltenes and (b) A1 asphaltenes (actual asphaltene concentrations for 3 and 8 wt% of A1 samples were 2.7 and 7.9 wt% respectively).

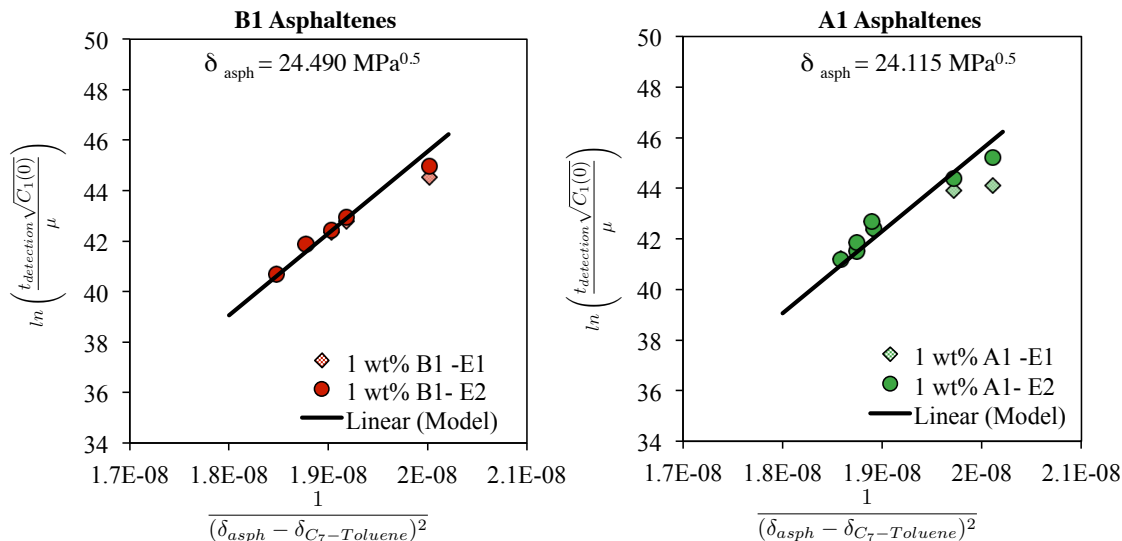


Figure 3.7: Plot of $\ln(t_{detection} \sqrt{C_1(0)}/\mu)$ vs. $1/(\delta_{asph} - \delta_{solution})^2$ for 1 wt% of B1 and A1 asphaltenes in toluene using extrapolations E1 and E2 with respect to master curve.

for B1 and A1). The effect of soluble asphaltene in modifying the solution’s solubility parameter is expected to be negligible for 1 wt% samples and therefore $\delta_{solution}$ could be calculated from the volumetric average of the solubility parameters of toluene and heptane. As discussed earlier, at high asphaltene concentrations due to increase in amount of soluble asphaltene, $\delta_{solution}$ could be higher than $\delta_{C_7-Toluene}$.

As shown in Figure 3.7 the values of 24.490 and 24.115 $\text{MPa}^{0.5}$ are reasonable estimates for the solubility parameters of B1 and A1 asphaltene respectively. The E1 extrapolation underestimates the fraction precipitated at low precipitant concentrations (corresponding to large $1/(\delta_{asph} - \delta_{solution})^2$ values), and the predictions based on E2 provide a slightly better match with master curve. However, the analyses reveal that the predictions of the model are only slightly sensitive to the extrapolation method used for estimating the fraction precipitated. The solubility parameter values

obtained from Figure 3.7 were used to predict the aggregation rate of asphaltenes at other asphaltene and precipitant concentrations.

Figures 3.8(a) and 3.9(a) show experimentally measured $\ln(t_{\text{detection}}\sqrt{C_1(0)}/\mu)$ vs. $1/(\delta_{\text{asph}} - \delta_{\text{solution}})^2$ for different concentrations of B1 and A1 asphaltenes using extrapolations E1 and E2, where δ_{solution} is the volumetric average of the solubility parameters of toluene and heptane ($\delta_{C_7\text{-Toluene}}$). It is clear that **without** accounting for the effect of soluble asphaltenes in the solution's solubility parameter, the aggregation rates for high asphaltene concentrations significantly deviate from the master curve. However after taking the effect of soluble asphaltenes into account (i.e. $\delta_{C_7\text{-Toluene-asph}}$), the trend follows the master curve as shown in Figures 3.8(b) and 3.9(b). The solubility parameter of the solution in Figures 3.8(b) and 3.9(b) was calculated using the volumetric average of the solubility parameters of heptane, toluene and soluble asphaltenes.

$$\delta_{C_7\text{-Toluene-asph}} = \phi_{C_7}\delta_{C_7} + \phi_{\text{Toluene}}\delta_{\text{Toluene}} + \phi_{\text{solubleasphaltenes}}\delta_{\text{asphaltenes}} \quad (3.2)$$

The solubility parameters of soluble and insoluble asphaltenes are assumed to be equal and are obtained from Figure 3.7 as discussed earlier.

It should now be clear that the aggregation rate of asphaltenes strongly depends on the asphaltene content of the solution. The proposed aggregation model accounts for both the changes in the collision frequency and the changes in the coagulation efficiency as a result of an increase in asphaltene concentration. The model provides reasonable predictions for the aggregation rate of B1 and A1 asphaltenes at different asphaltene concentrations. Figures 3.8(b) and 3.9(b) demonstrate that the competing effects of the increase in the number of aggregating asphaltenes and the

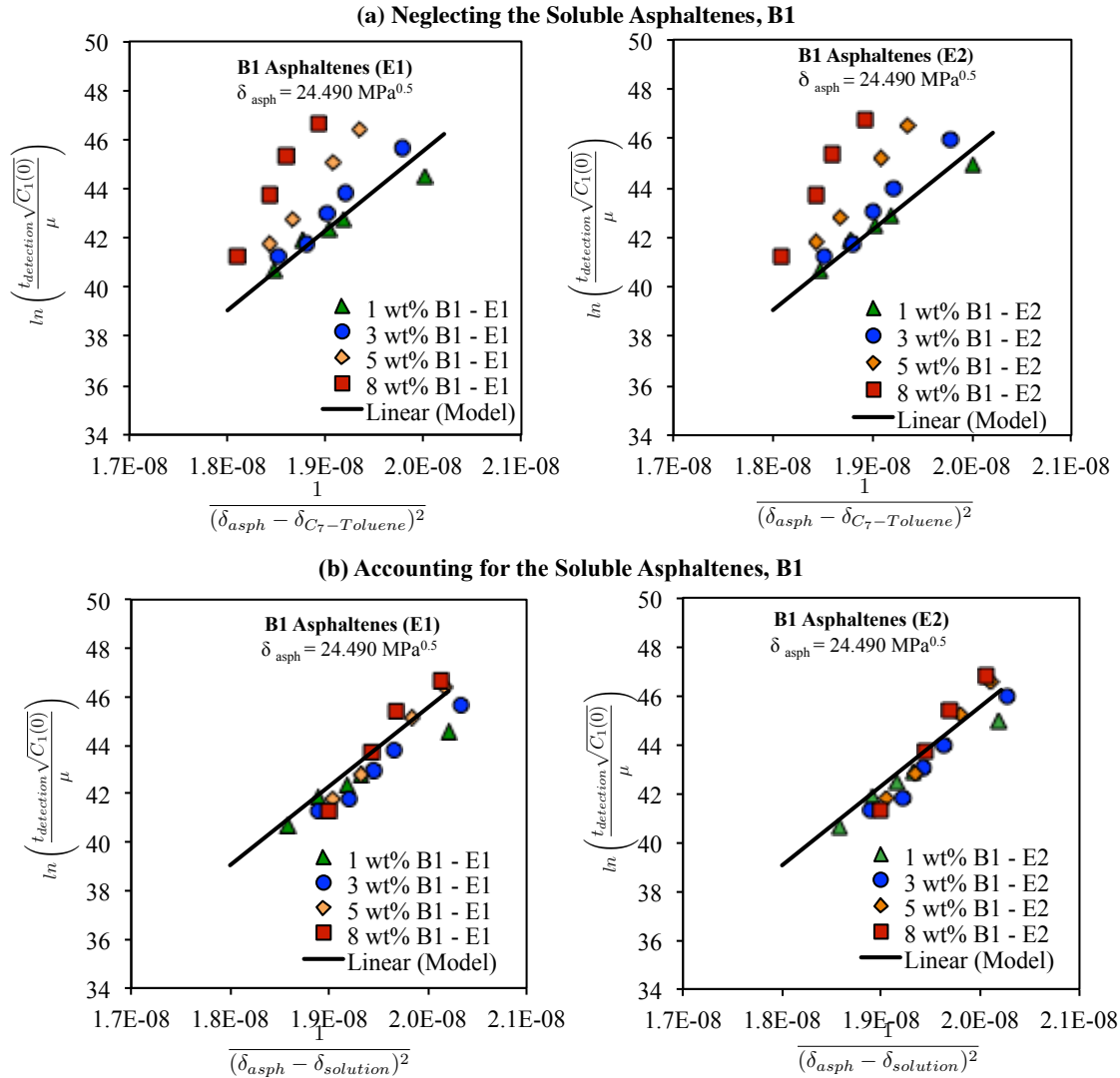


Figure 3.8: Plot of $\ln(t_{\text{detection}}\sqrt{C_1(0)}/\mu)$ vs. $1/(\delta_{\text{asph}} - \delta_{\text{solution}})^2$ for 1, 3, 5 and 8 wt% B1 asphaltenes in toluene with respect to master curve using extrapolations E1 and E2: (a) Before accounting for the contribution of soluble asphaltenes and (b) After accounting for the contribution of soluble asphaltenes.

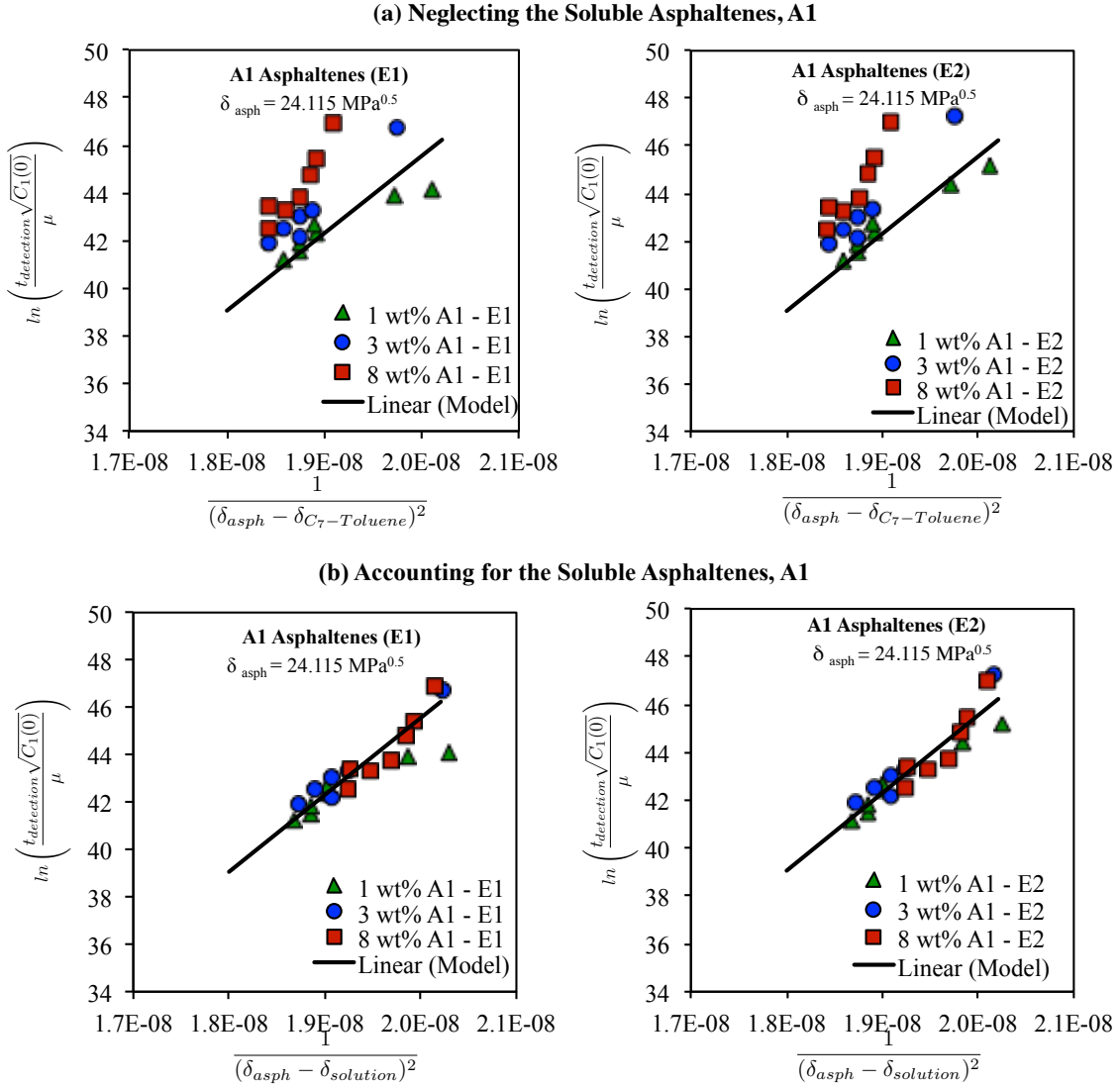


Figure 3.9: Plot of $\ln(t_{\text{detection}} \sqrt{C_1(0)}/\mu)$ vs. $1/(\delta_{\text{asph}} - \delta_{\text{solution}})^2$ for 1, 3 and 8 wt% A1 asphaltene in toluene with respect to master curve using extrapolations E1 and E2: (a) Before accounting for the contribution of soluble asphaltene and (b) After accounting for the contribution of soluble asphaltene.

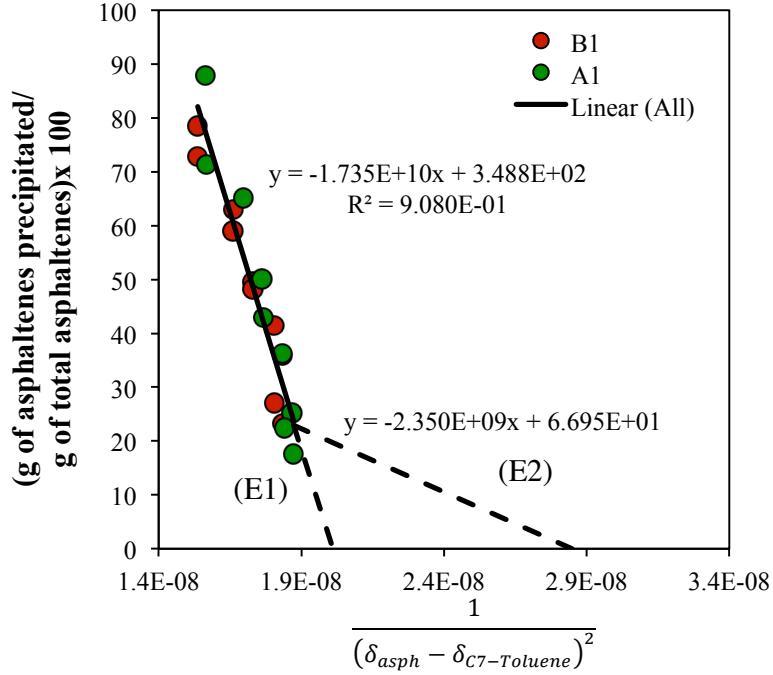


Figure 3.10: **Fraction of B1 and A1 asphaltenes precipitated as a function of $1/(\delta_{asph} - \delta_{solution})^2$.**

change in the solvency power can be successfully predicted with this model. It is also clear from these analyses that the change in $\delta_{solution}$ has a much greater impact on the aggregation rate than the change in $C_1(0)$. This behavior is not surprising because asphaltenes aggregate through a reaction-limited aggregation process for the range of asphaltene concentrations investigated for B1 and A1 samples [40]. For a reaction-limited process, any change in coagulation efficiency is expected to have a greater impact on the aggregation rate than a change in collision frequency. Therefore, slight changes in the solubility parameter of solution could significantly influence the aggregation rates and offset the effect of the change in the number concentration.

For K1 samples, the analyses were not as straight forward as those for B1 and A1 samples owing to the lack of centrifugation data needed for estimating $C_1(0)$.

Figure 3.10 shows the plot of the fraction of B1 and A1 asphaltenes precipitated as a function of $1/(\delta_{asph} - \delta_{C_7-Toluene})^2$. The fraction precipitated shown in Figure 3.10 follows a single linear curve. Therefore, it can be used for estimating the fraction precipitated for K1 samples. In order to use Figure 3.10, solubility parameter of K1 asphaltenes should be known. However, to obtain the solubility parameter of asphaltenes from master curve, the fraction of precipitated asphaltenes needs to be known. A trial and error approach was therefore applied with an initial guess for solubility parameter of K1 asphaltenes. The initial guess was first used to calculate the fraction precipitated from Figure 3.10. Two extremes for extrapolation of the fraction precipitated are available in Figure 3.10. E1 is the extrapolation of fraction precipitated from B1 and A1 samples to lower precipitant concentrations (i.e. high $1/(\delta_{asph} - \delta_{C_7-Toluene})^2$ values) and more likely represents the lower limit. The upper limit was generated by connecting the last data point to the value of $1/(\delta_{asph} - \delta_{C_7-Toluene})^2$ corresponding to pure toluene (no precipitant) with fraction precipitated being equal to zero (E2). The fraction precipitated from both extrapolations was then used to obtain a new guess for solubility parameter of asphaltenes using detection time measurements for 0.5 and 1 wt% K1 asphaltenes in toluene. The modifying effect of soluble asphaltenes for 0.1, 0.5 and 1 wt% samples is expected to be minimal. However, due to large experimental uncertainty for 0.1 wt% asphaltenes, only the results for 0.5 and 1 wt% were utilized. The new solubility parameter was then used to correct the fraction precipitated from Figure 3.10. This procedure was repeated until the solubility parameter converged to a single value. The solubility parameter value of 24.225 MPa^{0.5} provided reasonable matches with master curve for 0.5 and 1 wt% microscopy results.

Figure 3.11 shows the model predictions for the aggregation rate of K1 asphaltenes at different concentrations before and after taking the effect of soluble asphaltenes

into account. Similar to B1 and A1 asphaltenes, the large deviations observed in Figure 3.11(a) disappear in Figure 3.11(b).

For K1 samples, a few experimental measurements deviate from the master curve (Figure 3.11(b)). This deviation could be due to inaccuracies in the estimates of the fraction of K1 asphaltenes precipitated obtained from Figure 3.10. Any inaccuracy in estimating the fraction of precipitated asphaltenes can influence the values of $C_1(0)$ and $\delta_{solution}$ used in our aggregation model. Another source of inaccuracy could be due to the assumption that the fraction of asphaltenes precipitated at identical heptane/toluene ratio is independent of asphaltene content. Nevertheless, as can be seen from Figure 3.6, at low precipitant concentrations (i.e., 38 and 40 vol% heptane in toluene) for B1 asphaltenes, the fraction precipitated for the 8 wt% samples is smaller than the fraction precipitated for the 3 wt% samples. For A1 asphaltenes precipitated at 50 vol% heptane in toluene (Figure 3.6), the fraction precipitated for the 8 wt% is also smaller than the 3 wt%. Therefore, the centrifugation results presented in this chapter suggest that despite the fact that the samples have identical heptane concentration, the fraction of asphaltenes precipitated for solutions with different asphaltene concentrations (wt%) might not be identical. However, due to large experimental uncertainties, this conclusion cannot be generalized. A possible explanation for this behavior is the weaker thermodynamic driving force (i.e. larger value of $\delta_{solution}$) in the 8 wt% samples compared to the 3 wt% samples.

In addition to possible errors in estimating the fraction of soluble and insoluble asphaltenes, neglecting the reduction in diffusion coefficient due to increase in asphaltene concentration can be another source of error. Larger reductions in diffusivity are expected in solutions with higher asphaltene contents because of an increased number density. However, as discussed earlier, we believe that the reduction in diffusion coefficient is insignificant for our samples.

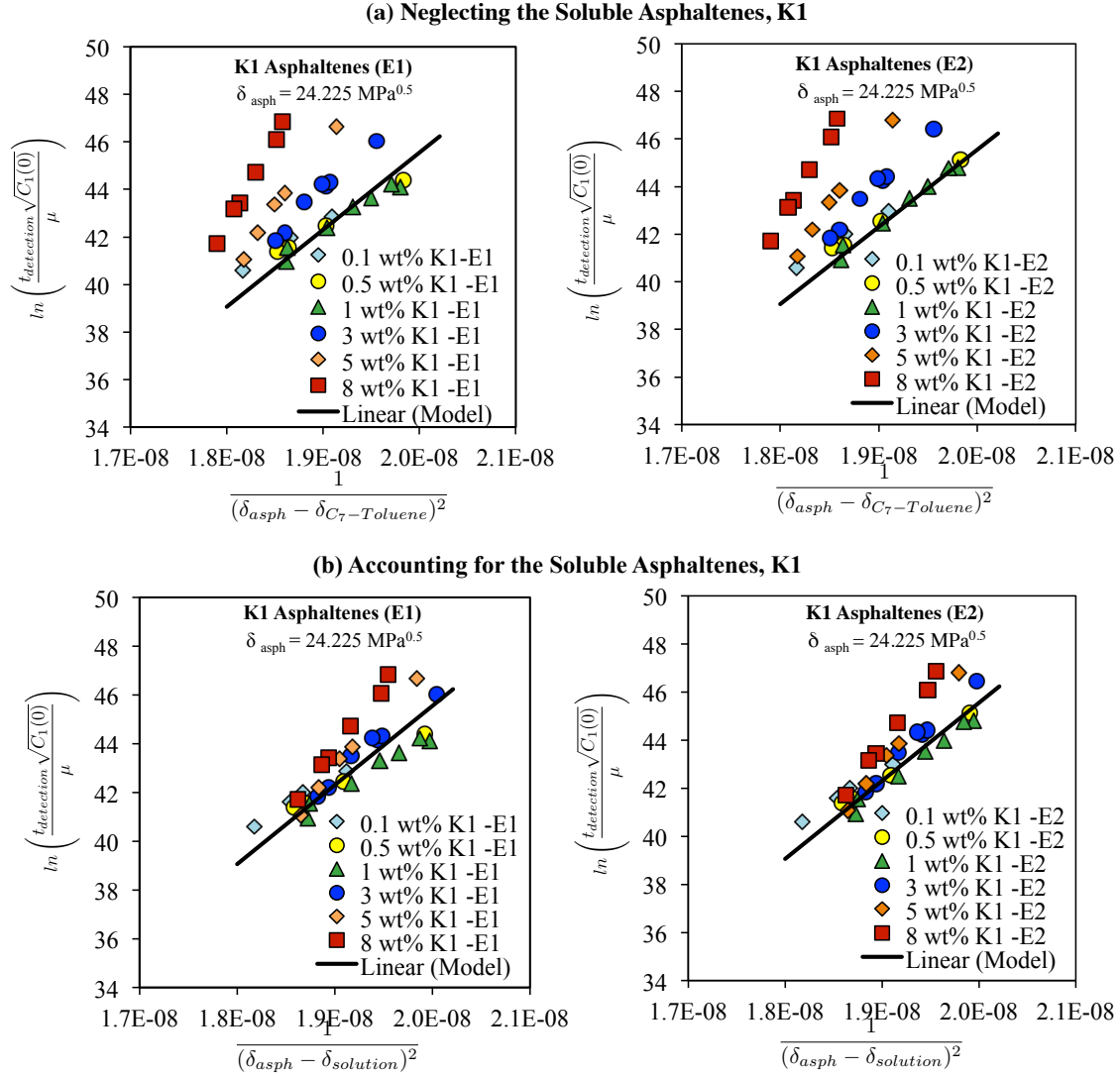


Figure 3.11:

Plot of $\ln(t_{\text{detection}}\sqrt{C_1(0)}/\mu)$ vs. $1/(\delta_{\text{asph}} - \delta_{\text{solution}})^2$ for 0.1, 0.5, 1, 3, 5 and 8 wt% K1 asphaltenes in toluene with respect to master curve using extrapolations E1 and E2: (a) Before accounting for the contribution of soluble asphaltenes and (b) After accounting for the contribution of soluble asphaltenes.

3.5 Conclusions

In this study, the effect of asphaltene concentration on the aggregation tendencies and precipitation kinetics of asphaltenes was investigated. Our findings challenge the intuitive expectation that higher asphaltene concentration would lead to accelerated precipitation kinetics. Instead, two distinct regions for the effect of asphaltene concentration were identified: 1) For asphaltene concentrations below 1 wt%, the aggregation rate of asphaltenes increases with increasing concentration, 2) For concentrations above 1 wt%, the aggregation rate decreases with increasing asphaltene concentration. In addition, centrifugation experiments show that the total amount of precipitated asphaltenes is a monotonically increasing function of asphaltene concentration. The differences in aggregation behavior for concentrations below and above 1 wt% are attributed to two competing effects. First, there is an increase in the number of unstable asphaltenes as the total asphaltene concentration increases, thus leading to an increase in collision frequency. Second, there is an increase in the solvency power of the solution (i.e. the solubility parameter) as a result of an increase in the amount of stable asphaltenes leading to a decrease in coagulation efficiency. The aggregation behavior at concentrations below 1 wt% is dictated by the increase in collision frequency while at concentrations above 1 wt%, the rate is controlled by the reduction in coagulation efficiency. By accounting for the existence of soluble asphaltenes in the solubility parameter of the solution, we were able to successfully model the aggregation behavior of asphaltenes using Smoluchowski's aggregation model. The model provides reasonable predictions for the effect of asphaltene concentration.

Bibliography

- [1] Nasim Haji-Akbari, Phitsanu Teeraphakul, and H. Scott Fogler. Effect of asphaltene concentration on the aggregation and precipitation tendency of asphaltenes. *Energy Fuels*, 2014.
- [2] C. W. Dwiggin Jr. A small angle x-ray scattering study of the colloidal nature of petroleum. *The Journal of Physical Chemistry*, 69:3500–3506, 1965.
- [3] D. A. Storm, E. Y. Sheu, and M. M. DeTar. Macrostructure of asphaltenes in vacuum residue by small-angle x-ray scattering. *Fuel*, 72:977–981, 1993.
- [4] J.-N. Roux, D. Broseta, and B. Demé. Sans study of asphaltene aggregation: concentration and solvent quality effects. *Langmuir*, 17(16):5085–5092, 2001.
- [5] B. Zhao and J. M. Shaw. Composition and size distribution of coherent nanostructures in athabasca bitumen and maya crude oil. *Energy Fuels*, 21(5):2795–2804, 2007.
- [6] T. F. Headen, E. S. Boek, J. Stellbrink, and U. M. Scheven. Small angle neutron scattering (sans and v-sans) study of asphaltene aggregates in crude oil. *Langmuir*, 25(1):422–428, 2009.
- [7] F. Mostowfi, K. Indo, O. C. Mullins, and R. McFarlane. Asphaltene nanoaggregates studied by centrifugation. *Energy Fuels*, 23(3):1194–1200, 2009.
- [8] J. Eyssautier, P. Levitz, D. Espinat, J. Jestin, J. Gummel, I. Grillo, and L. Barré. Insight into asphaltene nanoaggregate structure inferred by small angle neutron and x-ray scattering. *J. Phys. Chem. B*, 115(21):6827–6837, 2011.
- [9] R. Dutta Majumdar, M. Gerken, R. Mikula, and P. Hazendonk. Validation of the yen–mullins model of athabasca oil-sands asphaltenes using solution-state 1h nmr relaxation and 2d hsqc spectroscopy. *Energy Fuels*, 27, 2013.
- [10] S. S. Betancourt, G. T. Ventura, A. E. Pomerantz, O. Vilorio, F. X. Dubost, J. Zuo, G. Monson, D. Bustamante, J. M. Purcell, R. K. Nelson, R. P. Rodgers, C. M. Reddy, A. G. Marshall, and O. C. Mullins. Nanoaggregates of asphaltenes in a reservoir crude oil and reservoir connectivity. *Energy Fuels*, 23, 2009.

- [11] O. C. Mullins, D. J. Seifert, J. Y. Zuo, and M. Zeybek. Clusters of asphaltene nanoaggregates observed in oilfield reservoirs. *Energy Fuels*, 27, 2013.
- [12] James G. Speight. *The Chemistry and Technology of Petroleum*. CRC Press, fourth edition, 2006.
- [13] Oliver C. Mullins. The modified yen model. *Energy & Fuels*, 24(4):2179–2207, 2010.
- [14] N. V. Lisitza, D. E. Freed, P. N. Sen, and Y.-Q. Song. Study of asphaltene nanoaggregation by nuclear magnetic resonance (nmr). *Energy Fuels*, 23(3):1189–1193, 2009.
- [15] Gaëlle Andreatta, Neil Bostrom, and O. C. Mullins. High-q ultrasonic determination of the critical nanoaggregate concentration of asphaltenes and the critical micelle concentration of standard surfactants. *Langmuir*, 21(7):2728–2736, 2005.
- [16] E. Rogel, G. Torres O. León, and J. Espidel. Aggregation of asphaltenes in organic solvents using surface tension measurements. *Fuel*, 79(11):1389–1394, 2000.
- [17] S. I. Andersen and K. S. Birdi. Aggregation of asphaltenes as determined by calorimetry. *J. Colloid Interface Sci.*, 142(2):497–502, 1991.
- [18] S. I. Andersen and S. D. Christensen. The critical micelle concentration of asphaltenes as measured by calorimetry. *Energy Fuels*, 14(1):38–42, 2000.
- [19] Tabish Maqbool, Arjames T. Balgoa, and H. Scott Fogler. Revisiting asphaltene precipitation from crude oils: A case of neglected kinetic effects. *Energy Fuels*, 23:3681–3686, 2009.
- [20] Tabish Maqbool, Sasanka Raha, Michael P. Hoepfner, and H. Scott Fogler. Modeling the aggregation of asphaltene nanoaggregates in crude oilprecipitant systems. *Energy Fuels*, 25, 2011.
- [21] N. Haji-Akbari, P. Masirisuk, M. P. Hoepfner, and H. S. Fogler. A unified model for aggregation of asphaltenes. *Energy Fuels*, 27, 2013.
- [22] J. S. Buckley. Predicting the onset of asphaltene precipitation from refractive index measurements. *Energy Fuels*, 13, 1999.
- [23] G. Porte, H. Zhou, and V. Lazzeri. Reversible description of asphaltene colloidal association and precipitation. *Langmuir*, 19, 2003.
- [24] Irwin A. Wiehe. *Process Chemistry of Petroleum Macromolecules*. CRC Press, 2008.

- [25] M. R. Gray, R. R. Tykwinski, J. M. Stryker, and X. Tan. Supramolecular assembly model for aggregation of petroleum asphaltenes. *Energy Fuels*, 25, 2011.
- [26] Shengqun Wang, Jianjun Liu, Liyan Zhang, Jacob Masliyah, and Zhenghe Xu. Interaction forces between asphaltene surfaces in organic solvents. *Langmuir*, 26, 2010.
- [27] A. Natarajan, J. Xie, S. Wang, J. Masliyah Q. Liu, H. Zeng, and Z. Xu. Understanding molecular interactions of asphaltenes in organic solvents using a surface force apparatus. *J. Phys. Chem. C*, 115, 2011.
- [28] I. Yudin, G. Nikolaenko, E. Gorodetskii, E. Markhashov, V. Agayan, M. Anisimov, and J. Sengers. Crossover kinetics of asphaltene aggregation in hydrocarbon solutions,” physica a: Statistical mechanics and its applications. *Physica A: Statistical Mechanics and its Applications*, 251, 1998.
- [29] I. K. Yudin and M. A. Anisimov. Dynamic light scattering monitoring of asphaltene aggregation in crude oils and hydrocarbon solutions. In O. C. Mullins, E. Y. Sheu, A. Hammami, and A. G. Marshall, editors, *Asphaltenes, Heavy Oils, and Petroleomics*. Springer New York, 2007.
- [30] K. Oh, T. A. Ring, and M. D. Deo. Asphaltene aggregation in organic solvents. *J. Colloid Interface Sci.*, 271(1), 2004.
- [31] K. Rastegari, W.Y. Svrcek, and H.W. Yarranton. Kinetics of asphaltene flocculation. *Industrial Engineering Chemistry Research*, 43, 2004.
- [32] J.-A. Östlund, S.-I. Andersson, and M. Nydén. Studies of asphaltenes by the use of pulsed-field gradient spin echo nmr. *Fuel*, 80, 2001.
- [33] E. Durand, M. Clemancey, A.-A. Quoineaud, J. Verstraete, and and J.-M. Lancelin D. Espinat. 1h diffusion-ordered spectroscopy (dosy) nuclear magnetic resonance (nmr) as a powerful tool for the analysis of hydrocarbon mixtures and asphaltenes. *Energy Fuels*, 22, 2008.
- [34] E. Durand, M. Clemancey, J.-M. Lancelin, J. Verstraete, D. Espinat, and A.-A. Quoineaud. Effect of chemical composition on asphaltenes aggregation. *Energy Fuels*, 24, 2010.
- [35] L. Zielinski, I. Saha, D. E. Freed, M. D. Hürlimann, and Y. Liu. Probing asphaltene aggregation in native crude oils with low-field nmr. *Langmuir*, 26, 2010.
- [36] L. Barre, S. Simon, and T. Palermo. Solution properties of asphaltenes. *Langmuir*, 24, 2008.
- [37] M. P. Hoepfner, C. Vilas Bôas Fávero, N. Haji-Akbari, and H. S. Fogler. The fractal aggregation of asphaltenes. *Langmuir*, 29, 2013.

- [38] P. Matthew Spiecker, Keith L. Gawrys, and Peter K. Kilpatrick. Aggregation and solubility behavior of asphaltenes and their subfraction. *Journal of Colloid and Interface Science*, 267, 2003.
- [39] Jianxin Wang. *Predicting Asphaltene Flocculation in Crude Oils*. PhD thesis, New Mexico Institute of Mining and Technology, 2000.
- [40] Y. G. Burya, I. K. Yudin, V. A. Dechabo, V. I. Kosov, and M. A. Anisimov. Light-scattering study of petroleum asphaltene aggregation. *Appl. Opt.*, 40, 2001.

CHAPTER IV

Effect of *n*-Alkane Precipitants on Precipitation Kinetics of Asphaltenes

4.1 Introduction

It has been shown that temperature [1], asphaltene concentration (Chapter III) and the solvency power of the crude oil (Chapter II) play significant roles in controlling the kinetic behavior of asphaltenes. Moreover, the properties of the precipitated asphaltenes depend on the chemical identity of the precipitant used for their destabilization, therefore the type of the precipitant is also expected to be important. Investigating the effect of different *n*-alkane precipitants on the kinetics of asphaltene precipitation can help us better understand the behavior of asphaltenes in blend of incompatible crude oils. Crude oil blending is a common process in the oil industry for improving certain properties of the heavy crudes (e.g., viscosity or distillation yield) by mixing them with lighter crude oils [2, 3]. Light crude oils are usually rich in paraffins and could act as a precipitant for asphaltenes.

Asphaltenes are typically named after *n*-alkane precipitant used for their destabilization and the most commonly investigated precipitant in the literature is *n*-heptane (i.e. C_7 -asphaltenes). Two trends are reported for the role of *n*-alkane precipitants on

the precipitation behavior of asphaltenes. At high precipitant concentrations (~ 90 vol% precipitant blended with crude oils), the yield of precipitated asphaltenes has shown to increase by decreasing the chain length of n -alkanes (Figure 1.1) [4]. This behavior suggests that shorter chain n -alkanes are stronger precipitants for asphaltenes compared to their longer counterparts. Weaker precipitating power of the longer chain n -alkanes is consistent with their smaller solubility parameters. On the other hand, experimental measurements of onset volume (i.e. the amount of precipitant needed for immediate destabilization of asphaltenes, moderate precipitant concentration) as a function of precipitant carbon number, has shown that the onset volumes pass through a maximum [5]. The chain length of n -alkane at the maximum varies among different crudes oils and carbon numbers ranging from 7–10 are reported in the literature [5]. Existence of a maximum in the onset volume suggests that the precipitating power of precipitants do not change monotonically with change in their chain length. In other words, precipitating power of n -alkanes decreases with an increase in their carbon number up to the maximum and then increases beyond the maximum. This phenomenon is referred to as a paradox and is attributed to the mixing of molecules with different sizes and has been explained by accounting for the polydispersity of asphaltenes using the Flory-Huggins theory [5, 6].

Despite our current understanding of the phase behavior of asphaltenes at high precipitant concentrations, the effect of n -alkane precipitants on precipitation kinetics is not extensively investigated. Asphaltenes kinetic behavior in different n -alkanes can indeed be attributed to various factors. The first factor is the increase of viscosity with an increase in chain length of the n -alkane precipitants. Higher viscosity is expected to decrease aggregation rates and thus increase the time needed for detecting asphaltene instability. The second factor is the increase in the solubility parameter of the mixture that can result in smaller coagulation efficiency between aggregating asphaltenes,

leading to slower aggregation rates [7]. Finally, as discussed earlier, the yield of the precipitated asphaltenes decreases with increasing the chain length, suggesting that the properties and thus the aggregation tendencies of asphaltene that are involved in the aggregation process might vary among different *n*-alkane precipitants. For example, Fuhr *et al.*[8] and Calles *et al.*[9] have shown that the molecular weights and aromaticities of asphaltenes precipitated using different *n*-alkanes are not identical.

It is generally difficult to obtain a thorough understanding of the role of different *n*-alkane precipitants on the aggregation kinetics due to potential involvement of multiple factors in this process. Balgoa [10] investigated the kinetics of asphaltene precipitation from GM2 crude oil using six different precipitants (i.e., *n*-C₆, *n*-C₇, *n*-C₈, *n*-C₉, *n*-C₁₀ and *n*-C₁₅). Despite the differences in the solubility parameter and the viscosity of *n*-alkanes ranging from C₇–C₁₀, no significant change in the aggregation rate of asphaltenes was detected (Figure 4.1). His results also revealed that the precipitation rate of asphaltenes destabilized by hexane and pentadecane are faster than C₇–C₁₀ *n*-alkanes. Balgoa [10] explained his results by the competing effects between the collision frequency (i.e. change in viscosity) and the coagulation efficiency (i.e. difference in aggregation tendency of asphaltenes destabilized in different *n*-alkanes). In addition, he investigated the precipitation rate of asphaltenes in the blends of hexane and octane at different ratios (octane 1:3, 1:1 and 3:1). The blends were mixed with GM2 crude at 33 vol%, 31 vol% and 27 vol% of precipitant (Figure 4.2). The results showed that the experimentally measured detection time from microscopy experiments increases non-linearly with an increase in the *n*-octane volume fraction and the stronger precipitant (C₆) governs the kinetic behavior of the blend.

Balgoa's hypotheses provide qualitative explanations for the observed experimental trends but do not quantitatively describe the aggregation behavior of asphaltenes

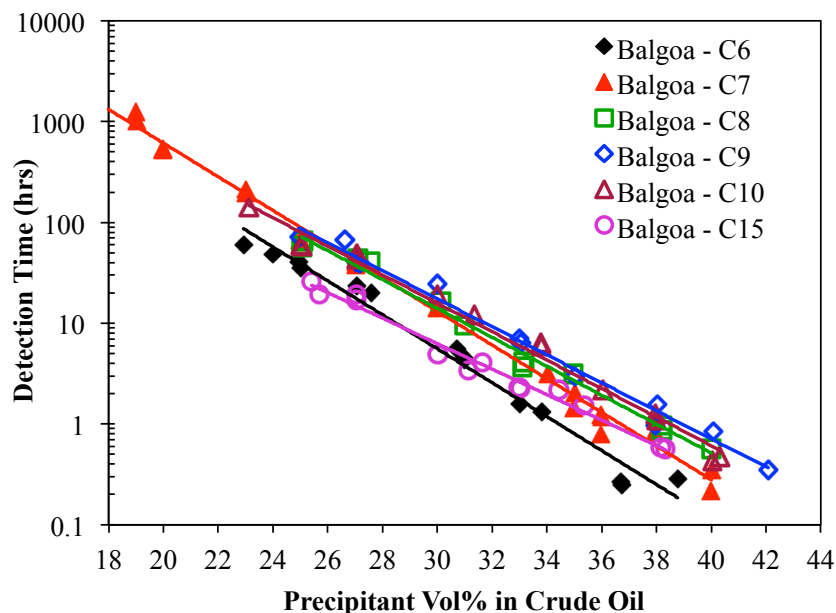


Figure 4.1: **Precipitation detection time vs. precipitant vol% for different n -alkanes mixed with GM2 crude oil** (Image reproduced from [10]).

in different n -alkanes. The aggregation model developed in Chapter II can be used to account for the competing effects of the collision frequency and the coagulation efficiency and can quantitatively model the aggregation rate of asphaltenes in different n -alkanes. In this study, first the kinetics of asphaltene precipitation in different n -alkane precipitants and the blends of n -alkanes is investigated. Then, the aggregation model is utilized to describe the kinetic behavior of asphaltenes in each sample.

4.2 Experimental Section

4.2.1 Materials and Methods

Asphaltenes were extracted from K1 crude oil to be used for model mixture preparation. High performance liquid chromatography (HPLC)-grade toluene was used as

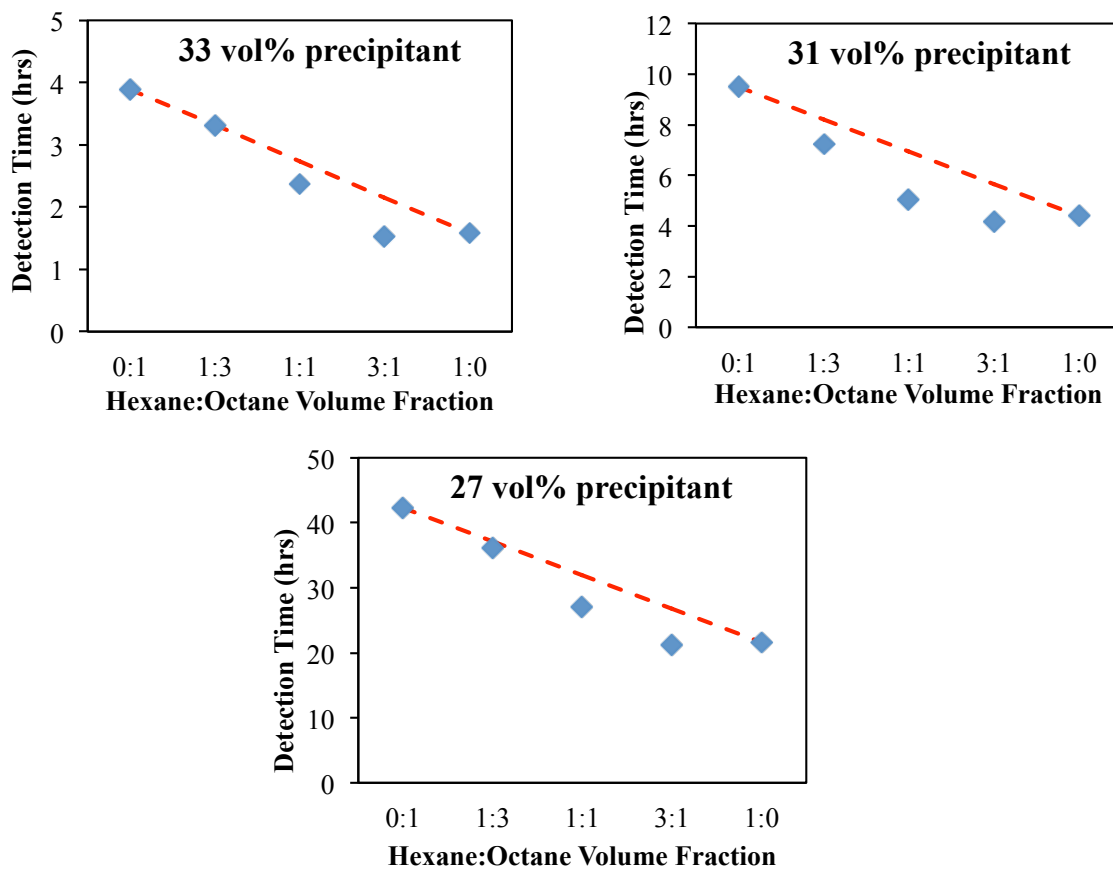


Figure 4.2: Precipitation detection time for different concentrations of *n*-hexane–*n*-octane blend mixed with GM2 crude oil (Images reproduced from [10]).

the solvent. HPLC-grade *n*-hexane (*n*-C₆), *n*-heptane (*n*-C₇), *n*-octane (*n*-C₈), *n*-nonane (*n*-C₉), *n*-decane (*n*-C₁₀), *n*-dodecane (*n*-C₁₂) and *n*-pentadecane (*n*-C₁₅) from Fisher were used as the precipitant. K1 crude oil was mixed with heptane in 1:25 volume ratio and was kept well mixed for 24 hours. The solution was then centrifuged with a Sorvall Legend X1R at 3500 rpm for 1 hour to separate precipitated asphaltenes. The asphaltenes were Soxhlet-washed for 24 hours to wash any non-asphaltenic material trapped in the cake. The asphaltenes were then dried in a vacuum oven at 75 °C. To prepare model mixture, 1 wt% of dried asphaltenes was dissolved in toluene and sonicated until the proper dissolution was achieved.

Table 4.1: Physical properties of compounds at room temperature.

Compound	Density (g/ml) [11]	Viscosity (cP) [11]	Solubility Parameter (MPa ^{0.5}) [12]
<i>n</i> -Hexane	0.660	0.32	14.90
<i>n</i> -Heptane	0.679	0.41	15.20
<i>n</i> -Octane	0.703	0.54	15.40
<i>n</i> -Nonane	0.718	0.70	15.60
<i>n</i> -Decane	0.726	0.93	15.80
<i>n</i> -Dodecane	0.749	1.56	16.0 [6, 13]
<i>n</i> -Pentadecane	0.768	2.81	16.30 [13]
Toluene	0.866	0.60	18.30
GM2 Crude Oil	0.868	15.69	17.59*

*Calculated from refractive index of GM2 crude oil using the correlation proposed by Wang and Buckley [14]

Microscopy Experiments: A known volume of model oil (1 wt% K1 asphaltenes in toluene) was placed in a 4 mL vial. The desired concentrations of precipitants/blend of precipitants (below the instantaneous onset point) were slowly added to the model oil using a syringe pump at 20 mL/h flow rate. All solutions were kept well mixed during precipitant addition (samples were prepared on a mass basis). After sample preparation, a droplet of well-stirred sample was placed under a Nikon microscope

(model: Eclipse E600) with 40x objective lens and 10x eyepiece and a Nikon camera (DS-Fi2) was used to shoot images off the microscope. Similar to previous chapters, the time at which asphaltenes were detected for the first time under the microscope was defined as *detection time* (detection limit $\sim 0.5 \mu\text{m}$).

4.3 Results and Discussion

4.3.1 Individual Precipitants

For a polydispersed mixture such as asphaltenes, detection time likely represents the aggregation rate of the most unstable asphaltenes. Figure 4.3 shows the detection time measurements for seven different n -alkane precipitants (C_6 , C_7 , C_8 , C_9 , C_{10} , C_{12} , C_{15}) mixed with the model oil (1 wt% K1 asphaltenes in toluene). For the precipitants ranging from C_6 – C_{10} only slight differences in the aggregation rates are observed, while for C_{12} and C_{15} , the rates increase with increasing the carbon number. Although these trends are opposite to the trend expected from the increase in the viscosity and the solubility parameter of the solution, the results are in good agreement with Balgoa’s observations [10]. The only difference between results shown in Figure 4.3 and Balgoa’s results (Figure 4.1) is the aggregation rate of asphaltenes in C_6 . In Balgoa’s experiments, C_6 behaved identical to C_{15} but in our experiments C_6 ’s behavior is similar to C_7 , C_8 , C_9 and C_{10} .

This unexpected trend in the observed rates indicates the involvement of a competing factor that cancels out the effect of increase in viscosity and solubility parameter of solution. We believe that this competing effect arises due to the polydispersity of asphaltenes. Note that the existing definition of asphaltenes captures a broad distribution of molecules with different physical and chemical properties. Mass spectrometry experiments have shown that asphaltenes are composed of around 7000 distinct

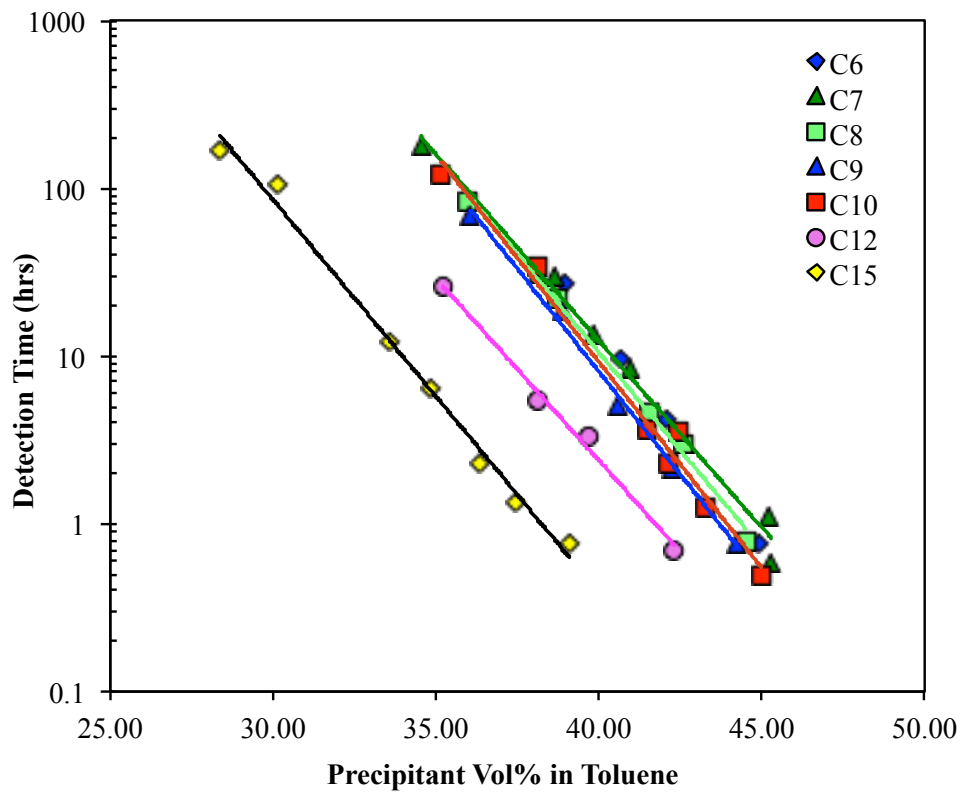


Figure 4.3: Detection time as a function of precipitant concentration for 1 wt% of K1 asphaltenes dissolved in toluene and then mixed with seven different precipitants (C_6 , C_7 , C_8 , C_9 , C_{10} , C_{12} , C_{15}).

molecules [15]. In addition, sub-fractions of asphaltenes have been shown to possess different properties in terms of their molecular weight, solubility, size and structure. Owing to extreme polydispersity of asphaltenes, different n -alkane precipitants are expected to destabilize different fractions of the asphaltenes solubility class.

As discussed in the introduction (4.1), it is shown that the amount of precipitated asphaltenes decreases with increasing the chain length of n -alkane, suggesting that the longer chain n -alkanes can only precipitate the most unstable fraction of total asphaltenes. Fuhr *et al.* [8] investigated the properties of asphaltenes precipitated using several n -alkanes (n -C₅, n -C₆, n -C₈, n -C₉) and they observed that the aromaticity and the molecular weight of precipitated asphaltenes increase with an increase in the carbon number of precipitant. It is well known that increasing the size and aromaticity, increases the magnitude of dispersion energy and thus the solubility parameter [16]. Therefore, it can be concluded that the solubility parameter of the precipitated asphaltenes increases with increasing the chain length of n -alkane. This behavior might appear counter-initiative due to the weaker destabilizing power of the higher carbon number precipitants. However, it should be noted that weaker precipitants (e.g. pentadecane), are only capable of precipitating the most unstable fraction of asphaltenes i.e. asphaltenes with the highest solubility parameter. On the other hand for stronger precipitants such as hexane, they precipitate a wider spectrum of asphaltenes with the solubility parameter of precipitated asphaltenes being the average of the different fractions rather than the most unstable fraction. Figure 4.4 represents a schematic of solubility parameter distribution for asphaltenes destabilized from different n -alkanes.

In summary at this point, increasing the n -alkane carbon number increases the solubility parameter of both the precipitant and asphaltenes. The aggregation tendency (i.e. coagulation efficiency) of asphaltens is controlled by the difference between the

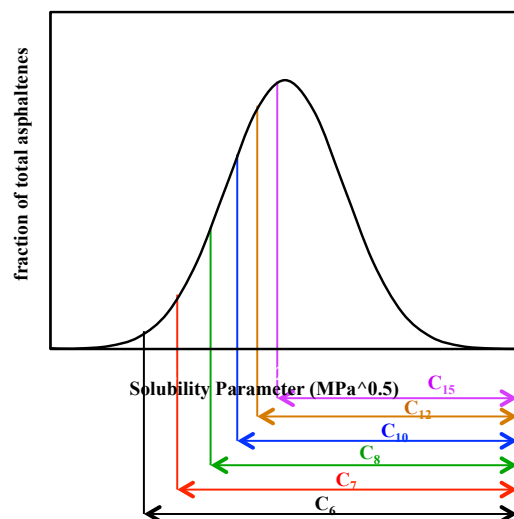


Figure 4.4: **Schematic of the solubility parameter distribution for asphaltene precipitated using different *n*-alkanes.**

solubility parameters of the asphaltene and the environment surrounding them [7]. Therefore for different *n*-alkane precipitants, the coagulation efficiency can either increase or decrease depending on the magnitude of changes in the solubility parameter of asphaltene and the precipitant. This hypothesis can also easily explain the existence of a maximum in the plot of onset volume vs. the precipitant carbon number. One simple approach to qualitatively characterize the polydispersity of asphaltene is to calculate the solubility parameter of different fractions.

Asphaltene are solid and complex compounds and it is experimentally difficult to measure their solubility parameter (Section 1.2.3 of Chapter I). However, the solubility parameter of asphaltene can be easily obtained from the master curve relationship between the detection time and the solubility parameters derived in Chapter II. The following equation can be used for correlating the experimentally measured detection times to the differences in the solubility parameters:

$$\ln \left(\frac{t_{detection} \sqrt{C_1(0)}}{\mu} \right) \propto \frac{1}{(\delta_{asph} - \delta_{solution})^2} \quad (4.1)$$

where δ_{asph} and $\delta_{solution}$ are the solubility parameters of the asphaltenes and the solution respectively, μ is the local viscosity and $C_1(0)$ is the number concentration of aggregating asphaltenes. $\delta_{solution}$ and μ can be simply calculated from the volumetric averaging and logarithmic averaging of the solubility parameters and viscosities of the solvent and precipitant respectively. $C_1(0)$ can be calculated from the fraction of unstable asphaltenes. It is shown in Chapter III that the fraction of the precipitated asphaltenes is related to the $1/(\delta_{asph} - \delta_{solution})^2$. Therefore, by knowing the detection time, a simple trial and error approach can be implemented to obtain the solubility parameter of asphaltenes (i.e. δ_{asph}) precipitated using different n -alkanes. The solubility parameter of asphaltenes are obtained both for Balgoa's results shown in Figure 4.1 and also for our results shown in Figure 4.3.

Figure 4.5 shows the agreement between the model and the experiments for obtaining the solubility parameter of asphaltenes in this work and in Balgoa's study and confirms that the utilized model can successfully explain the precipitation kinetics of asphaltenes in different n -alkanes. Tables 4.2 and 4.3 and Figure 4.6 show the solubility parameters of asphaltenes precipitated from different precipitants as a function of their carbon number. The solubility parameters obtained from the model, increase with increasing the precipitants carbon number. This trend is in agreement with the observed reduction in the precipitating power of n -alkanes as their carbon number increases (Figure 1.1), leading to the destabilization of the most unstable asphaltenes only, that are the asphaltenes with the highest solubility parameter. Figure 4.6 also reveals that the solubility parameter of K1 asphaltenes has

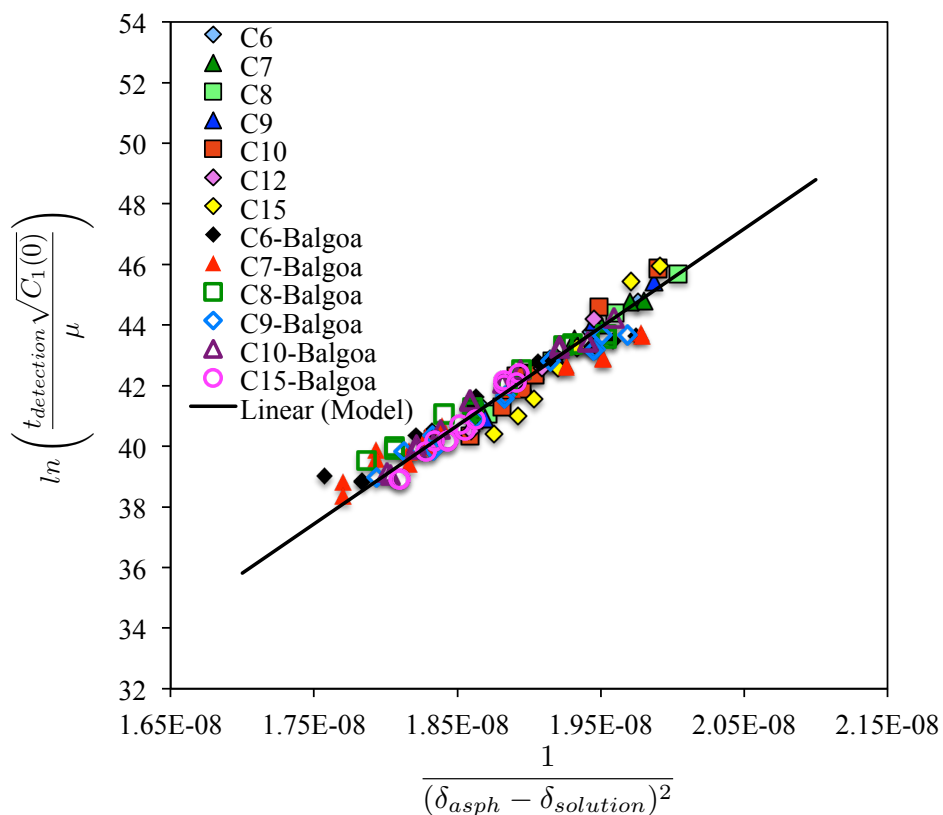


Figure 4.5: **Plot of $\ln(t_{\text{detection}} \sqrt{C_1(0)} / \mu)$ vs. $1/(\delta_{\text{asph}} - \delta_{\text{solution}})^2$ for seven different precipitants ($C_6, C_7, C_8, C_9, C_{10}, C_{12}, C_{15}$) mixed with 1wt% K1 asphaltenes in toluene and six different precipitants ($C_6, C_7, C_8, C_9, C_{10}, C_{15}$) mixed with GM2 crude oil.**

a wider distribution compared to GM2 asphaltenes, indicating that K1 asphaltenes have greater polydispersity.

Solubility parameter of asphaltenes shown in Figure 4.6 along with the master curve can be used to calculate the detection times and evaluate the accuracy of the model in describing individual data points. Figures 4.7 and 4.8 show model predictions vs. actual experimental data for K1 and GM2 respectively. The experiments follow the model reasonably well in all samples. The modeling results for K1-toluene

Table 4.2: Solubility parameter of asphaltenes destabilized with different *n*-alkanes (K1 asphaltenes in toluene).

Name Precipitant	Solubility Parameter of Asphaltenes ($MPa^{0.5}$)
<i>n</i> -Hexane	24.09
<i>n</i> -Heptane	24.22
<i>n</i> -Octane	24.32
<i>n</i> -Nonane	24.42
<i>n</i> -Decane	24.51
<i>n</i> -Dodecane	24.66
<i>n</i> -Pentadecane	24.82

Table 4.3: Solubility parameter of asphaltenes destabilized with different *n*-alkanes (GM2 crude oil).

Name Precipitant	Solubility Parameter of Asphaltenes ($MPa^{0.5}$)
<i>n</i> -Hexane	24.09
<i>n</i> -Heptane	24.15
<i>n</i> -Octane	24.19
<i>n</i> -Nonane	24.22
<i>n</i> -Decane	24.32
<i>n</i> -Pentadecane	24.53

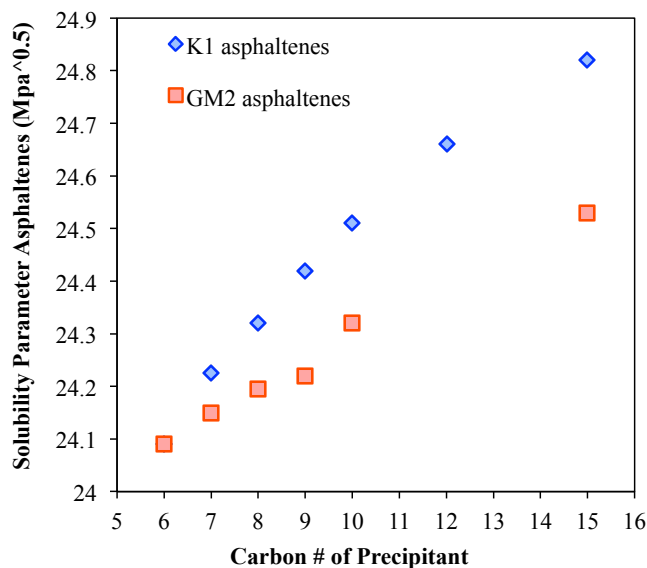


Figure 4.6: **Plot of asphaltene solubility parameter vs. the precipitant carbon number (K1 and GM2).**

mixtures slightly deviate from the experimental observations for the samples destabilized with pentadecane (Figure 4.7). Precipitation of asphaltene from GM2 crude oil shows no such deviations. The deviation of K1 samples could be due to significant difference between the molar volume of heptane and pentadecane. Our model was developed based on the differences in solubility parameters and does not account for the changes in molar volumes. To account for the changes in molar volumes, the molar volumes of asphaltene and crude oils need to be known. Measuring the molecular weights (and molar volumes) of the asphaltene and crude oils is usually very challenging. In fact, the molecular weight of asphaltene has been the subject of extensive debate for decades due to their strong tendency to self-associate and it has not been until very recently that some reasonable estimates were reported [17]. Molecular weights (and molar volumes) of crude oils might also depend on the particular

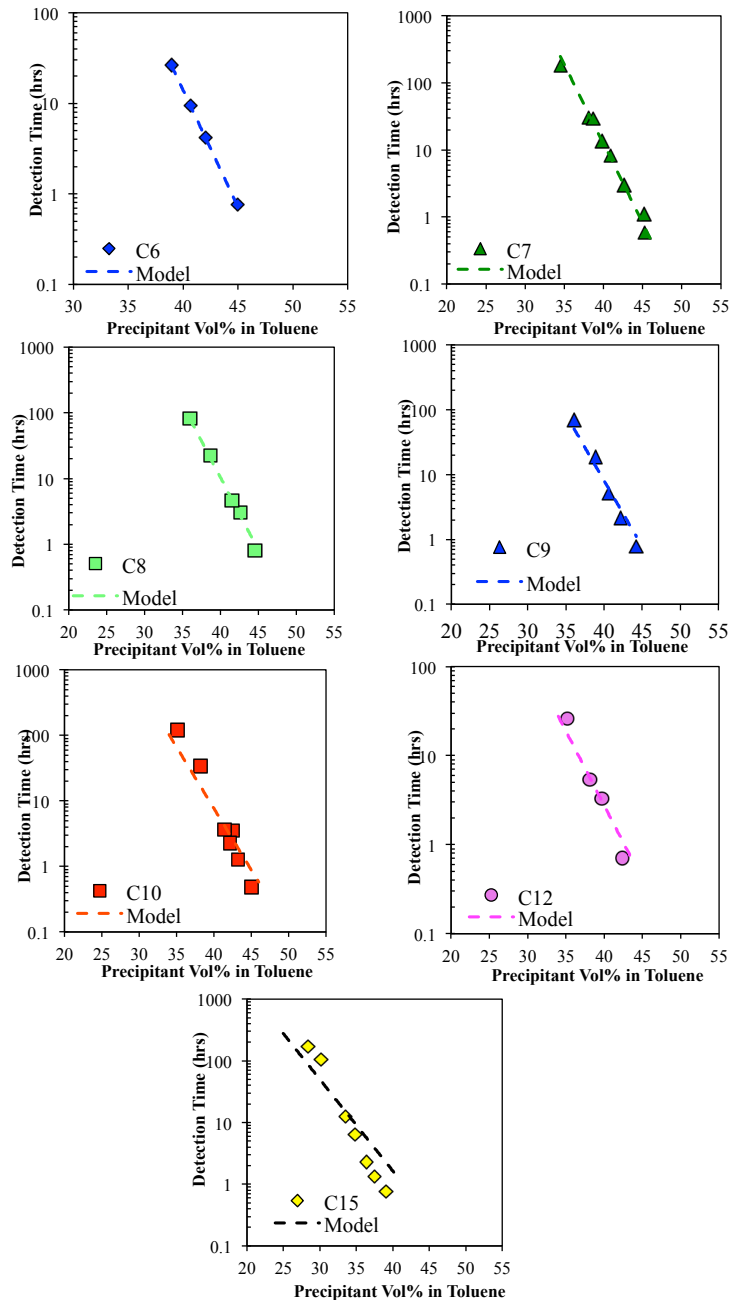


Figure 4.7: Modeling results compared to experimental measurements of detection time for seven different precipitants mixed with 1wt% K1 asphaltenes in toluene.

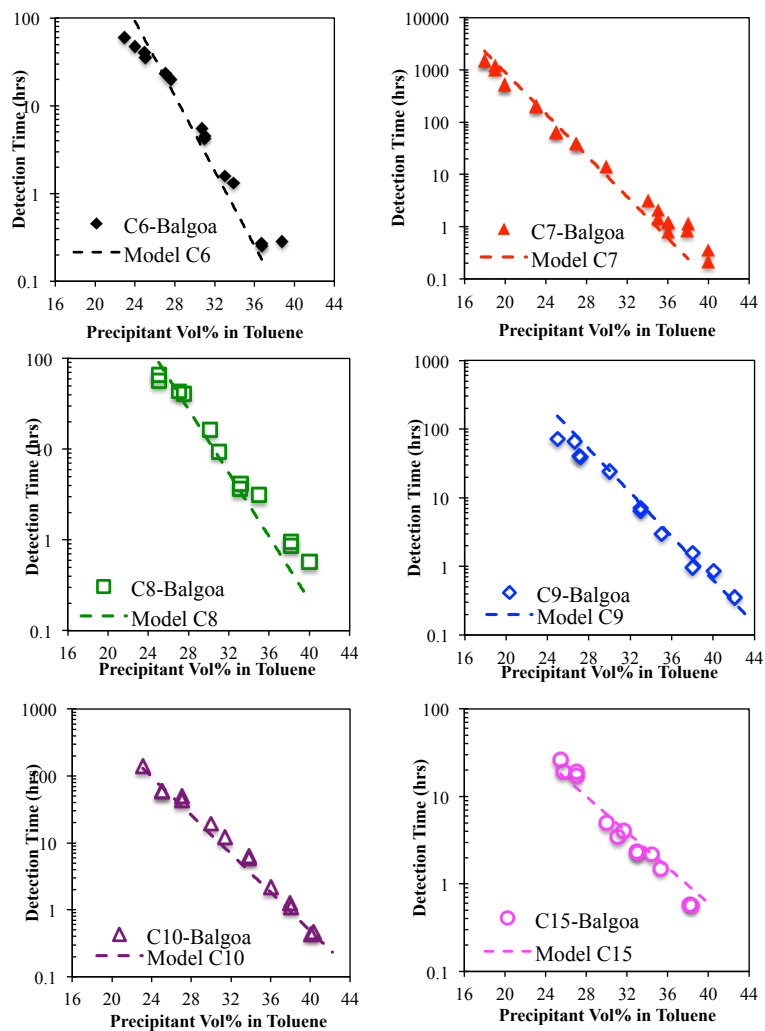


Figure 4.8: Modeling results compared to experimental measurements of detection time for six different precipitants mixed with GM2 crude oil.

experimental procedure used for measuring them [6]. Despite not accounting for the changes in molar volumes, our model can still successfully describe the experimental observations both for K1 asphaltenes and GM2 crude oil.

4.3.2 Blend of Precipitants

The aggregation model can be used for predicting the precipitation rate of asphaltenes in the blends of different n -alkanes. The precipitation rate of asphaltenes in the blend of two, three, four and five n -alkane precipitants is investigated. To predict the precipitation rates in the blend, the solubility parameter of asphaltenes needs to be known. Properties of the precipitated asphaltenes in the blend of n -alkanes are expected to be the averages of properties of asphaltenes precipitated in each of the constituent individual precipitants. Therefore, instead of fitting the detection time measurements to the master curve, solubility parameter of asphaltenes in the blend is calculated from the volumetric average of the asphaltenes solubility parameter in each n -alkane:

$$\delta_{asph-blend} = \phi_{C_n} \delta_n + \phi_{C_m} \delta_m + \phi_{C_p} \delta_p + \dots \quad (4.2)$$

$\delta_{asph-blend}$ stands for the solubility parameter of asphaltenes in the blend of C_n , C_m and C_p precipitants. ϕ s represent the volume fraction of precipitants in the blend and δ_n , δ_m and δ_p stand for the solubility parameter of asphaltenes precipitated from individual precipitants (Tables 4.2 and 4.3).

Table 4.4 shows the calculated values of the viscosities and the solubility parameters of the blends and asphaltenes for the blends of two, three, four and five different precipitants at different ratios. For the blends of 50:50 $C_7 - C_{12}$, 30:30:40

$C_7 - C_{10} - C_{12}$ and 20:20:20:20:20 $C_6 - C_7 - C_{10} - C_{12} - C_{15}$, the viscosities and the solubility parameters are all identical. Therefore, despite the differences in the composition of the precipitant, the precipitation rate of asphaltenes is expected to be identical. This expected trend is confirmed experimentally from the results shown in Figure 4.9 and can be qualitatively predicted from the master curve (Figure 4.10).

Table 4.4: Calculated values of viscosities and solubility parameters used for predicting detection times in Figure 4.10

Blend Composition	Solubility Parameter of Blend($MPa^{0.5}$)	Solubility Parameter of Asphaltenes($MPa^{0.5}$)	Viscosity of Blend (cP)
$C_7 - C_{15}$ 0.75:0.25	15.48	24.37	0.67
0.5:0.5	15.75	24.52	1.07
0.25:0.75	16.03	24.67	1.74
$C_7 - C_{12}$ 0.5:0.5	15.60	24.44	0.80
$C_7 - C_{10} - C_{12}$ 0.3:0.3:0.4	15.70	24.48	0.89
$C_7 - C_{10} - C_{12} - C_{15}$ 0.2:0.2:0.2:0.4	15.92	24.61	1.36
$C_6 - C_7 - C_{10} - C_{12} - C_{15}$ 0.2:0.2:0.2:0.2:0.2	15.64	24.46	0.88

Figure 4.10 shows the model predictions for the detection times as well as the actual experimental measurements for the blends shown in Table 4.4. All predicted detection times are calculated from the master curve (i.e. Equation 4.1) with known values for the viscosities and solubility parameters. The agreement between the model predictions and the experiments is remarkable for all the samples. It should be emphasized that **no fitting** parameter is used for obtaining the predictions presented in Figure 4.10. Our findings reveal that Equation 4.2 provides accurate estimates of

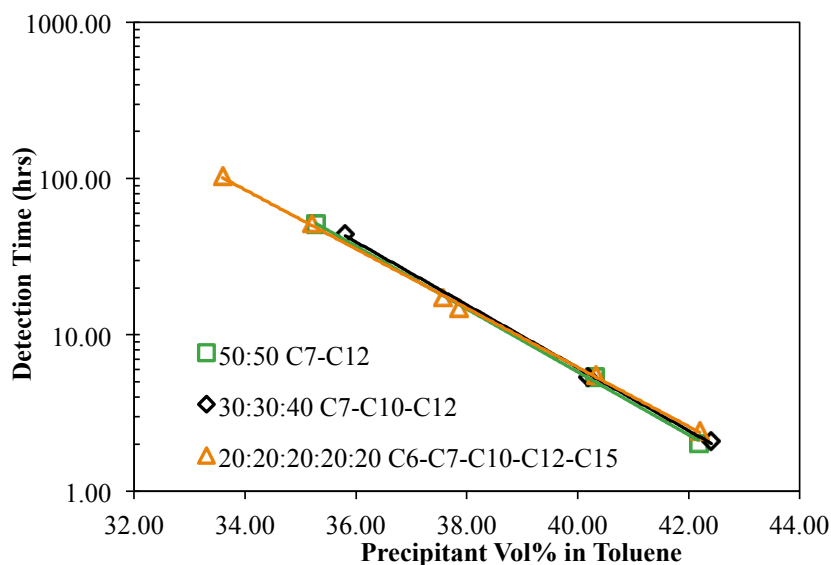


Figure 4.9: **Detection times vs. precipitant concentration for blends of 0.5:0.5 $C_7 - C_{12}$, 0.3:0.3:0.4 $C_7 - C_{10} - C_{12}$ and 0.2:0.2:0.2:0.2:0.2 $C_6 - C_7 - C_{10} - C_{12} - C_{15}$ precipitants.**

the solubility parameters of asphaltenes precipitated at different ratios of the same blend (i.e. $C_7 - C_{15}$) and also in different blend compositions.

Similar analysis using Equations 4.1 and 4.2 was performed on the results for the blends of C_6 and C_8 investigated by Balgoa (Figure 4.2). Figure 4.11 shows the comparison between the experiments and the master curve for the blends investigated in this work and Balgoa's work altogether. Overall ten different blends have been investigated and all of them perfectly follow the predicted trend from the master curve. Excellent agreement between the master curve and the experimental data can be interpreted as a close match between the detection time predictions vs. experimentally measured values.

In previous investigations, Flory-Huggins theory has been used to describe the phase behavior of asphaltenes in different n -alkanes [6, 18]. However, without ac-

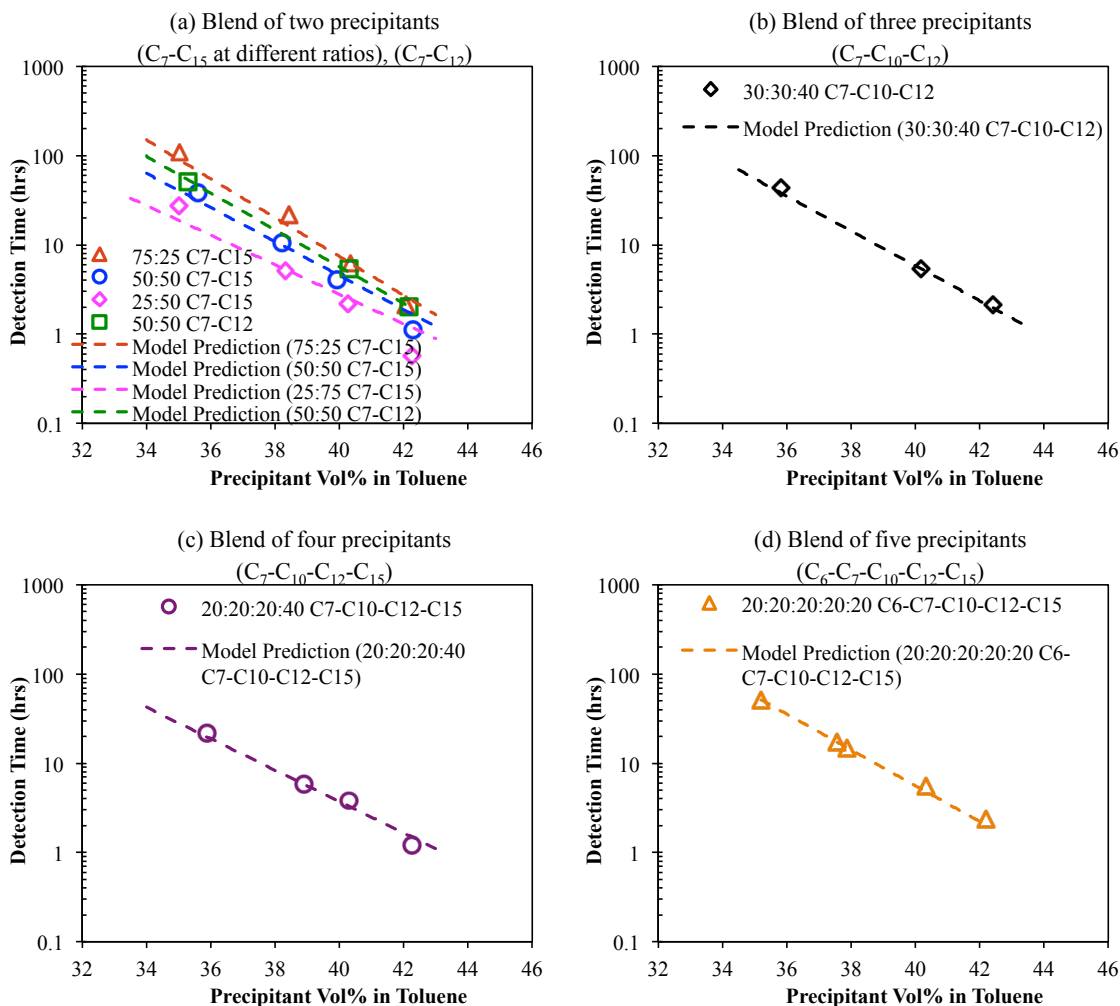


Figure 4.10: Model predictions compared to the experimental measurements of detection time for blends of precipitants mixed with 1wt% K1 model oil in toluene: (a) heptane and pentadecane at different ratios (0.25:0.75 $C_7 - C_{15}$, 0.5:0.5 $C_7 - C_{15}$, 0.75-0.25 $C_7 - C_{15}$), heptane and dodecane (0.5:0.5 $C_7 - C_{12}$), (b) 0.3:0.3:0.4 $C_7 - C_{10} - C_{12}$, (c) 0.2:0.2:0.2:0.4 $C_7 - C_{10} - C_{12} - C_{15}$, (d) 0.2:0.2:0.2:0.2:0.2 $C_6 - C_7 - C_{10} - C_{12} - C_{15}$.

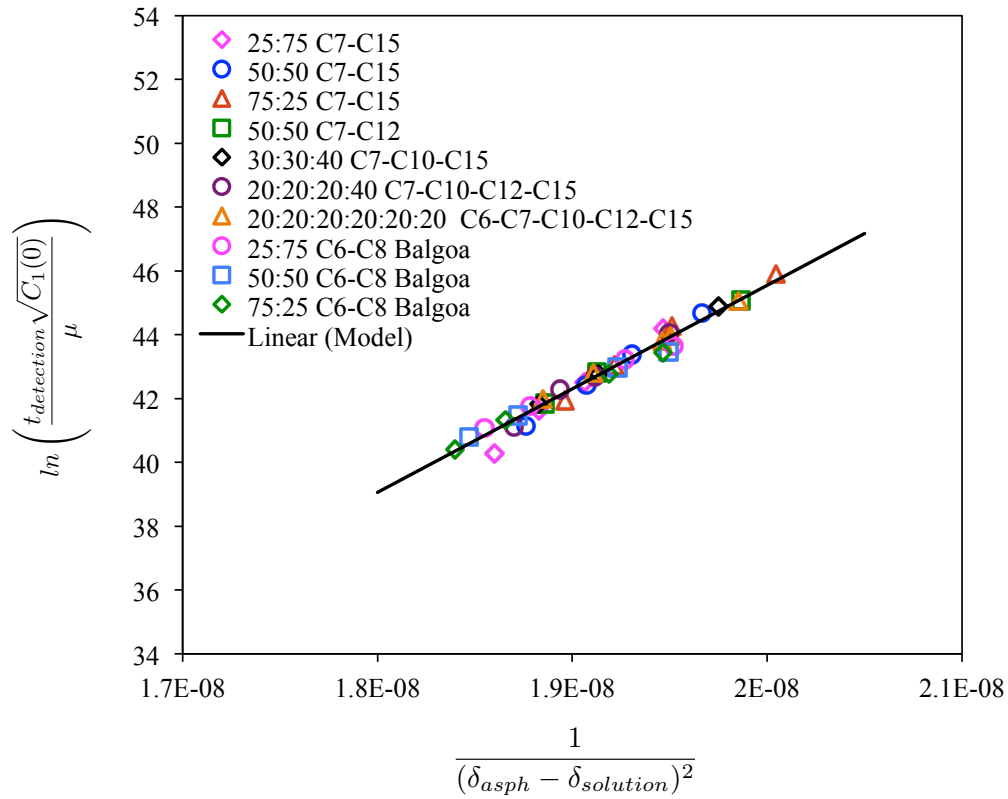


Figure 4.11: Plot of $\ln(t_{\text{detection}} \sqrt{C_1(0)}/\mu)$ vs. $1/(\delta_{\text{asph}} - \delta_{\text{solution}})^2$ (i.e. master curve) compared to the experimental measurements for ten different blends of precipitants (K1 model oil and GM2 crude oil).

counting for the polydispersity of asphaltenes Flory-Huggins theory could not provide a quantitative description of asphaltenes behavior [6, 18]. For example, in Wang's [6] model two fitting parameters (i.e., the solubility parameter and molar volume of asphaltenes) were used as input to Flory-Huggins theory. Mathematical fits for different precipitants was obtained by changing the solubility parameter of the precipitated asphaltenes. No monotonic trend between the solubility parameter of precipitated asphaltenes and carbon number of n -alkane precipitants was observed in his model. In our study the solubility parameter of precipitated asphaltenes in individual precipitants is calculated by fitting the measured detection times to the unified aggregation curve (Chapter II). However, opposite to Wang's work a monotonic trend in the solubility parameter of precipitated asphaltenes as a function of n -alkanes chain length was observed both in the model oils (K1 asphaltenes in toluene) and in the crude oils (GM2 investigated by Balgoa). The increasing trend of the asphaltenes solubility parameter as a function of n -alkane chain length is expected due to the monotonic change in the precipitating power of n -alkanes and polydispersity of asphaltenes. Our investigation is the first to study and predict the precipitation rate of asphaltenes in the blends of more than two different precipitants. Blend of up to five precipitants were investigated and the results were all successfully predicted with our model. These results can help in developing new tools for predicting potential asphaltene problems in blend of more than two crude oils at different blend ratios.

4.4 Conclusions

Precipitation kinetics as a function of chain length of the n -alkane precipitants was investigated. Despite a monotonic change in the viscosity and the solubility parameter of n -alkane precipitants as a function of their carbon number, the precipitation rate

of asphaltenes does not vary monotonically. This behavior can be well explained by the polydispersity of asphaltenes and differences in the precipitating power of *n*-alkanes. Our model successfully predicted the precipitation rates in different *n*-alkanes and showed that longer chain *n*-alkanes tend to precipitate the most unstable fraction of asphaltenes with the highest solubility parameter. In addition, the model predicted the precipitation rate of asphaltenes from blends of different precipitants after characterizing asphaltenes polydispersity from individual precipitants. These results provide new paradigm for predicting the precipitation rate of asphaltenes in blends of incompatible crude oils.

Bibliography

- [1] T. Maqbool, P. Srikiratiwong, and H. S. Fogler. Effect of temperature on the precipitation kinetics of asphaltenes. *Energy Fuels*, 25, 2011.
- [2] S. Li, J. Liu, B. Shen, X. Xu, Q. Fan, J. Chen, and G. Zhao. Distillation yields from blending cabinda crude oil and oman crude oil. *Petroleum Science and Technology*, 24, 2006.
- [3] N. Shigemoto, R.S. Al-Maamari, B.Y. Jibril, and A. Hirayama. A study of the effect of gas condensate on the viscosity and storage stability of omani heavy crude oil. *Energy Fuels*, 20, 2006.
- [4] D.L. Mitchell and J.G. Speight. The solubility of asphaltenes in hydrocarbon solvents. *Fuel*, 52:149–152, 1973.
- [5] Irwin A. Wiehe, Harvey W. Yarranton, Kamran Akbarzadeh, Parviz M. Rahimi, and Alem Teclemariam. The paradox of asphaltene precipitation with normal paraffins. *Energy Fuels*, 19, 2005.
- [6] Jianxin Wang. *Predicting Asphaltene Flocculation in Crude Oils*. PhD thesis, New Mexico Institute of Mining and Technology, 2000.
- [7] N. Haji-Akbari, P. Masirisuk, M. P. Hoepfner, and H. S. Fogler. A unified model for aggregation of asphaltenes. *Energy Fuels*, 27, 2013.
- [8] B. J. Fuhr, C. Cathrea, L. Coates, H. Kalra, and A. I. Majeed. Properties of asphaltenes from a waxy crude. *Fuel*, 70, 1991.
- [9] J.A. Calles, J. Dufour, J. Marugán, J.L. Peña, R. Giménez-Aguirre, and D. Merino-García. Properties of asphaltenes precipitated with different n-alkanes. a study to assess the most representative species for modeling. *Energy Fuels*, 22, 2008.
- [10] Arjames T. Balgoa. Kinetics of asphaltene precipitation: Effect of different n-alkane precipitants. Master's thesis, The Petroleum and Petrochemical College, Chulalongkorn University, 2009.

- [11] 94, editor. *Handbook of Chemistry and Physics*. CRC, 2013.
- [12] 2, editor. *Handbook of Solubility Parameters and Other Cohesion Parameters*. CRC, 1991.
- [13] K. C. Chao and J. D. Seader. A general correlation of vapor-liquid equilibria in hydrocarbon mixtures. *AIChE Journal*, 1961.
- [14] J. X. Wang and J. S. Buckley. A two-component solubility model of the onset of asphaltene flocculation in crude oils. *Energy Fuels*, 15(5):1004—1012, 2001.
- [15] Geoffrey C. Klein, Sunghwan Kim, Ryan P. Rodgers, Alan G. Marshall, and Andrew Yen. Mass spectral analysis of asphaltenes. ii. detailed compositional comparison of asphaltenes deposit to its crude oil counterpart for two geographically different crude oils by esi ft-icr ms. *Energy Fuels*, 20, 2006.
- [16] Charles M. Hansen. *Hansen Solubility Parameters*. CRC Press, 2nd edition, 2007.
- [17] Oliver C. Mullins. The modified yen model. *Energy & Fuels*, 24(4):2179–2207, 2010.
- [18] Hussein Alboudwarej, Kamran Akbarzadeh, James Beck, William Y. Svrcek, and Harvey W. Yarranton. Regular solution model for asphaltene precipitation from bitumens and solvents. *AIChE Journal*, 49(11):2948–2956, 2003.

CHAPTER V

Polydispersity and Aggregation Tendency of Asphaltenes

5.1 Introduction

The definition of asphaltenes captures a broad distribution of molecules with different chemical and physical properties. The properties of asphaltenes can greatly influence their destabilization tendencies. Numerous studies have focused on characterizing the properties of different asphaltenes and asphaltene sub-fractions with the aim of identifying the most problematic fractions. Leon *et al.* [1] used various characterization techniques to obtain the molecular weight (MW), aromaticity and H/C ratio of asphaltenes precipitated from different crude oils. By determining the precipitation onset point using titration technique, they concluded that an increase in the H/C ratio and a decrease in aromaticity enhances the stability of asphaltenes in the crude oil. They also dissolved extracted asphaltenes in different solvents (cyclohexane, tetrahydrofuran, carbon tetrachloride) to study the effect of asphaltenes structure on their self-aggregation through surface tension measurements. However, they were not able to establish a general relationship between self-aggregation and properties characterized in their study [1].

Spiecker *et al.* [8] fractionated asphaltenes into soluble and insoluble fractions and showed that the insoluble fraction tend to form larger aggregates in toluene [8]. Buckley *et al.* [2] showed that asphaltenes precipitated from a single crude oil using different precipitants behave differently in terms of their stability and precipitation tendency. For instance, they observed that asphaltenes precipitated from shorter chain *n*-alkanes are more stable. Calles *et al.* [3] compared properties of asphaltenes precipitated from C_5 , C_6 and C_7 . They showed that the aromaticity of precipitated asphaltenes increases as a result of increase in the carbon number of precipitant. They also investigated differences in elemental composition in terms of C, N and S content of asphaltenes and found that the only difference is that C_5 asphaltenes have less nitrogen compared to C_6 and C_7 asphaltenes.

Field deposits are typically more unstable compared to asphaltenes extracted in the laboratory from dead crude oils [5, 6]. Wattana [5, 6] compared the asphaltenes collected from field deposits and precipitated from both unstable and stable crude oils and showed that field deposits have different metal content, molecular weight and polarity. She also showed that field deposits and the asphaltenes extracted from unstable oils have a higher fraction of polar components. In addition, Wattana [5] investigated the properties of asphaltene sub-fractions fractionated from methylene chloride using different precipitant concentrations and found out that the metal content and the polarity of each sub-fraction is different . Similar to Wattana's observations, Maqbool [7] also reported slight differences in the metal content of asphaltene sub-fractions precipitated at different heptane concentrations. Higher metal contents and polarities are typically associated with lower stability of asphaltenes. Moreover, Maqbool [7] fractionated asphaltenes precipitated at different times in a single precipitation experiment. His results suggested that asphaltenes precipitating first have higher dielectric constants compared to other fractions.

Kinetics of asphaltenes aggregation is directly related to the interactions between asphaltenes and is expected to depend on asphaltene properties. However, the role of asphaltenes polydispersity on their aggregation kinetic has not been extensively investigated (only dielectric constant measurements are done by Maqbool [7]). For example, it is not clear if the overall properties of asphaltenes participating in the aggregation process at a fixed precipitant concentration are identical or vary over time. We hypothesize that the asphaltenes that precipitate first are the most problematic fraction and have the highest tendency for aggregation. To evaluate our hypothesis asphaltenes are fractionated into smaller sub-fractions and different techniques such as small angle X-ray scattering(SAXS), elemental composition measurements and microscopy experiments are utilized to study the importance of polydispersity on kinetics.

5.2 Experimental Section

5.2.1 Materials

Crude oil A and model oil composed of asphaltenes extracted from crude A were used in our characterization experiments. Crude oil was first centrifuged at 3500 rpm for 10 hours using a Sorvall Legend X1R centrifuge to separate sand, clay, water and other insoluble particles prior to our precipitation experiments. HPLC-grade toluene and heptane from Fisher were used as the solvent and the precipitant for asphaltenes respectively.

Microscopy experiments: An optical microscope from Nikon (model: Eclipse E600) with 40x objective lens and 10x eyepiece was used for detecting asphaltene particles and a Nikon camera (DS-Fi2) was used for shooting images off the microscope. The *detection times* (i.e. the earliest time to detect particles around 0.5 μm in size)

as a function of heptane concentration were measured from microscopy experiments for each sub-fraction.

Small Angle X-ray Scattering (SAXS): For all scattering experiments asphaltenes were dissolved in toluene. Two different SAXS facilities were utilized in this study: Bruker Nanostar SAXS Equipment at University of Michigan and Advanced Photon Source (APS) in Argonne National Laboratory. For Bruker Nanostar, the X-ray generator was set at 40 kV and 35 mA with 0.5 second per frame and 900 seconds per sample. For APS, X-ray generator was operated at 12 keV and samples were loaded to a quartz flow-through capillary with a 1.5 mm inner diameter. The results from APS are converted to the absolute scale by using toluene as the standard.

5.2.2 Fractionation Experiments

All fractionation experiments for the crude oil and model oil were conducted at or above the instantaneous onset concentration (i.e. the amount of heptane needed to immediately detect asphaltenes instability under optical microscope) in order to avoid slow kinetics and to collect enough asphaltenes for characterization.

5.2.2.1 Separation of Asphaltene sub-Fractions from Crude Oil

50 vol% heptane (\sim instantaneous onset) was added to the crude oil using syringe pump at 5 mL/min flow rate. After 1 hour the entire sample was centrifuged at 3500 rpm for 4 hours using Sorvall Legend X1R centrifuge. The cake was separated from supernatant to generate *Cut_{C1}* asphalttenes. *Cut_{C1}* asphaltenes were washed with heptane and then dried in the oven. The supernatant was stored in a stirred flask to allow remaining asphaltenes to precipitate. As will be discussed in the results section, *Cut_{C1}* asphaltenes has some wax contamination. Similar procedure was repeated after 72, 833 and 2253 hours for generating *Cut_{C2}*, *Cut_{C3}* and *Cut_{C4}*. After separating

Cut_C4, 50 vol% heptane in crude oil sample has almost reached to the thermodynamic equilibrium (micro centrifugation experiments were used as a guideline) and more heptane was added to increase concentration to 75 vol% heptane in crude oil. *Cut_C6* and *Cut_C7* asphaltenes were then generated 1 hour and 1096 hours after heptane addition. At each heptane concentration (i.e., 50 vol% and 75 vol%) after separating the last cut some of the supernatant was used to precipitate soluble asphaltenes by mixing it with heptane in 1:40 volume ratio. The soluble asphaltenes in 50 vol% and 75 vol% are referred to as *Cut_C5* and *Cut_C8* respectively.

In a separate experiment, crude oil was mixed with heptane in 1:40 volume ratio and was kept stirred for 24 hours. The precipitated asphaltenes were then centrifuged at 10000 rpm for an hour. The separated asphaltene cake was washed three times (not Soxhlet wash) with heptane to remove trapped oil. Washed asphaltenes were dried in the oven and are referred to as *Asphaltenes_C*.

5.2.2.2 Separation of Asphaltene sub-Fractions from Model Oil

Model Oil Preparation: Asphaltenes were precipitated out of the crude oil using experimental procedure discussed earlier (i.e. extraction of total asphaltenes). However, before dissolving asphaltenes in toluene, they were Soxhlet washed for 24 hours to ensure that all non-asphaltinic materials such as waxes are washed out (*Asphaltenes_M*). Therefore, due to slight differences in sample preparation, the results from the model oil and crude oil are not directly comparable. The asphaltene content of model oil was 8 wt% asphaltenes in toluene with the instantaneous onset concentration of around 60 vol% heptane.

Fractionation Experiments (Model Oil): 60 vol% heptane was added to the model oil. After 1 day and 25 days the entire sample was centrifuged to generate *Cut_M1* and *Cut_M2* similar to fractionation of crude oil. After separating *Cut_M2*,

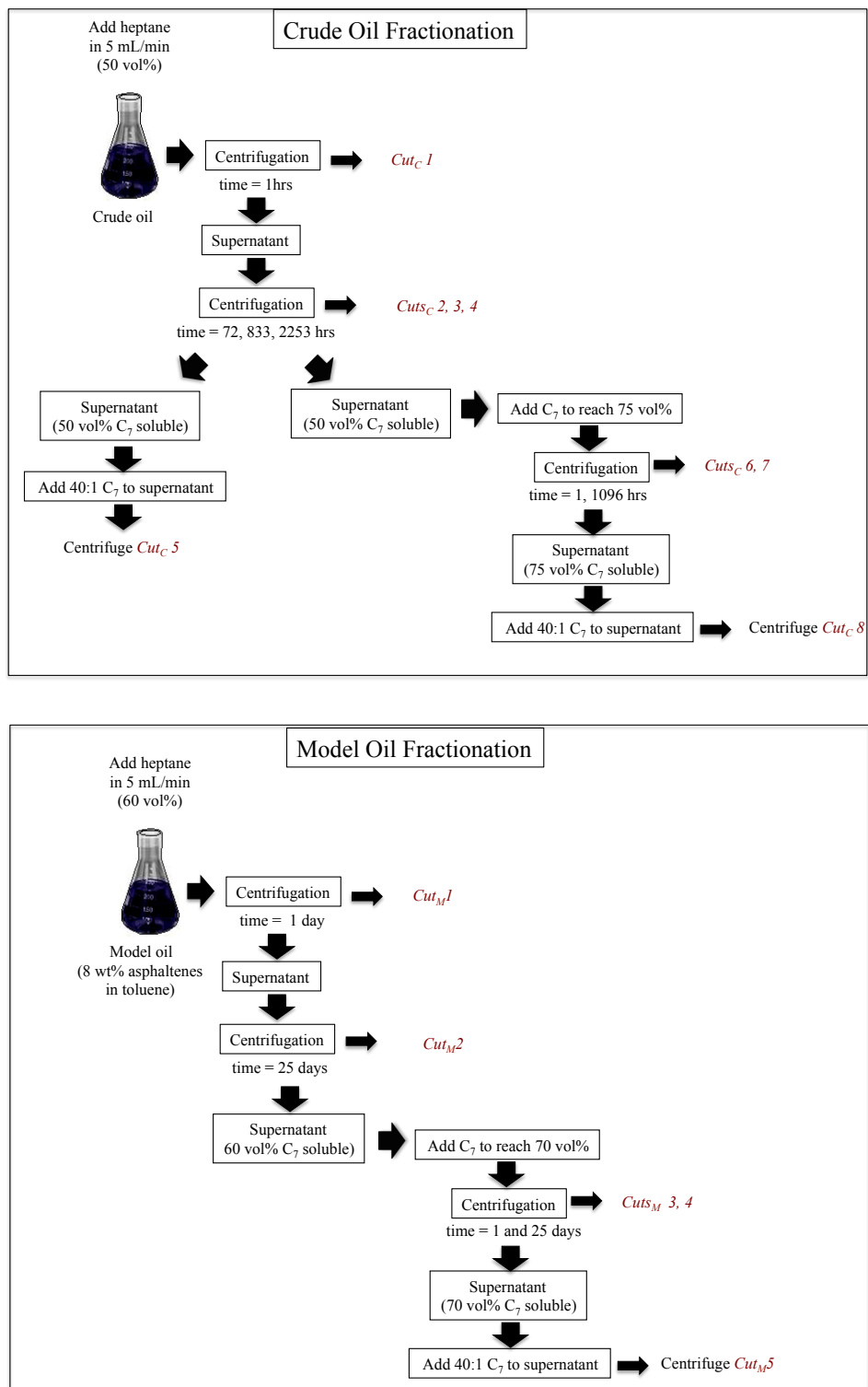


Figure 5.1: Schematic of asphaltene fractionation from crude oil and model oil.

70 vol% heptane was added to the supernatant to generate Cut_M3 and Cut_M4 after 1 day and 25 days. Finally the soluble asphaltenes remaining in the 70 vol% solution were precipitated by adding 1:40 volume ratio heptane to generate Cut_M5 .

In this chapter, subscripts C and M refer to the fractions separated from crude oil and model oil respectively. Figure 5.1 shows a schematic for experimental procedure.

5.3 Results and Discussion

Table 5.1: Elemental composition for crude oil sub-fractions.

#of Cut	wt%					H/C	ppm	
	C	H	N	O	S		Ni	V
Cut_C1	82.86	11.12	0.55	2.70	4.33	1.61	88	237
Cut_C3	80.90	17.48	1.15	2.17	7.70	1.11	172	537
Cut_C4	81.41	7.35	1.11	2.79	7.60	1.08	160	495
Cut_C5	81.18	7.81	1.02	1.82	7.26	1.15	139	442
Cut_C6	81.27	7.77	1.07	2.13	7.48	1.15	148	453
Cut_C7	80.61	7.56	0.98	1.94	7.36	1.13	142	424
Cut_C8	81.07	7.79	1.01	3.79	7.06	1.15	129	394
$Asphaltenes_C$	81.50	7.79	1.05	2.21	7.2	1.15	152	479

5.3.1 Elemental Composition

Table 5.1 shows the carbon, hydrogen, heteroatoms (N, O and S) and metal contents (Ni and V) for different cuts separated from crude oil. The measurements were performed in Shell labs. H/C ratio for asphaltenes is typically around 1-1.2 [9] and for waxes is around 2. Thus, the 1.61 value for H/C ratio of Cut_C1 asphaltenes is much higher than typical values expected for asphaltenes and is likely due to wax contamination and will be discussed in further detail later. Figure 5.2 depicts the H/C ratios, heteroatom contents and metal contents of different cuts. For all cuts (except Cut_C1), no significant difference in H/C ratio is detected. In addition, there

is no correlation between the oxygen content and the stability of the cuts. However, asphaltenes precipitated earlier in each heptane concentration (with the exception of *Cut_{C1}*) have slightly higher nitrogen, sulfur and metal content in their structure compared to the other cuts. Higher heteroatom and metal content would imply higher polarity. Therefore, these findings indicate that asphaltenes that precipitate earlier are slightly more polar compared to other sub-fractions. Also, the asphaltenes precipitated at lower heptane concentrations (i.e. 50 vol%) have higher heteroatom and metal content, an observation in agreement with previous studies [5, 7].

As mentioned earlier, high H/C ratio of *Cut_{C1}* is likely due to wax contamination. Waxes are composed of alkane hydrocarbons and the main driving force for their precipitation is changes in temperature. All our experiments were performed in room temperature, therefore we believe that insoluble waxes were present inside the crude oil before adding heptane (waxes are typically more soluble in heptane than in crude oil). However, due to similar densities of waxes and crude oil, waxes were not separated in pretreatment of crude oil by centrifugation. After heptane addition, due to reduction in the density and the viscosity of the solution, waxes were centrifuged alongside the precipitated asphaltenes. Therefore, all the waxes are likely separated in the first centrifugation after heptane addition (*Cut_{C1}*) and are not expected to contaminate the subsequent cuts.

The H/C ratio of asphaltenes is surprisingly constant even among asphaltenes extracted from different crude oils (i.e. 1-1.2) [9]. Therefore, due to the almost constant H/C ratio among all the cuts, wax/asphaltene content of *Cut_{C1}* can be estimated by assuming that the H/C content of its asphaltenes is identical to the H/C content of other cuts. By using the average H/C ratio of other cuts (1.13) for *Cut_{C1}* and H/C ratio of 2 for waxes, the asphaltene content of *Cut_{C1}* is estimated to be around 44.8% (wax content \sim 55.2%). Waxes are saturated molecules with

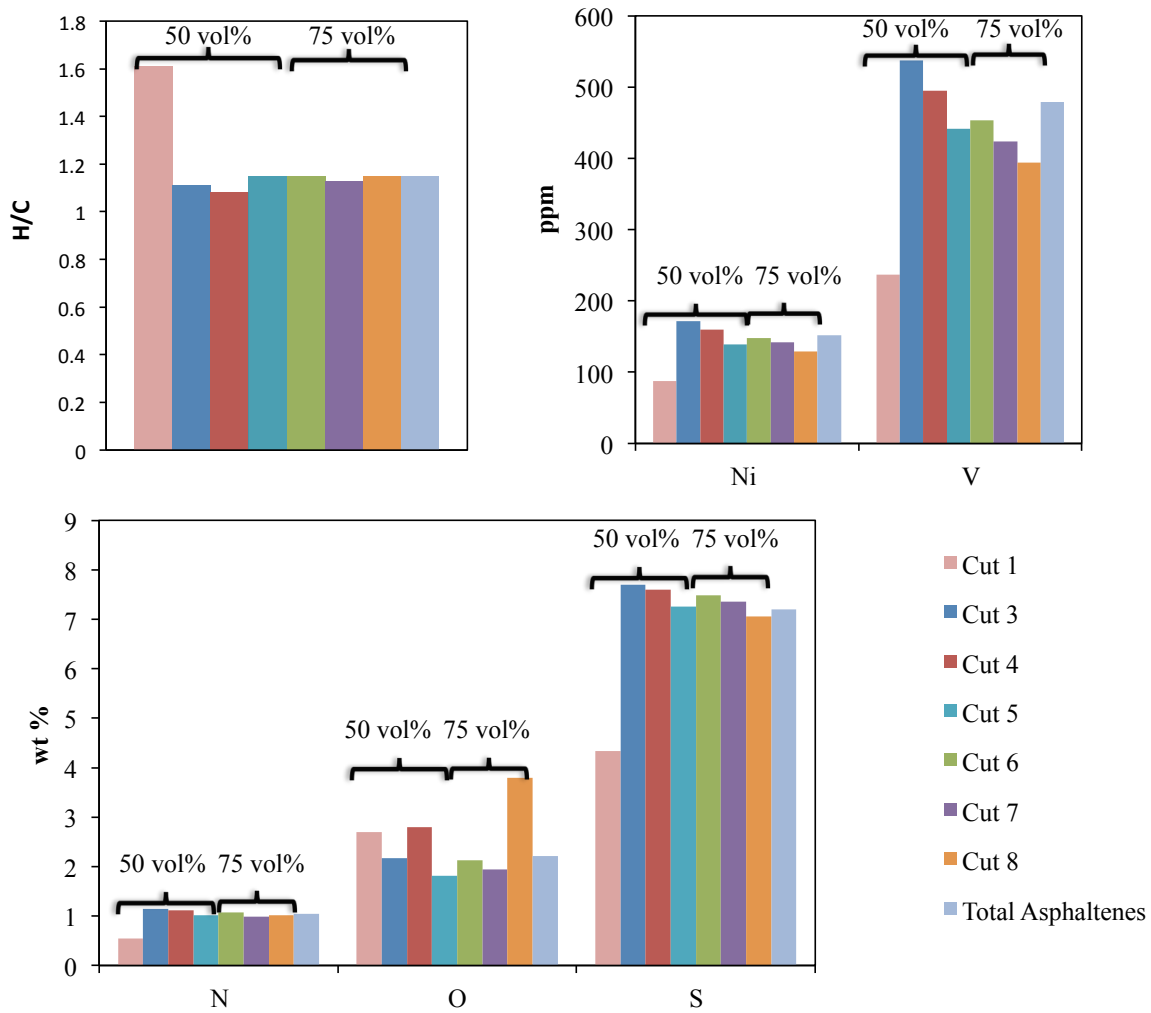


Figure 5.2: Elemental composition for crude oil sub-fractions.

no metals or heteroatoms in their structure. Therefore actual heteroatom and metal content of *Cut_C1* asphaltenes can be estimated from its asphaltene content. Table 5.2 shows the corrected values. After correcting for wax contamination, a clear correlation is observed between the nickel and sulfur content of asphaltenes and their stability. In other words, asphaltenes precipitated first have slightly higher metal and heteroatom content compared to those separated in other cuts. However, such differences are so insignificant that cannot lead to any general conclusions about the relationships between stability and chemical composition. Differences in chemical composition were not investigated for asphaltenes fractionated from the model oil.

Table 5.2: Corrected elemental composition of *Cut_C1*.

#of Cut	wt%					H/C	ppm	
	C	H	N	O	S		Ni	V
<i>Cut_C1</i>	77.0	7.2	1.14	5.6	8.9	1.13	196	529

5.3.2 Small Angle X-ray Scattering (SAXS)

Asphaltenes usually exist in the aggregated form (i.e., nano-particles) even in pure solvents. It is believed that there exists a correlation between the sizes of these nano-particles and the aggregation tendency of their constituent molecules; asphaltenes in larger nano-aggregates are generally thought to be more prone to precipitation, and therefore less stable. Therefore characterizing the size distribution of different asphaltene sub-fractions– in a single solvent– can be used as a tool for evaluating variations in their stability. Different asphaltene cuts from the crude oil and the model oil were dissolved in toluene (1 wt%) separately and were investigated by SAXS. Optical microscopy was used for confirming the dissolution of asphaltenes in the micron scale before scattering experiments. All the samples were soluble in

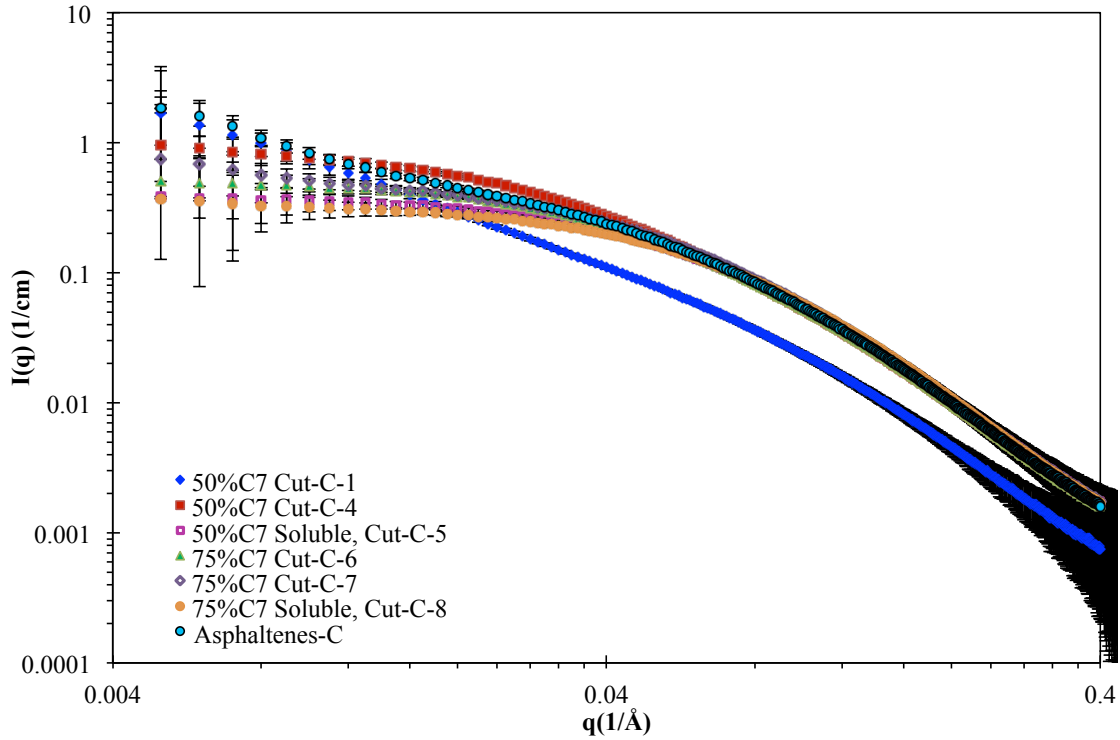


Figure 5.3: **Scattering intensity as a function of scattering vector for crude oil sub-fractions.**

toluene in the micron scale except for Cut_C1 . The insolubility of Cut_C1 was likely due to existence of the insoluble wax. Cut_C1 was therefore centrifuged at 14000 rpm for 10 minutes to separate the insoluble fraction. Figure 5.3 shows scattering results for different cuts from crude oil characterized using APS equipment.

The size of the nano-particles in each fraction is estimated by Guinier approximation:

$$I(q) = I_0 \exp\left(-\frac{(qR_g)^2}{3}\right) \quad (5.1)$$

where I is the scattering intensity, I_0 is the zero angle intensity, $q(1/\text{\AA})$ is the scattering vector and $R_g(\text{\AA})$ is the Guinier radius of gyration. Due to large error bars in

Figure 5.3 for small values of q , the smallest value of q used in the Guinier analysis was around 0.009 ($1/\text{\AA}$). For Cut_C1 , $I(q)$ does not plateau for low values of q (Figure 5.3), suggesting that the asphaltene particles are too large to be characterized by Guinier approximation. Large size of Cut_C1 asphaltenes can be attributed to their higher instability and therefore their higher tendency to form strong associations (i.e. large nano-particles). In addition, it is possible that despite the centrifugation of Cut_C1 sample, some of the larger wax particles are still left in the solution and cause surface scattering. The radius of gyration values for cuts from crude oil are included in Tables 5.3.

Table 5.3: Radius of gyration of crude oil sub-fractions.

Name of fraction	$R_g(\text{\AA})$
50 vol% heptane	
- Cut_C1	-
- Cut_C4	49.7 ± 1.9
- Cut_C5 soluble	31.0 ± 0.5
75 vol% heptane	
- Cut_C6	37.3 ± 0.8
- Cut_C7	36.1 ± 0.7
- Cut_C8 soluble	28.1 ± 0.4
$Asphaltenes_C$	84.1 ± 10.3

These scattering experiments clearly show that for the 50 vol%, asphaltenes that precipitated first come from the larger nano-aggregates in the solution. In addition, asphaltenes precipitated in 50 vol% (i.e., Cut_C1 and Cut_C4) heptane are more unstable than asphaltenes precipitated in 75 vol% heptane (i.e., Cut_C6 and Cut_C7). The sizes of nano-particles present in Cut_C6 and Cut_C7 are identical, suggesting that the properties of their constituent asphaltenes are also identical and the main reason for the precipitation kinetics at 75 vol% is the aggregation of similar type of asphaltenes. Figure 5.4 and Table 5.4 show scattering results and radius of gyration values for

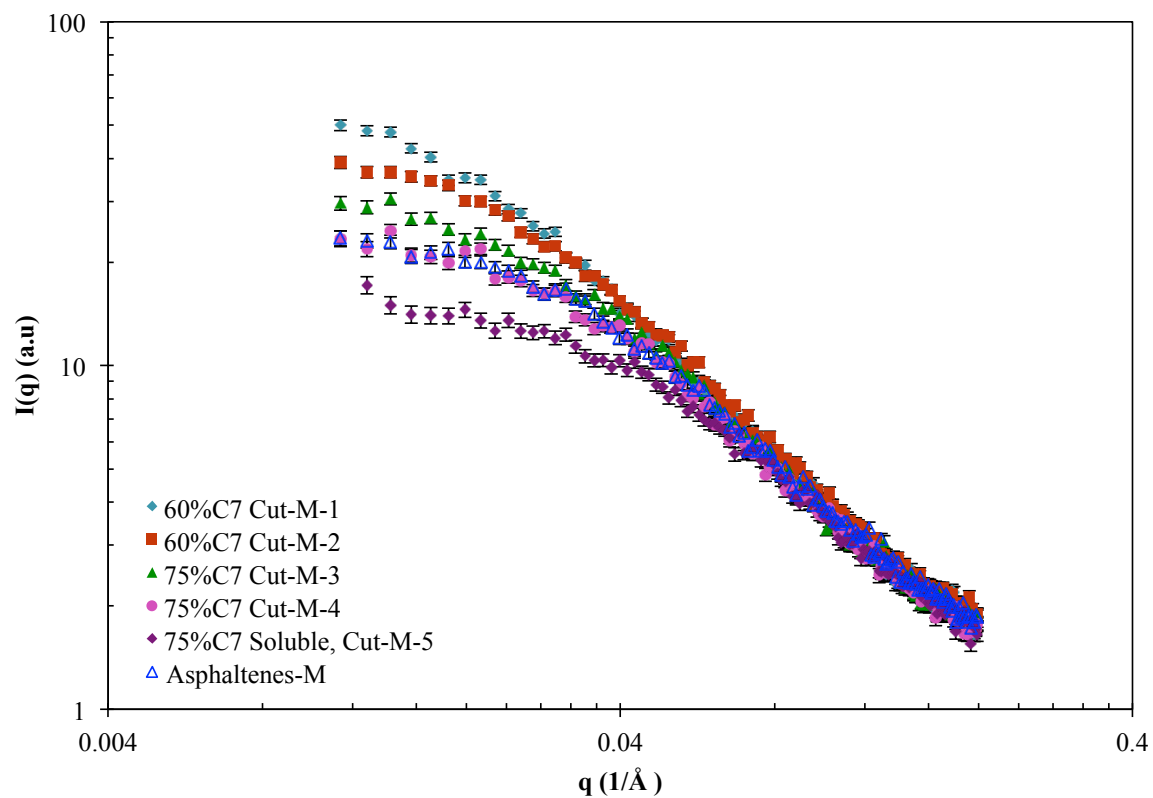


Figure 5.4: Scattering intensity as a function of scattering vector for the model oil sub-fractions.

asphaltenes fractionated from model oil. The results are obtained using the NanoS-tar equipment at the University of Michigan. Similar to the asphaltenes fractionated from the crude oil, the size of nano-particles formed in toluene is consistently smaller for asphaltenes precipitated later in time. Moreover, the size and polydispersity of asphaltenes decreases by increasing the heptane concentration (i.e. 70 vol%).

In summary, the scattering results suggest that properties of asphaltenes precipitated at different times and precipitant concentrations are not identical. In other words, the most unstable asphaltenes precipitate first and an inverse correlation exists between the stability and the precipitation time. By increasing the precipitant concentration (i.e., to 75 vol% in the crude oil or to 70 vol% in the model oil), the polydispersity decreases significantly in both systems and stable asphaltenes with more uniform properties start coming out of the solution.

Table 5.4: Radius of gyration of the model oil sub-fractions

Name of fraction	$R_g(\text{\AA})$
60 vol% heptane	
- $Cut_M 1$	62.1 ± 3.6
- $Cut_M 2$	50.7 ± 2.3
70 vol% heptane	
- $Cut_M 3$	43.6 ± 1.7
- $Cut_M 4$	39.6 ± 1.5
- $Cut_M 5$ soluble	26.9 ± 0.8
$Asphaltenes_M$	35.1 ± 1.1

5.3.3 Microscopy Experiments

Scattering results suggest that the aggregation tendency of asphaltenes varies among different sub-fractions. In the next step, microscopy experiments were utilized to measure the aggregation tendency of each sub-fraction after adding the precipitant. Due to the limited quantity of asphaltenes, microscopy experiments are only

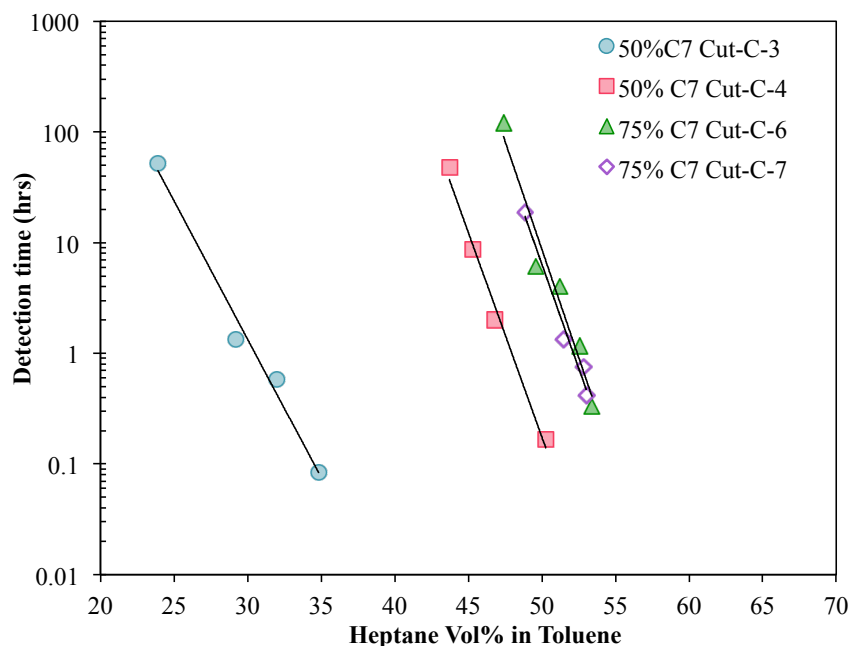


Figure 5.5: **Detection time as a function of heptane concentration for crude oil sub-fractions**

performed for some of the cuts. To perform the experiments 2 wt% of each cut from the crude oil fractionation and 1 wt% of each cut from the model oil fractionation were dissolved in toluene. Figure 5.5 shows the detection time measurements after the addition of heptane for crude oil cuts. Cut_C3 is the one that precipitated the earliest compared to the other cuts shown in Figure 5.5 and has therefore the fastest precipitation rate and the lowest stability.

In addition, precipitation rate of Cut_C4 asphaltenes is faster compared to the Cut_C6 and Cut_C7 . However, no difference in precipitation tendency is observed between Cut_C6 and Cut_C7 . Identical aggregation rates of Cut_C6 and Cut_C7 is in agreement with identical sizes of their nano-particles when dissolved in toluene. It appears that polydispersity plays a significant role in dictating the behavior of asphaltenes at small thermodynamic driving forces (i.e. at low precipitant concentrations) and once

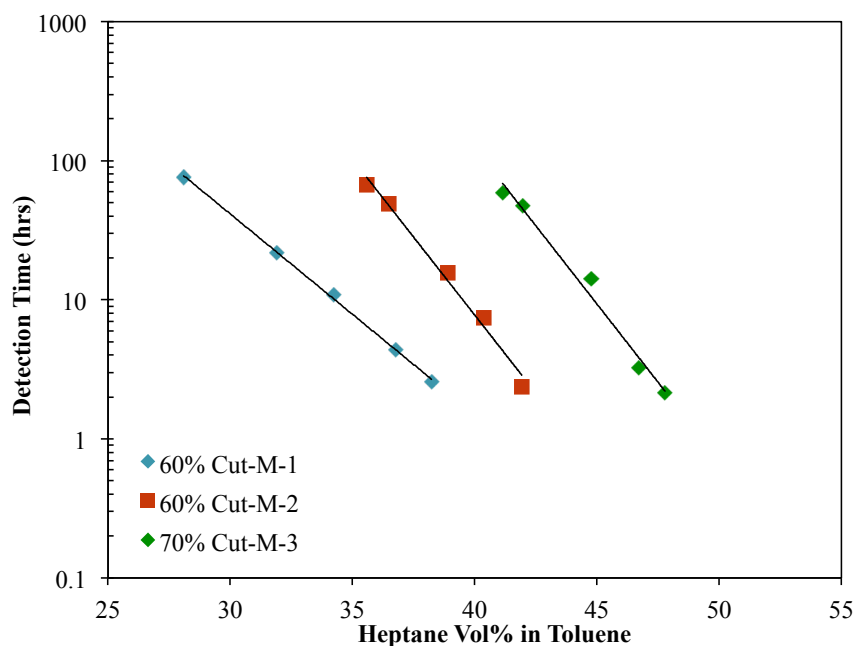


Figure 5.6: **Detection time as a function of heptane concentration for crude oil sub-fractions**

the most unstable asphaltene precipitate out of the solution, the rates are controlled by aggregation of asphaltene with similar properties. Unfortunately, elemental analysis did not show any significant differences in properties, therefore it is unclear at this point, what are the structural properties of most unstable asphaltene (the ones precipitated the earliest). Similar conclusions are valid for asphaltene fractionated from the model oil (Figure 5.6).

Figures 5.5 and 5.6 along with the master curve developed in Chapter II can be used to calculate the solubility parameter distribution in different cuts. Master curve correlates the *detection time* to the difference in the solubility parameter of asphaltene and the solution and with known detection times it can be used to obtain the solubility parameter of asphaltene. Figure 5.7 shows the agreement between the measurements and the master curve.

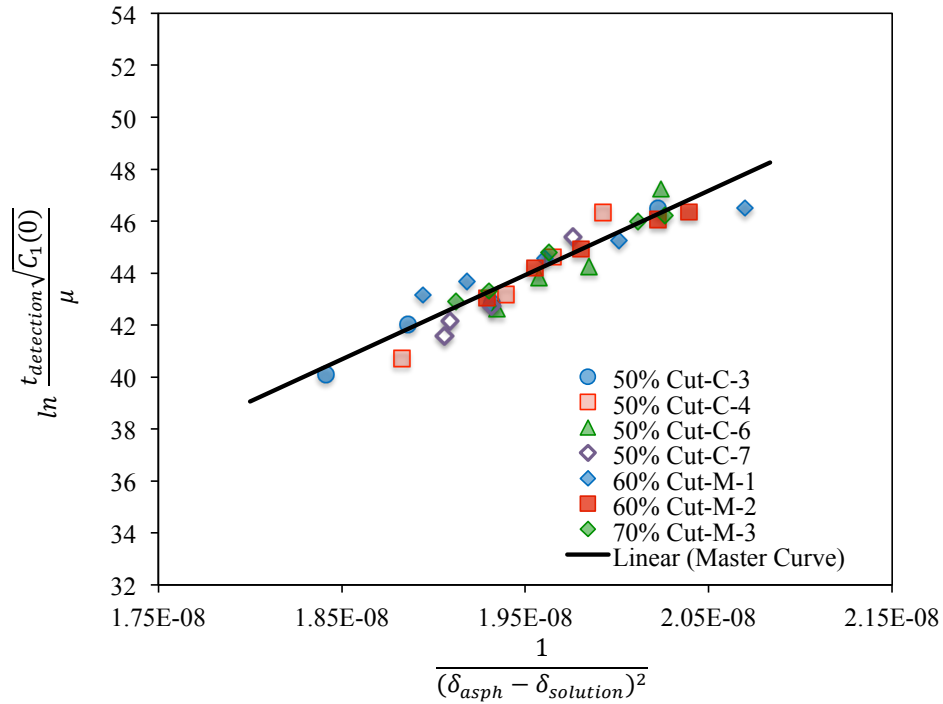


Figure 5.7: **Plot of $\ln(t_{\text{detection}}\sqrt{C_1(0)}/\mu)$ vs. $1/(\delta_{\text{asph}} - \delta_{\text{solution}})^2$ for crude oil and model oil sub-fractions compared to the master curve.**

Table 5.5: Solubility parameter of crude oil sub-fractions obtained from Figure 5.7.

Name of fraction	Solubility Parameter (MPa ^{0.5})
50 vol% heptane	
- <i>Cut_C3</i>	24.59
- <i>Cut_C4</i>	24.03
75 vol% heptane	
- <i>Cut_C6</i>	23.86
- <i>Cut_C7</i>	23.90

The solubility parameters obtained from Figure 5.7 are shown in Tables 5.5 and 5.6. For samples fractionated from the crude oil, there is a significant change in solubility parameters from Cut_C3 to Cut_C7 ($\sim 0.7 \text{ MPa}^{0.5}$). The solubility parameter of heptane and toluene are 15.2 and 18.3 $\text{MPa}^{0.5}$ respectively and only 3 units of difference in their solubility parameters dictates the difference between a solvent and a precipitant. Therefore, a difference of 0.7 $\text{MPa}^{0.5}$ in solubility parameter of asphaltenes from Cut_C3 to Cut_C7 is considered to be significant. For cuts fractionated from the model oil, the variations of the solubility parameters falls into a narrower range ($\sim 0.4 \text{ MPa}^{0.5}$).

Table 5.6: Solubility parameter of model oil sub-fractions obtained from Figure 5.7.

Name of fraction	Solubility Parameter ($\text{MPa}^{0.5}$)
60 vol% heptane - Cut_M1	24.38
- Cut_M2	24.20
70 vol% heptane - Cut_M3	24.05

5.4 Conclusions

The properties of asphaltenes precipitated at different times and precipitant concentrations were investigated in this study. No significant differences in the chemical composition of different cuts was detected, and only slight differences in metal contents and some of heteroatom contents were observed. In addition, it was shown that different asphaltene sub-fractions tend to form different sizes of nano-aggregates and the ones precipitating first form the largest nano-particles in toluene. Moreover, despite small changes in the chemical composition, the aggregation rates measured from

microscopy experiments varied significantly at small driving forces, indicating that asphaltenes are extremely polydispersed. At higher driving forces, the polydispersity decreases significantly.

Due to the extreme complexity of asphaltenes, the bulk properties such as elemental composition do not provide adequate information about the instability of asphaltene sub-fractions and instead aggregation rates and estimation of solubility parameter distribution appears to be a more appropriate way to characterize differences in properties of asphaltenes. In addition, the findings presented in this chapter support the hypothesis that asphaltenes precipitating first (i.e. ones precipitating in the slow kinetics region) are in fact the most problematic fractions. Therefore, it is extremely important to be able to understand and predict their behavior under different experimental conditions which have been the main focus of this thesis.

Bibliography

- [1] O. León, E. Rogel, J. Espidel, and G. Torres. Asphaltenes: structural characterization, self-association, and stability behavior. *Energy Fuels*, 14(1), 2000.
- [2] J. Wang and J.S. Buckley. Asphaltene stability in crude oil and aromatic solvents—the influence of oil composition. *Energy Fuels*, 17, 2003.
- [3] J.A. Calles, J. Dufour, J. Marugán, J.L. Peña, R. Giménez-Aguirre, and D. Merino-García. Properties of asphaltenes precipitated with different n-alkanes. a study to assess the most representative species for modeling. *Energy Fuels*, 22, 2008.
- [4] D. Merino-Garcia and S.I. Anderson. Application of isothermal titration calorimetry in the investigation of asphaltene association. In O.C. Mullins, A.G. Marshall, E.Y. Sheu, and A. Hammami, editors, *Asphaltene, Heavy Oils and Petroleomics*. Springer New York, 2007.
- [5] P. Wattana. *Precipitation and Characterization of Petroleum Asphaltenes*. PhD thesis, University of Michigan, 2004.
- [6] P. Wattana and H.S. Fogler. Characterization of polarity-based asphaltene subfractions. *Energy Fuels*, 2005.
- [7] Tabish Maqbool. *Understanding the Kinetics of Asphaltene Precipitation from Crude Oils*. PhD thesis, University of Michigan, 2011.
- [8] P. Matthew Spiecker, Keith L. Gawrys, and Peter K. Kilpatrick. Aggregation and solubility behavior of asphaltenes and their subfraction. *Journal of Colloid and Interface Science*, 267, 2003.
- [9] James G. Speight. *The Chemistry and Technology of Petroleum*. CRC Press, fourth edition, 2006.

CHAPTER VI

Conclusions

In this dissertation the key factors effecting the aggregation behavior of asphaltenes at small thermodynamic driving forces are investigated. It is shown that the solvent, asphaltene concentration and the precipitant can influence the precipitation and aggregation kinetics to varying extents. Overall, the effect of solvent is found to be more prominent. On the other hand, some interesting trends for the roles of asphaltene concentration and chemical identity of precipitant are observed which highlight the importance of self-stabilization and polydispersity of asphaltenes on their aggregation and precipitation tendencies.

The aggregation behavior of asphaltenes for different solvents and crude oils is investigated in Chapter II mainly by using optical microscopy. The results demonstrate that precipitation kinetics strongly depends on the properties of the crude oil or the solvent under investigation. To quantitatively explain this behavior, a novel aggregation model based on Smoluchowski's population balance approach is developed. Our analysis reveals that the detection times measured from optical microscopy can be estimated from the number concentration of unstable asphaltenes, viscosity and collision efficiency (i.e. coagulation efficiency). Due to the complexity of asphaltenes and their unknown structure, the exact type and magnitude of forces involved in the

aggregation process are unknown. Therefore a simple form is proposed to predict the changes in collision efficiency. The proposed correlation relates the collision efficiency to the difference in the solubility parameters of asphaltenes and the solution and can successfully explain the differences in aggregation behavior of asphaltenes in different solvents and crude oils. With this new model, all aggregation curves collapse onto a single master curve that can be utilized as a tool for obtaining the solubility parameters of the most unstable asphaltenes for each asphaltene type.

In Chapter III the effect of asphaltene concentration on their precipitation rate is investigated. It is intuitively expected from the literature that the nature and strength of interparticle forces between aggregating asphaltenes do not change by changing their concentration above 1 wt%. Therefore the collision efficiency is expected to remain constant and the aggregation rate is simply expected to increase by increasing the number of aggregating particles. However, the microscopy experiments revealed that the aggregation rate of asphaltenes passes through a maximum at around 1 wt%. In other words, the precipitation rate increases by increasing the concentration up to 1 wt% (as expected) and then decreases upon a further increase in asphaltene concentration. This interesting phenomenon has not been reported for any other system and it is believed to be due to a change in the degree of interparticle interactions between asphaltenes as their concentration increases. Although the detailed picture of such changes are unknown at this point, we believe this behavior is due to the existence of soluble asphaltenes remaining in the solution. The soluble asphaltenes can be viewed as being part of the solvent and can therefore increase the overall solubility parameter of the solution. From the model developed in Chapter II, any increase in solubility parameter of solution results in smaller aggregation tendency. Therefore, the results can be easily explained by the competing effects of the changes in number concentration of aggregating asphaltenes and changes in their

aggregation tendency. At concentrations below 1 wt%, the increase in number concentration overcomes the increase in solubility parameter (small quantity of soluble asphaltenes to alter the solvency power). However, at concentrations above 1 wt%, precipitation rates are dictated by the changes in the collision efficiency (i.e. change in the solubility parameter). The self-stabilizing effect of asphaltenes is neglected in all existing models and is successfully predicted using the analysis developed in Chapter II.

The effect of different *n*-alkane precipitants on the kinetics of precipitation is investigated in Chapter IV. By increasing the chain length of the *n*-alkane precipitant—i.e. the carbon number—, both the viscosity and the solubility parameter of the solution increases and as a result, the precipitation rate is expected to decrease. However, the actual behavior of the system is more subtle. Indeed, the precipitation rate either remains constant, or increases, or passes through a maximum as *n* increases. This behavior can be explained by accounting for the polydispersity of asphaltenes. Due to their higher solubility parameters, precipitants with longer chains are believed to be weaker. Therefore they tend to precipitate the more unstable asphaltenes with higher average solubility parameter. The aggregation tendency is controlled by the difference in solubility parameters of asphaltenes and solution surrounding them and thus depending on the magnitude of differences in solubility parameters of asphaltenes and precipitants, the precipitation rate can either increase or decrease. The findings from Chapter IV show that the polydispersity of asphaltenes can be characterized using a distribution of solubility parameters and our model successfully predicts the increasing trend in the solubility parameter of precipitated asphaltenes as a function of an increase in *n*. The solubility parameter distribution obtained from the model can also successfully predict the precipitation rate of asphaltenes in blends of different *n*-alkane precipitants (blends of two, three, four and five precipitants are investigated).

Finally, Chapter V provides direct experimental evidence for the importance of studying asphaltene kinetic at weak thermodynamic driving forces. The asphaltenes are fractionated into smaller sub-fractions based on the time that it takes for them to aggregate to a separable size ($\sim 0.2\text{--}0.5\ \mu\text{m}$) at identical and different driving forces (i.e. heptane concentration). The elemental composition of different asphaltene sub-fractions shows minor differences in their chemical composition. Our findings suggest that asphaltenes precipitated earlier are more polar (i.e., with higher metal and heteroatom content). Moreover, SAXS and microscopy experiments clearly show that asphaltenes that precipitate first are the ones with the highest aggregation tendency and solubility parameter. Therefore, they are expected to be the most problematic fraction of total asphaltenes.

The fractionation approach utilized in Chapter V allowed us to investigate the stability of each cut independently. In reality however, asphaltenes that precipitate under stronger driving forces also include the ones that would have precipitated under weaker driving forces as well. As a result, one might expect that the asphaltene-related problems will be more severe due to the larger quantity of total asphaltenes that would precipitate under strong driving forces. However, as discussed in Chapter III, the presence of more stable asphaltenes tend to increase the stability of the less stable fractions. Therefore larger mass of more stable and less stable asphaltenes is not necessarily more problematic than the smaller fraction of unstable asphaltenes. For example, in the case of deposited asphaltenes, the solvent remediation is more likely to be effective in removing the asphaltenes deposited at stronger driving forces compared to the ones that have deposited at weaker driving forces. It should be emphasized that this discussion does not mean that operating at strong driving forces is not problematic. In general, it is important to avoid operating at any conditions that can result in instability and therefore deposition of asphaltenes. However, investigating

the destabilization of asphaltenes in strong driving forces can help in predicting only a **fraction** of potential problems but studying asphaltenes behavior in weak driving forces provides the lower limit for the instability and can help in identifying **all** of problematic operational conditions.

CHAPTER VII

Future Work

7.1 Studying Asphaltene Model Compounds

As has been discussed throughout this thesis, asphaltenes are a complex solubility class composed of more than 7000 unique molecules [1] with strong tendency for self-association and phase separation from crude oil. The general consensus is that asphaltenes are composed of rigid polyaromatic cores surrounded by flexible alkyl side chains. The core-core interactions are considered to be the main intra-asphaltene attractive forces that are countered by the steric repulsion emanating from side chains. The magnitude of attraction and repulsion forces are controlled by various factors such as the size of polyaromatic cores and the lengths and configurations of alkyl side chains [2]. However, since the structural details and the polydispersity of asphaltenes are unknown, it is extremely difficult to quantitatively characterize the attractive and repulsive forces that are in play during their aggregation and precipitation.

In this thesis, a simple phenomenological approach is proposed for estimating the effectiveness of collisions between unstable asphaltenes. Our model captures the asphaltenes behavior at ambient conditions reasonably well. However because of the complexity of asphaltenes, it is difficult to explain why such simple correlations can

work so well. In addition it is not clear if such correlations accurately represent the types of interactions involved in the aggregation process. Studying model compounds with known structures and controlled polydispersity can help us better understand the process and address some of these unanswered questions. Existing theories for attractions and steric stabilization can be utilized for estimating the range and strength of interactions between asphaltenes and help in testing the validity of the theories that correctly describe the behavior of asphaltenes model compounds. One can start by adding alkyl side chains of different lengths at different locations of the aromatic core like coronene. The stability and destabilization of model compounds at different conditions (e.g., pure solvent or at different ratios of solvent/precipitant) can then be investigated using techniques such as XRD, SAXS, SANS or NMR. Despite the advantages of model compounds over asphaltenes, it should be mentioned that some of the asphaltenes unique characteristics could simply be due to their extreme polydispersity and not due to structural details of individual molecules. Therefore, one should keep in mind that experiments on model compounds might not result in behaviors similar to asphaltenes.

7.2 Further Investigating the Polydispersity of Asphaltenes

The nontrivial behavior of asphaltenes in different *n*-alkanes in Chapter IV is attributed to their polydispersity. This hypothesis can be further investigated by fractionating asphaltenes precipitated by different *n*-alkanes and studying the aggregation tendency of each fraction separately. The instability of asphaltene sub-fractions is expected to increase by increasing the carbon number of *n*-alkane precipitant. The aggregation tendency and the solubility parameter of each fraction can be measured in toluene-heptane mixtures. The solubility parameter distribution from toluene-

heptane can be compared to the values obtained from the approach presented in Chapter IV.

7.3 Precipitation Kinetics in Blend of Incompatible Crude Oils

One of the main reasons for the destabilization of asphaltenes in the oil industry is the blending of incompatible crude oils. Blending different crude oils is a common process in the oil industry, which is carried out either to improve mixture properties or to reduce transportation costs [3, 4]. However, blending of crude oils might change the stability of asphaltenes in the mixture and can cause problems such as fouling in the pipelines and refinery equipments [5]. Our preliminary results indicate that blend of incompatible crude oils show similar behavior in terms of precipitation kinetics as the crude oils mixed with a precipitant such as heptane. Figure 7.1 shows the detection time plot for the blend of crude A and L1 crude oil at different ratios. L1 is a paraffinic crude oil with an asphaltene content of approximately 0.03 wt% while crude A has an asphaltene concentration of 3.25 wt%. L1 crude oil appears to be acting as a precipitant for asphaltenes in crude A. This behavior is not surprising because L1 is a paraffinic oil with high concentration of *n*-alkanes.

The initial results show that kinetic effects exist in blends of incompatible crude oils. Neglecting these effects could lead to significant economic and operational problems. In cases where blending occurs between two types of oils only, one can easily perform microscopy experiments similar to those explained in this thesis. However, if three or more different types of oils are to be blended, the number of possible combinations will be too large for the experimental approach to be practical. Consequently, there is a need for predictive models for foreseeing the kinetic behavior of such blends

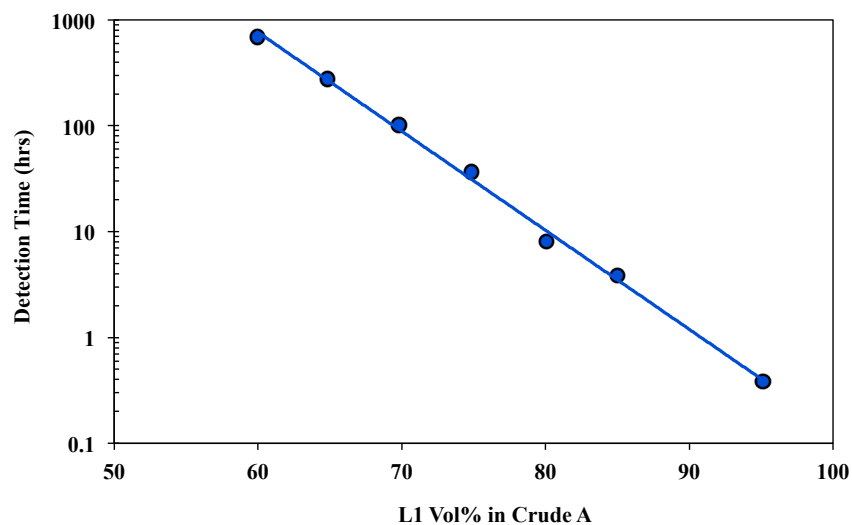


Figure 7.1: **Detection time as a function of blend composition for blends of incompatible oils.**

and the validity of aggregation model developed in this thesis can be investigated for blends of incompatible crude oils at different ratios.

7.4 Precipitation Kinetics in Live Oils

Pressure depletion is one of the major reasons for asphaltene precipitation and deposition during oil production. Expansion of light ends (i.e. dissolved gas) due to reduction in pressure, decreases the solubility parameter of the solution and can therefore result in asphaltene destabilization [6]. Although laboratory experiments at high pressures are typically challenging, it is interesting from an operational point of view to investigate the existence of precipitation kinetics for pressure destabilization. High pressure experiments can be performed in PVT cells equipped with laser-based particle detection systems [7] or high pressure microscopes [6]. If precipitation kinetics in these systems are similar to precipitations kinetics in oil-precipitant mixtures, the

validity of the model developed in this thesis can be tested for these systems as well. The solubility parameter of live oils can be obtained using an equation of state or from the correlations between the refractive index and solubility parameter by knowing the amount of dissolved gas [8–10].

Bibliography

- [1] Geoffrey C. Klein, Sunghwan Kim, Ryan P. Rodgers, Alan G. Marshall, and Andrew Yen. Mass spectral analysis of asphaltenes. ii. detailed compositional comparison of asphaltenes deposit to its crude oil counterpart for two geographically different crude oils by esi ft-icr ms. *Energy Fuels*, 20, 2006.
- [2] Shengqun Wang, Jianjun Liu, Liyan Zhang, Jacob Masliyah, and Zhenghe Xu. Interaction forces between asphaltene surfaces in organic solvents. *Langmuir*, 26, 2010.
- [3] S. Li, J. Liu, B. Shen, X. Xu, Q. Fan, J. Chen, and G. Zhao. Distillation yields from blending cabinda crude oil and oman crude oil. *Petroleum Science and Technology*, 24, 2006.
- [4] N. Shigemoto, R.S. Al-Maamari, B.Y. Jibril, and A. Hirayama. A study of the effect of gas condensate on the viscosity and storage stability of omani heavy crude oil. *Energy Fuels*, 20, 2006.
- [5] W.E.M. Schermer, P.M.J. Melein, and F.G.A.V.D. Berg. Simple techniques for evaluation of crude oil compatibility. *Petroleum Science and Technology*, 22, 2004.
- [6] A. Hammami and J. Ratulowski. Precipitation and deposition of asphaltenes in production systems: A flow assurance overview. In O. C. Mullins, A. Hammami E. Y. Sheu, and A. G. Marshall, editors, *Heavy Oils, and Petroleomics*, pages 617—660. Springer New York, 2007.
- [7] A. Hammami, C. H. Phelps, T. Monger-McClure, and T. M. Little. Asphaltene precipitation from live oils: an experimental investigation of onset conditions and reversibility. *Energy Fuels*, 14, 2000.
- [8] Sylvain Verdier, Diep Duong, and Simon I. Andersen. Experimental determination of solubility parameters of oils as a function of pressure. *Energy Fuels*, 19, 2005.
- [9] Sylvain Verdier and Simon Ivar Andersen. Internal pressure and solubility parameter as a function of pressure. *Fluid Phase Equilibria*, 231, 2005.

- [10] Julian Y. Zuo, O. C. Mullins, Denise Freed, and Dan Zhang. A simple relation between solubility parameters and densities for live reservoir fluids. *J. Chem. Eng. Data*, 55, 2010.

APPENDICES

APPENDIX A

Analytical Solution for Smoluchowski's Equation and Estimating Detection Time

A.1 Analytical Solution

Smoluchowski's Equation is given by ([1]):

$$\frac{dC_k}{dt} = \frac{1}{2} \sum_{i+j=k} K_{ij} C_i C_j - C_k \sum_{i \geq k} K_{ik} C_i \quad (\text{A.1})$$

where C_k is the number concentration of particle composed of k monomers and $C_1(0)$ is the number concentration of monomers (i.e. primary nano-particles) at $t = 0$. For a constant collision kernel, Smoluchowski's Equation has an analytical solution. Constant K_{ij} (i.e. size independent kernel [2]) can be estimated from following correlation (Chapter II):

$$K_{ij} = \frac{8k_B T}{3\mu} \beta \quad (\text{A.2})$$

where k_B is the Boltzmann constant, μ is the viscosity, T is the temperature and β is the collision efficiency. We want to solve Smoluchowski's Equation with a constant kernel analytically. We first define the dimensionless C_k as follows:

$$C'_k = \frac{C_k}{C_1(0)} \quad (\text{A.3})$$

Replacing C_k s with $C'_k C_1(0)$ in Equation A.1 we get:

$$\frac{dC'_k}{dt} = \frac{1}{2} C_1(0) \sum_{i+j=k} K_{ij} C'_i C'_j - C'_k C_1(0) \sum_{i \geq k} K_{ik} C'_i \quad (\text{A.4})$$

which must be solved alongside the following initial conditions for C'_1 :

$$C'_1(0) = \frac{C_1(0)}{C_1(0)} = 1 \quad (\text{A.5})$$

We define variable α as follows and substitute it in Equation A.4:

$$\alpha = K_{ij} C_1(0) = \frac{8k_B T}{3\mu} \beta C_1(0) \quad (\text{A.6})$$

$$\frac{dC'_k}{dt} = \frac{1}{2} \sum_{i+j=k} \alpha C'_i C'_j - C'_k \sum_{i \geq k} \alpha C'_i \quad (\text{A.7})$$

We then assume that the solution for Equation A.7 has the following mathematical form [1]):

$$C'_k(t) = A(t) [a(t)]^{k-1} \quad (\text{A.8})$$

Differentiating Equation A.8 and replacing it in Equation A.7 we get:

$$\frac{1}{C'_k} \frac{dC'_k}{dt} = \frac{1}{2C'_k} \alpha \sum_{i+j=k} C'_i C'_j - \alpha \sum_{i \geq k} C'_i = \frac{\dot{A}a^{k-1} + A\dot{a}(k-1)a^{k-2}}{A(t)[a(t)]^{k-1}} \quad (\text{A.9})$$

Substituting C 's from Equation A.8 in Equation A.9, it becomes:

$$\frac{\dot{A}}{A} + (k-1)\frac{\dot{a}}{a} = \frac{\alpha}{2}(k-1)\frac{A}{a} - \alpha A \sum_{i=1}^{\infty} a^{i-1} \quad (\text{A.10})$$

with the following initial conditions:

$$C'_1(0) = 1 \implies A(0) = 1$$

$$C'_k(0) = 0 \implies A(0) = 0$$

From Equation A.10 we get:

$$\frac{dA}{dt} = -\frac{\alpha A^2}{1-a} \implies \alpha = -\frac{(1-a)}{A^2} \frac{dA}{dt} \quad (\text{A.11})$$

and:

$$\frac{da}{dt} = -\frac{\alpha}{2}A \implies \alpha = \frac{2}{A} \frac{da}{dt} \quad (\text{A.12})$$

Combining Equations A.11 and A.12:

$$-(1-a)dA = 2Ada \implies \frac{dA}{A} = -2\frac{da}{1-a} \implies \ln A = \ln(1-a)^2 + a_1 \quad (\text{A.13})$$

From the initial conditions for A and a we get the constant a_1 in Equation A.13:

$$A(0) = 1 \text{ and } a(0) = 0 \implies a_1 = 0 \implies A(t) = (1 - a(t))^2 \quad (\text{A.14})$$

By replacing $A(t)$ in Equation A.12 we get $a(t)$:

$$\frac{da}{dt} = \frac{\alpha}{2}(1 - a)^2 \text{ and } a(0) = 0 \implies a(t) = \frac{\alpha t}{\alpha t + 2} \quad (\text{A.15})$$

Combining Equations A.14 and A.15 we get:

$$A(t) = \frac{4}{(\alpha t + 2)^2} \quad (\text{A.16})$$

Combining Equations A.8, A.15 and A.16, C_k can be calculated from the following correlation (analytical solution):

$$\frac{C_k(t)}{C_1(0)} = \frac{4}{(\alpha t + 2)^2} \left[\frac{\alpha t}{\alpha t + 2} \right]^{k-1} \quad (\text{A.17})$$

where $C_1(0)$ is the number concentration of particles at $t = 0$.

A.2 Estimating Detection Time

For our experiments minimum detectable size under optical microscope is around $0.5 \mu\text{m}$. In order to detect asphaltenes, the number concentration of particles at microscope's detection limit (i.e., $0.5\mu\text{m}$) should have reached a minimum value (i.e., C_M):

$$C_{k_0}(t_{\text{detection}}) \text{ at } 0.5 \mu\text{m} = C_M \quad (\text{A.18})$$

where k_0 is the number of primary nano-particles in the structure of an aggregate with size $0.5 \mu\text{m}$.

Substituting Equation A.18 in A.17 for detection time we get:

$$\frac{C_{k_0}(t)}{C_1(0)} = \frac{C_M}{C_1(0)} = \frac{4}{(\alpha t_{\text{detection}} + 2)^2} \left[\frac{\alpha t_{\text{detection}}}{\alpha t_{\text{detection}} + 2} \right]^{k_0-1} \quad (\text{A.19})$$

Let $\alpha t = t'$:

$$\begin{aligned} \frac{C_M}{C_1(0)} &= \frac{4}{(t' + 2)^2} \left[\frac{t'}{t' + 2} \right]^{k_0-1} = f(t')g(t') \\ f(t') &= \frac{4}{(t' + 2)^2} \text{ and } g(t') = \left[\frac{t'}{t' + 2} \right]^{k_0-1} \end{aligned} \quad (\text{A.20})$$

It is clear from Equation A.20 that the solution of t' depends on the values of C_M , k_0 and $C_1(0)$. C_M and k_0 are the characteristics of the detection point and therefore should be the same for all our samples. We are also assuming that $C_1(0)$ is a constant for the range of heptane concentrations investigated in each crude oil and model oil. Due to dilution effect resulting from heptane addition, the change in number concentration of the unstable asphaltenes (i.e. $C_1(0)$) could be insignificant. In order to solve Equation A.20, C_M and k_0 constants need to be known. k_0 can be estimated by knowing the size of primary nano-particles (typical size of asphaltene clusters is around 5 nm [3]) from following equation [4]:

$$k_0 \approx \left(\frac{d_a}{d_p} \right)^{Df} \approx \left(\frac{0.5 \times 10^{-6}}{5 \times 10^{-9}} \right)^{2.1} = 15848 \approx 15800 \quad (\text{A.21})$$

k_0 : number of primary nano-particles in the aggregates of size $0.5 \mu\text{m}$

D_f : fractal dimension (around 2.1 for reaction-limited aggregation [5])

d_p : size of aggregate ($0.5 \mu\text{m}$)

d_a : size of primary nano-particles

C_M is the minimum number of particles with size $0.5 \mu\text{m}$. Some rough calculations can be carried out to obtain a reasonable estimate for C_M .

Microscopy experiments are done using a small drop of solution placed between two microscopy slides ($22 \times 22 \text{ mm}$ with the surface area of 0.000484 m^2). The volume of one drop is around: $5 \times 10^{-8} \text{ m}^3$. Assuming that the droplet covers the entire microscopy slide, the thickness of sample between two slides is estimated to be around 0.1033 mm . An analysis of the microscopy pictures at detection times has revealed that around 30 of $0.5 \mu\text{m}$ particles need to be detectable in the field view for a sample to be called precipitated. Field of view approximately spans an area of $3.06 \times 10^4 \mu\text{m}^2$. Therefore the volume monitored under field view is around $3.16 \times 10^{-12} \text{ m}^3$. A value of $C_M = 10^{13}$ results in around 31 particles in the field of view. Therefore all calculations in this appendix are carried out using $C_M = 10^{13}$.

In addition to the values of C_M and k_0 , $C_1(0)$ also needs to be known for each crude oil and model oil. To calculate $C_1(0)$ (the number concentration of primary particles at $t = 0$), it is assumed that asphaltene primary particles are clusters composed of eight nano-aggregates, and nano-aggregates are composed of six asphaltene molecules with average molecular weight of 750 [3]. If the volume fraction of unstable asphaltene in solution is b (m^3 of asphaltene/ m^3 of solution), then $C_1(0)$ can be calculated using following formula:

$$\begin{aligned}
C_1(0) &= b \frac{m^3 \text{ asphaltenes}}{m^3 \text{ solution}} \frac{1200 \text{ kg asphaltenes}}{1 m^3 \text{ asphaltenes}} \frac{1000 \text{ g}}{1 \text{ kg}} \frac{1 \text{ mol asphaltenes}}{750 \text{ g}} \\
&\frac{N_A(\text{Avegado number})}{6 (\# \text{ of molecules in nano - aggregate})} \\
&\frac{1}{8 (\# \text{ of nano - aggregates in cluster})} = \\
&2.00738 \times 10^{25} b \frac{\# \text{ of primary particles (asphaltene clusters)}}{m^3 \text{ solution}} \\
C_1(0) &= 2.00738 \times 10^{25} b, \text{ where } b \text{ is : } \frac{m^3 \text{ asphaltenes}}{m^3 \text{ solution}} \tag{A.22}
\end{aligned}$$

Knowing $C_1(0)$, k_0 and C_M , Equation A.20 can be solved to obtain t' using trial and error. Table A.1 shows the solution for t' of ten different model oils and crude oils presented in Chapter II.

Table A.1: Analytical solution for results presented in Chapter II.

Name of Sample	$C_1(0)$	$t' (s)$	f'	g'
K1 Asphaltenes in 1-MN	1.82×10^{23}	253155	6.24×10^{-11}	0.882
B1 Asphaltenes in 1-MN	2.15×10^{23}	277086	5.21×10^{-11}	0.892
K1 Asphaltenes in Toluene	2.78×10^{23}	317138	3.98×10^{-11}	0.905
B1 Asphaltenes in Toluene	3.45×10^{23}	355063	3.17×10^{-11}	0.915
B1 asphaltenes in Toluene + 1-MN	2.57×10^{23}	304274	4.32×10^{-11}	0.901
Crude Oil A	2.51×10^{23}	300872	4.42×10^{-11}	0.900
Crude Oil B	3.03×10^{22}	92868	4.64×10^{-10}	0.711
Crude Oil C	6.70×10^{22}	147028	1.85×10^{-10}	0.806
Crude Oil D	8.63×10^{22}	169221	1.40×10^{-10}	0.829
Crude Oil E	5.57×10^{22}	132410	2.28×10^{-10}	0.787

Figure A.1 shows the changes in f' and g' as a function of $C_1(0)$. f' and g' are normalized with respect to their maximum value for better visualization. It can be seen that the normalized f' is a stronger function of $C_1(0)$ compared to normalized g' . Therefore one can assume that g' in Equation A.20 is a constant independent of

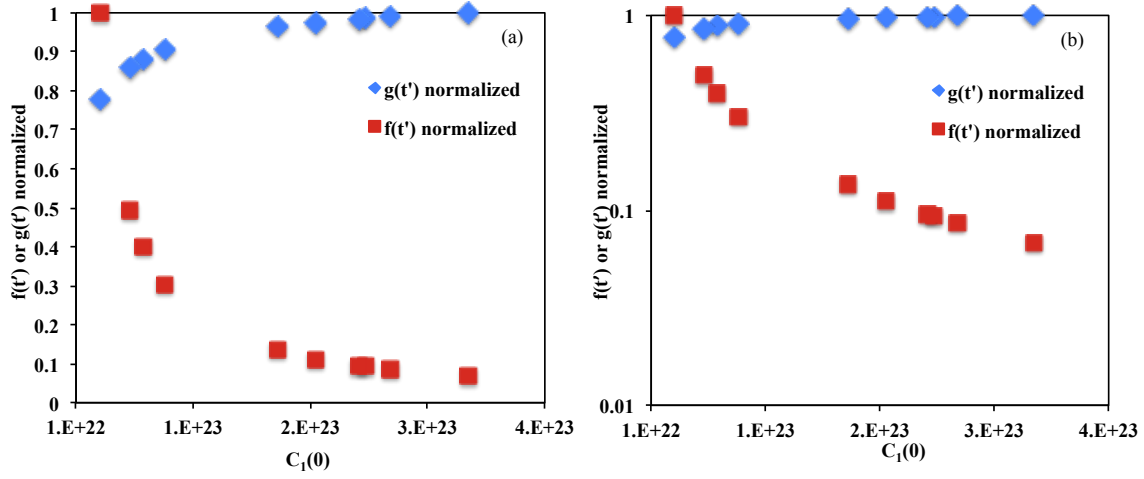


Figure A.1: Plot of f' and g' as a function of $C_1(0)$: (a) normal scale, (b) log scale.

crude oil under investigation . For the value of $C_M = 1 \times 10^{13}$ and $k_0 = 15800$, g' has the average value of 0.852 with the standard deviation of 0.0637.

Assuming that $g'(t) = \text{constant} = g$, the analytical solution (Equation A.20) can be simplified to the following form:

$$\frac{C_M}{C_1(0)} = \frac{4}{(t' + 2)^2} \left[\frac{t'}{t' + 2} \right]^{k_0 - 1} = \frac{4}{(t' + 2)^2} g \quad (\text{A.23})$$

In addition $t' \gg 2$ therefore Equation A.24 can be further simplified to the following form:

$$\frac{C_M}{C_1(0)} = \frac{4}{(t')^2} g \quad (\text{A.24})$$

$$t' = \alpha t_{detection} = 2\sqrt{\frac{C_1(0)g}{C_M}} = \frac{8k_B T}{3\mu} \beta C_1(0) t_{detection} \quad (\text{A.25})$$

Rearranging Equation A.25, we get:

$$t_{detection} = \frac{\mu}{\beta \sqrt{C_1(0)}} \left[\frac{3}{4k_B T} \sqrt{\frac{g}{C_M}} \right] \quad (\text{A.26})$$

The term inside the brackets in Equation A.26 is a constant, therefore the following equation for the change in *detection time* as a function of μ , β and $C_1(0)$ is obtained:

$$t_{detection} \propto \frac{1}{\sqrt{C_1(0)}} \frac{\mu}{\beta} \quad (\text{A.27})$$

Equation A.27 was used in Chapter II to obtain the unified master curve from plot of $\ln(t_{detection} \sqrt{C_1(0)}/\mu)$ vs. $(\delta_{asph} - \delta_{solution})^2$. To have a dimensionless form of y-axis, $\{t_{detection} \sqrt{C_1(0)}/\mu\}$ can be replaced by $\{t_{detection} \sqrt{C_M C_1(0)} k_B T / \mu\}$. Figure A.2 shows the master curve obtained from the plot of $\ln(t_{detection} \sqrt{C_M C_1(0)} k_B T / \mu)$ vs. $(\delta_{asph} - \delta_{solution})^2$ for C_M value of 10^{-3} .

A.3 Sensitivity Analysis of Asphaltenes Solubility Parameter

The solubility parameter of asphaltenes precipitated from different crude oils and model oils presented in Chapter II are obtained by searching for the global minimum of error squared between the predicted and the measured values of $\ln(t_{detection} \sqrt{C_1(0)}/\mu)$ (See Chapter II) and include up to five significant digits. The solubility parameter val-

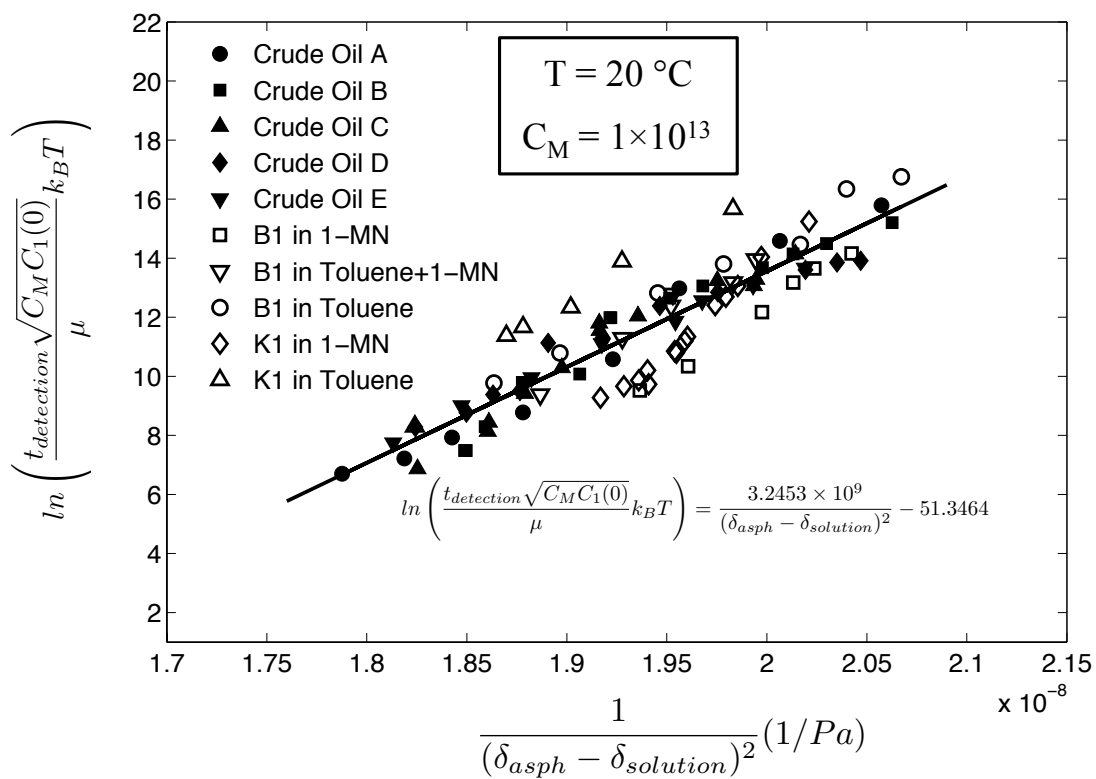


Figure A.2: Plot of $\ln(t_{\text{detection}} \sqrt{C_M C_1(0)} k_B T / \mu)$ vs. $(\delta_{\text{asph}} - \delta_{\text{solution}})^2$ for crude oils and model oils presented in Chapter II.

ues were also rounded to four, three and two significant digits. The analyses revealed that up to three significant digits, the model can successfully predict the behavior of asphaltenes in different crude oils and model oils (See Figures A.3 and A.4). Figures A.3 and A.4 also show the sensitivity of the model prediction from master curve to $\pm 100\text{Pa}^{0.5}$ change in the solubility parameter of asphaltenes in each sample. It is clear from these analyses that change in δ_{asph} has a great impact on the predicted aggregation rate. This behavior is not surprising because asphaltenes aggregation is assumed to happen through a reaction-limited process in our model and any change in the collision efficiency (due to change in δ_{asph}) is expected to have a significant influence on the aggregation rate. Phase behavior of asphaltenes modeled using Flory-Huggins theory is also shown to be very sensitive to the slight changes in the solubility parameters of precipitated asphaltenes [6].

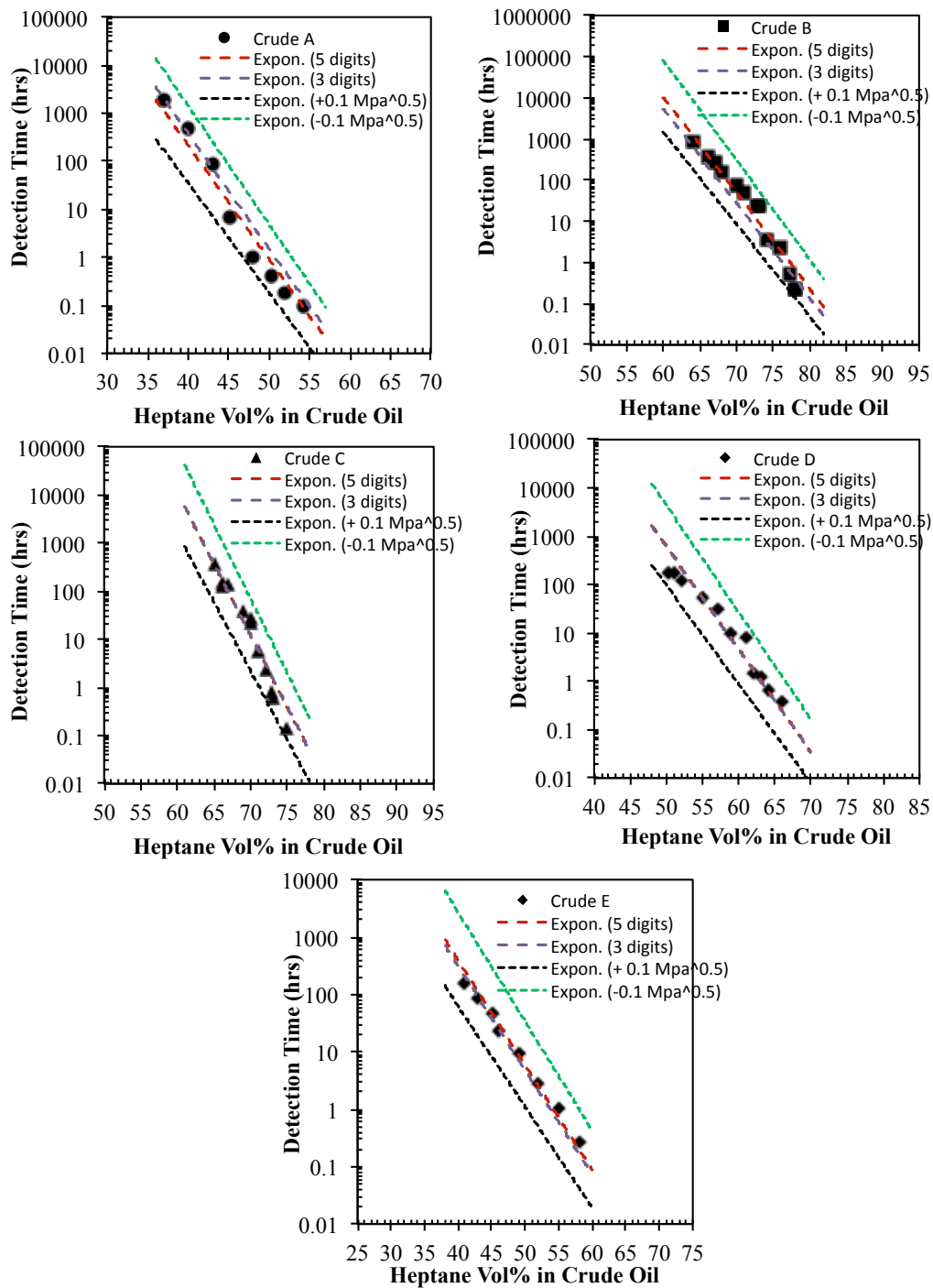


Figure A.3: Sensitivity of the model predictions from the master curve to the solubility parameter of asphaltenes in five different crude oils: data points represent experimentally measured detection times and dashed lines represent the model predictions for different solubility parameter values.

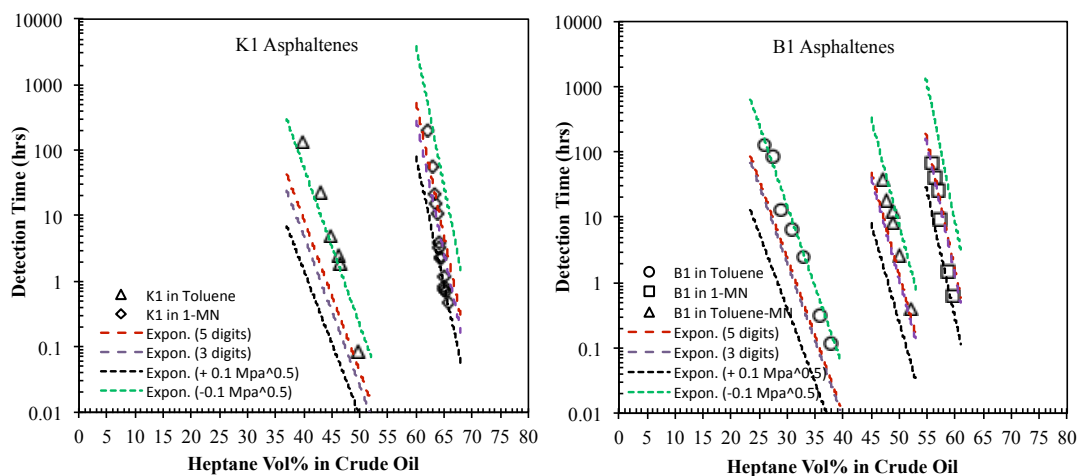


Figure A.4: Sensitivity of the model predictions from the master curve to the solubility parameter of two types of asphaltenes (K1 and B1) in different model oils: data points represent experimentally measured detection times and dashed lines represent the model predictions for different solubility parameter values.

Bibliography

- [1] P. L. Krapivsky, S. Redner, and E. Ben-Naim. *A Kinetic View of Statistical Physics*. Cambridge University Press, 2010.
- [2] M. Elimelech, X. Jia, J. Gregory, and R. Williams. *Particle Deposition and Aggregation: Measurement, Modelling and Simulation*. Butterworth-Heinemann, 1998.
- [3] Oliver C. Mullins. The modified yen model. *Energy & Fuels*, 24(4):2179–2207, 2010.
- [4] Tabish Maqbool, Sasanka Raha, Michael P. Hoepfner, and H. Scott Fogler. Modeling the aggregation of asphaltene nanoaggregates in crude oilprecipitant systems. *Energy Fuels*, 25, 2011.
- [5] R. C. Ball, D. A. Weitz, T. A. Witten, and F. Leyvraz. Universal kinetics in reaction-limited aggregation. *Physical Review Letters*, 58, 1987.
- [6] Jianxin Wang. *Predicting Asphaltene Flocculation in Crude Oils*. PhD thesis, New Mexico Institute of Mining and Technology, 2000.

APPENDIX B

Accounting for the Polydispersity of Asphaltenes in Different Solvents

B.1 Accounting for the Polydispersity of Asphaltenes in Different Solvents

To account for the polydispersity of asphaltenes precipitated in different solvents (i.e., toluene vs. 1-methylnaphthalene) (Chapter II) different values for the solubility parameter of asphaltenes can be used in each solvent (similar to the approach used in Chapter IV for different precipitants). Figure B.1 shows $\ln(t_{\text{detection}}\sqrt{C_1(0)}/\mu)$ vs. $(\delta_{\text{asph}} - \delta_{\text{solution}})^{-2}$ after accounting for asphaltenes polydispersity. The solubility parameter of asphaltenes in the blend of toluene-methylnaphthalene is calculated from the volumetric average of the solubility parameters of asphaltenes in toluene and in 1-methylnaphthalene. Table B.1 shows the solubility parameter values used in Figure B.1. As discussed in Chapter II, 1-methylnaphthalene is a stronger solvent for asphaltenes than toluene. Therefore the average solubility parameter of precipitated

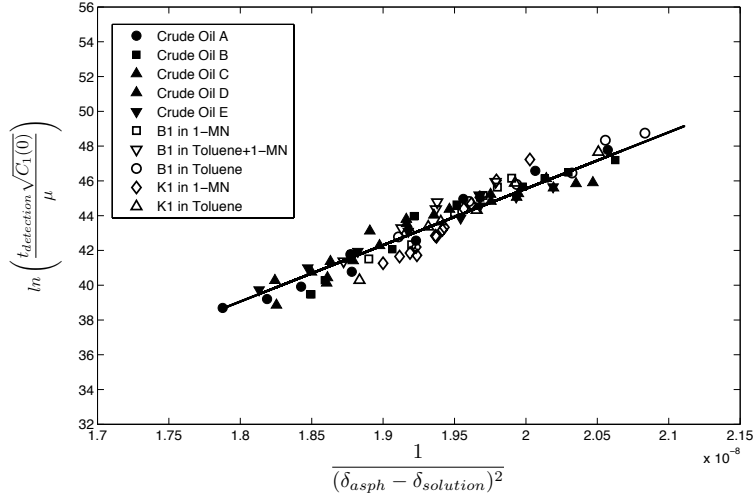


Figure B.1: **Plot of $\ln(t_{\text{detection}}\sqrt{C_1(0)}/\mu)$ vs. $(\delta_{\text{asph}} - \delta_{\text{solution}})^{-2}$ after accounting for polydispersity of asphaltenes in different solvents.**

asphaltenes in methylnaphthalene-heptane is expected to be higher than toluene-heptane. The predicted trend (Table B.1) for the solubility parameters from our model is well in agreement with this expected trend.

Table B.1: Solubility parameter of K1 and B1 asphaltenes.

Sample Name	Solubility Parameter Asphaltenes (Pa ^{0.5})
K1 Asphaltenes-Toluene	24050
K1 Asphaltenes-MN	24200
B1 Asphaltenes-Toluene	24420
B1 Asphaltenes-MN	24530

APPENDIX C

Aging of Asphaltenes

C.1 Aging of Asphaltenes

Asphaltenes for model mixture preparation were extracted from different crude oils. Crude oils were stored at ambient conditions under nitrogen environment. In order to precipitate asphaltenes, crude oils were mixed with heptane in 1:25 volume ratio and were kept well mixed for 24 hours. The arising solutions were then centrifuged with a Sorvall Legend X1R at 3500 rpm for 1 hour to separate precipitated asphaltenes. The asphaltenes were then Soxhlet-washed with heptane for 24 hours to wash any non-asphaltenic material trapped in the cake. The asphaltenes were then dried in the oven at 75°C.

Despite the identical procedure used for extracting asphaltenes in all the samples, the precipitation rates of asphaltenes extracted from the same crude at different times can be different. For example, Figure C.1 shows the precipitation rate of three separate batches of K1 asphaltenes in toluene as a function of their concentration. All three batches were extracted from K1 crude oil: Batch #1 at 2010, Batch #2

at 2011 and Batch #3 at 2013. Batch #1 and #2 asphaltenes were dried in the presence of air and batch #3 asphalttenes were dried in a vacuum oven. Although we get slightly different values for the rate of precipitation in different batches, the experimental trends– for the effect of asphaltene concentration on precipitation rate– are clearly preserved. The differences in precipitation rates between different batches could be attributed to the: aging of crude oil (e.g. due to oxidation), oxidation of asphaltenes at high temperatures (i.e. 75°C in the presence of air) and evaporation losses of light ends from crude oil over time. In addition, the number of washing cycles in the Soxhlet could also influence the composition of recovered asphaltenes. All the samples were washed for 24 hours, however minor fluctuations in the temperature of the coolant could affect the number of cycles and therefore the properties of the recovered asphaltenes.

Despite the differences in the results shown for K1 asphaltenes in Figure C.1, the relative differences between asphaltene concentrations among different batches are identical. For example, by shifting the batch #1 and batch #3 asphaltenes on x -axis by 3.3 and 4 units respectively, the results for all three batches perfectly overlap (Figure C.2).

In conclusion, the aging of asphaltenes can influence the absolute rates measured from microscopy experiments but it does not affect the experimental trends and the conclusions reached in this thesis. In order to investigate the effect of different factors on the precipitation rate of asphaltenes (e.g., solvent or asphaltene concentration), only asphaltenes extracted from the same batch were used to perform the experiments presented in this thesis. All the model oils for the same set of experiments were prepared at the same day and were not destabilized until at least one week after their preparation.

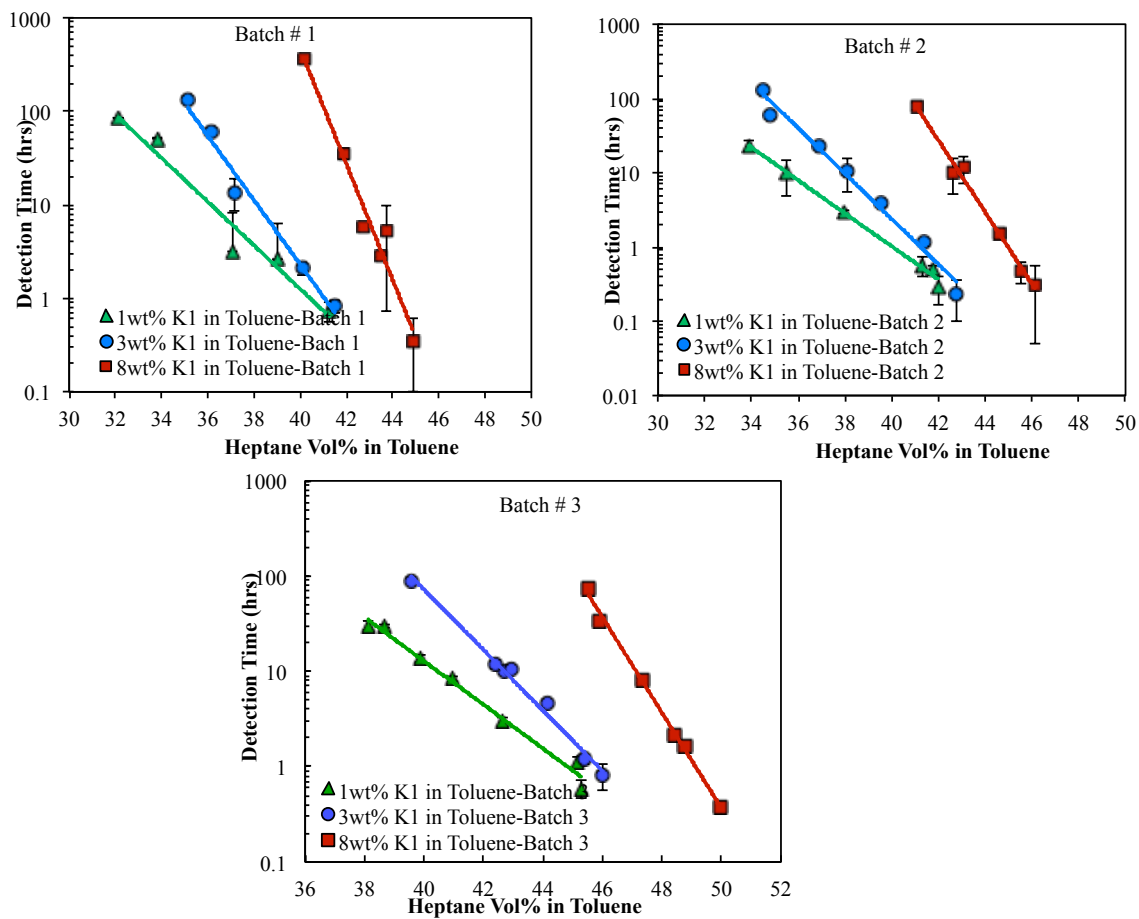


Figure C.1: Detection time as a function of heptane concentration for different batches of K1 asphaltenes in toluene.

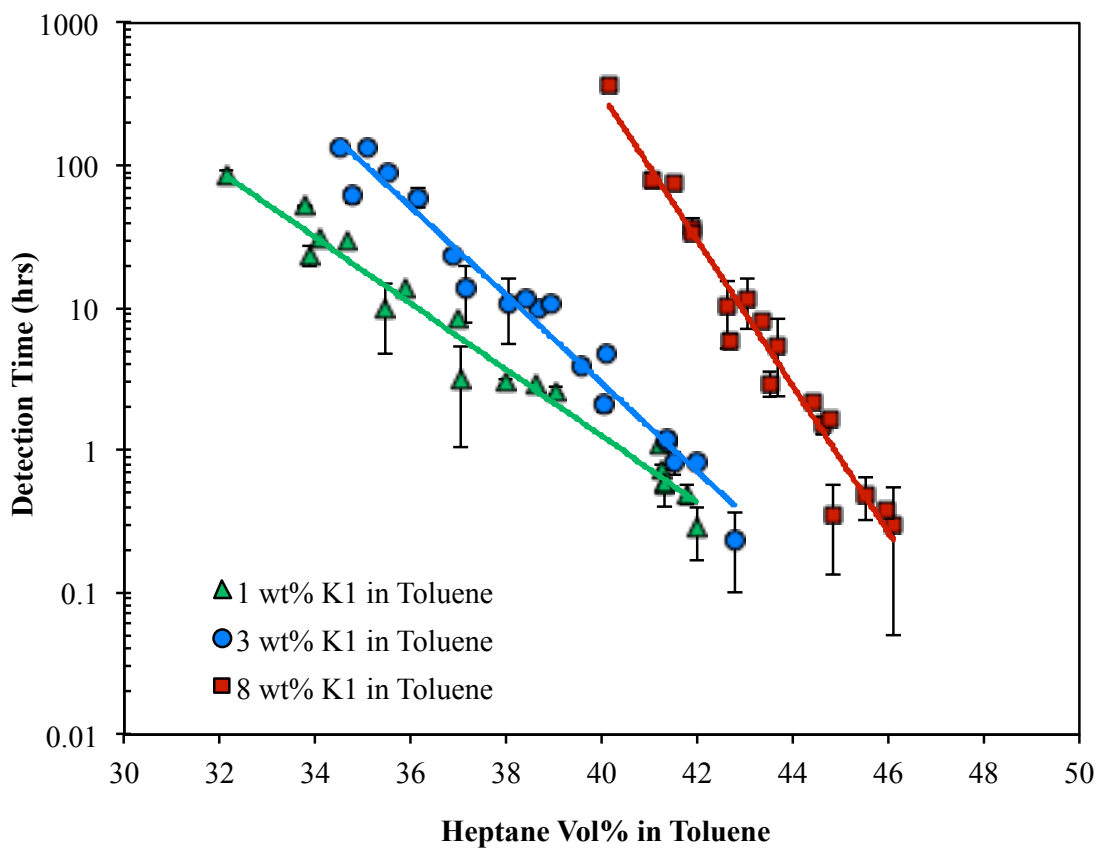


Figure C.2: **Detection time as a function of heptane concentration for different batches of K1 asphaltenes in toluene:** values for batches 1 and 3 are shifted 3.3 and 4 units on x-axis respectively to match batch 2.

APPENDIX D

Effect of Sonication

D.1 Effect of Sonication

In order to prepare samples with different asphaltene concentrations, all the samples were sonicated to insure complete sub-micron dispersion in toluene. Due to larger quantity of asphaltenes at higher asphaltene concentrations, their sonication time was typically longer than the time needed for lower concentrations. To insure that the results presented in Chapter III are not influenced by different sonication times, two batches of 1 wt% of K1 asphaltenes in toluene were prepared: 1) Batch #1 asphaltenes were sonicated until the background under optical microscope appeared clean (~ 15 minutes), 2) Batch #2 asphaltenes were sonicated for 45 minutes (sonication time used for 8 wt% K1 asphaltenes in toluene). Figure D.1 shows the detection time results for two batches of 1 wt% K1 asphaltenes, along with other concentrations. Sonication time might have a minor influence on the detection time measurements (the largest deviation is at small detection times with the highest experimental uncertainty), but the differences between results for 1 wt% and other concentration are still

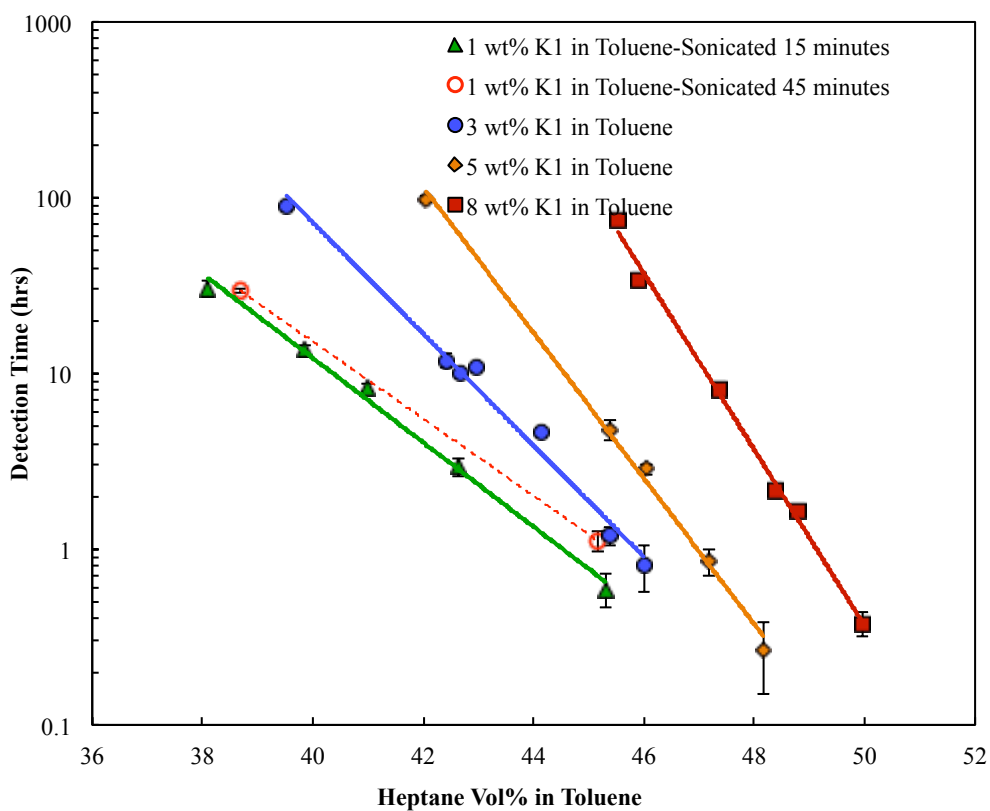


Figure D.1: **Plot of detection time as a function of heptane concentration for different asphaltene concentrations (effect of sonication).**

significantly large enough that the trends and conclusions presented in Chapter III are valid.

APPENDIX E

Small-Angle X-ray Scattering for Different Asphaltene Concentrations

E.1 Small-Angle X-ray Scattering for Different Asphaltene Concentrations

SAXS is a powerful technique that provides information about the size and structure of nano-particles. The scattering intensity for a particle in a solution is expressed as [1, 2]:

$$I(q) = \phi(1 - \phi)I_e\Delta\rho^2P(q)S(q) \quad (\text{E.1})$$

where ϕ is the volume fraction of the particle, I_e is the scattering intensity of an electron, $\Delta\rho$ is the difference between scattering density of the particles and the solution, $P(q)$ is the form factor which accounts for the size and shape of particles and $S(q)$ is the structure factor accounting for the position or orientation correlation

between scattering particles. For dilute samples, the position correlation between particles can be assumed to be negligible ($S(q) = 1$) and Guinier approximation can be used to obtain an average shape-independent size, radius of gyration:

$$I(q) = I_0 \exp\left(-\frac{(qR_g)^2}{3}\right) \quad (\text{E.2})$$

where I is the scattering intensity, I_0 is the zero angle intensity, $q(1/\text{\AA})$ is the scattering vector and $R_g(\text{\AA})$ is the Guinier radius of gyration.

At high asphaltene concentrations, due to close proximity of particles, the interactions between them become important and the structure factor is no longer equal to one. In such circumstances, $I(q)/\phi(1-\phi)$ at low q range decreases by increasing the asphaltene concentration in a solvent (i.e. repulsive interaction between asphaltenes) [1] and the Guinier approximation is not valid for estimating the size (e.g., 8 wt%). As heptane is added to the solvent, the overall concentration of asphaltenes decreases as a result of dilution. In addition, centrifugation of precipitated asphaltenes further reduces the concentration of remaining asphaltenes in the supernatant. Therefore, the influence of structure factor on the scattering of the centrifuged samples is significantly smaller compared to asphaltenes dispersed in toluene. Consequently direct comparison between solutions with different asphaltene concentrations might become feasible. SAXS was therefore applied to measure the change in the size of asphaltene nano-particles as a function of asphaltene and precipitant concentration. Bruker Nanostar SAXS equipment at the University of Michigan was used to perform scattering measurements. The X-ray generator was set at 40 kV and 35 mA with 0.5 s per frame.

The supernatant of the centrifuged samples (two months after heptane addition) in

Chapter III were collected and the scattering intensities of the asphaltenes remaining in the solution were measured using SAXS (Figures E.1 and E.2). All the plots in Figures E.1 and E.2 are background corrected and are corrected for the differences in the scattering density and the volume fraction of asphaltenes (Equation E.2) (I is not converted to the absolute scaling). The scattering densities of asphaltenes were calculated from their elemental composition shown in Table 3.1. It is clear from Figures E.1 and E.2 that the scattering intensities at Guinier region (low q) for 3 wt% samples are consistently higher than 8 wt% samples at identical heptane concentrations. The differences between 3 and 8 wt% samples of A1 asphaltenes at 55 and 60 vol% of heptane appear to be small, and scattering profiles overlap. However, the radius of gyration calculations show that the sizes of asphaltene nano-particles are different among these samples. Tables E.1 and E.2 show the size of nano-aggregates calculated using Guinier approximation for the results shown in Figures E.1 and E.2 respectively.

The size of nano-particles left in the solution decreases by increasing heptane concentration for B1 asphaltenes both in 3 and 8 wt% samples. These results might appear contra-initiative, because one would expect the size of asphaltenes to increase as a result of increase in heptane concentration. However, the most unstable asphaltenes tend to form the largest clusters in the solution. As heptane concentration increases, the unstable asphaltenes have already precipitated and been centrifuged out of the solution at the time of scattering measurements. Therefore the sizes measured in these experiments are due to the scattering of the remaining asphaltenes that are more stable, and thus tend to form smaller clusters in the solution. For A1 asphaltenes similar trends are observed except for 3 wt% asphaltenes at 50 and 55 vol% heptane. The increase in the size of stable nano-particles from 50 to 55 vol% heptane could be due to experimental error or could be attributed to an increase in

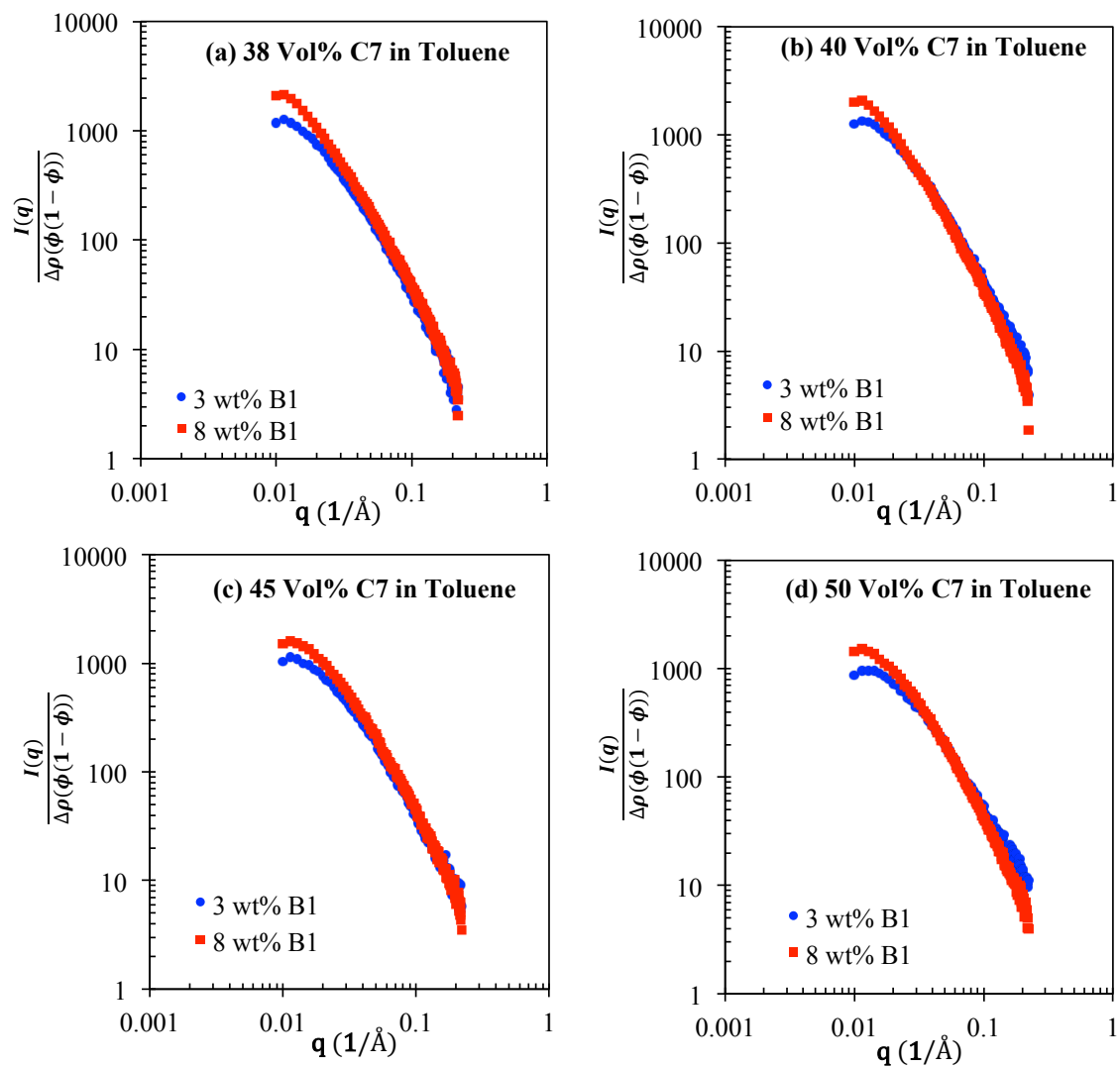


Figure E.1: Scattering results for supernatant of 3 and 8 wt% B1 asphaltenes at different heptane concentrations.

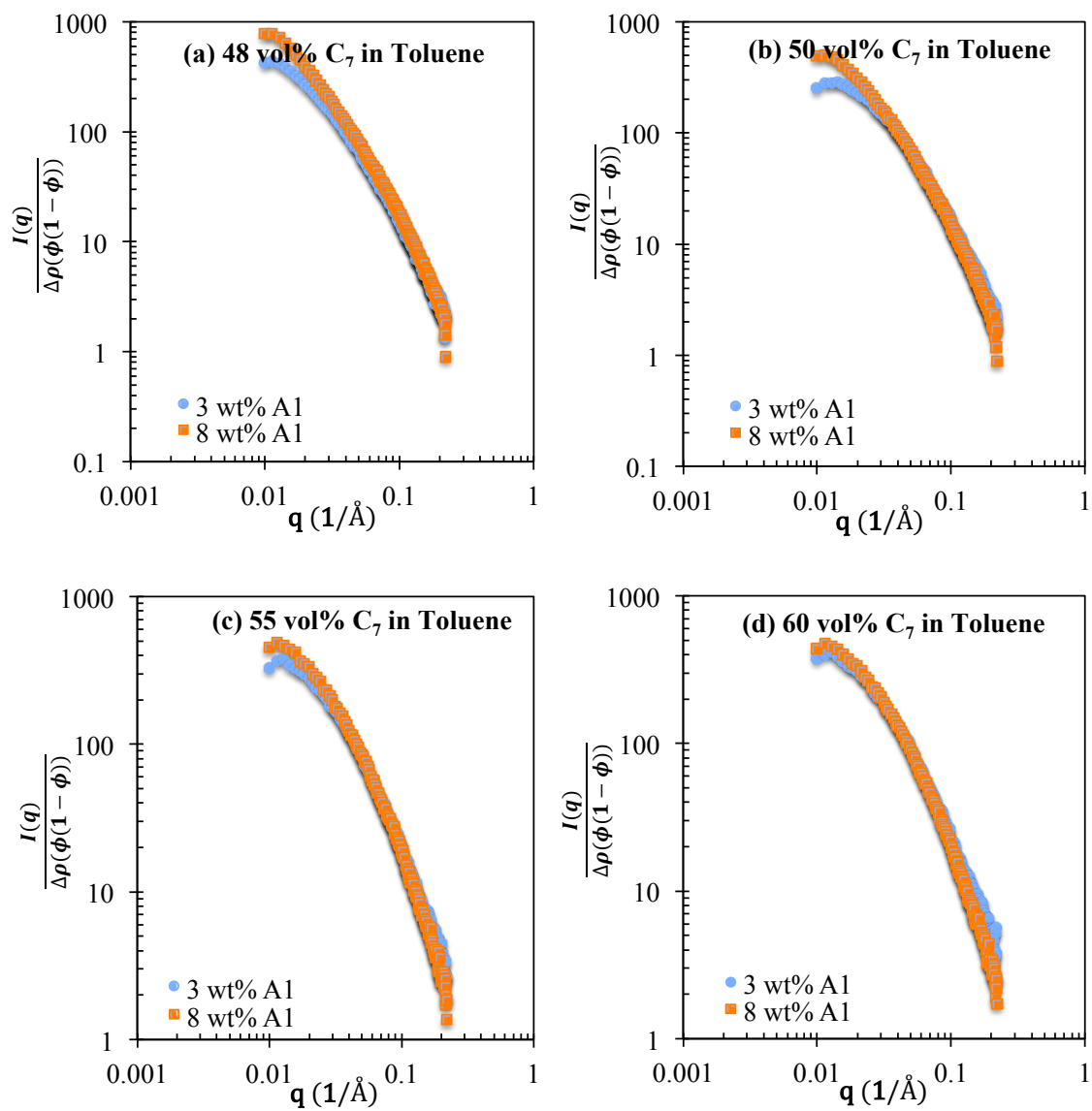


Figure E.2: Scattering results for supernatant of 3 and 8 wt% A1 asphaltenes at different heptane concentrations.

the size of remaining asphaltenes despite the fractionation and separation of unstable ones.

Table E.1: Radius of gyration from scattering results of B1 asphaltenes shown in Figure E.1

3 wt% B1 in Toluene		8 wt% B1 in Toluene	
C_7 Concentration	$R_g(\text{\AA})$	C_7 Concentration	$R_g(\text{\AA})$
38.57	71.40 ± 2.37	38.43	79.98 ± 1.61
40.59	68.54 ± 1.89	40.37	79.13 ± 1.62
45.61	61.92 ± 1.36	45.55	71.44 ± 3.97
50.61	56.01 ± 1.39	50.72	64.93 ± 1.08

Table E.2: Radius of gyration from scattering results of A1 asphaltenes shown in Figure E.2

3 wt% A1 in Toluene		8 wt% A1 in Toluene	
C_7 Concentration	$R_g(\text{\AA})$	C_7 Concentration	$R_g(\text{\AA})$
48.56	65.93 ± 1.85	48.11	80.49 ± 1.23
50.58	51.66 ± 0.87	50.20	68.20 ± 1.50
55.18	53.46 ± 1.29	55.36	59.80 ± 1.20
60.00	49.65 ± 0.89	60.49	56.91 ± 0.90

The results from Tables E.1 and E.2 indicate that at a fixed heptane concentration, the sizes of asphaltene nano-particles in 3 wt% are always smaller than their sizes in 8wt%. Smaller sizes of asphaltenes in 3 wt% compared to 8 wt% samples are surprising because asphaltenes are equally polydispersed in both samples. These results indicate that asphaltenes tend to fractionate differently in these two samples. It appears that at identical heptane concentration, higher fraction of unstable asphaltenes has precipitated in 3 wt% compared to 8 wt%. This behavior is only possible, if the thermodynamic driving force is different between these two samples and asphaltenes have lower tendencies for phase separation in 8 wt% samples. Change in

thermodynamic driving force can be attributed to changes in solubility parameter of solution.

One other plausible explanation for higher radius of gyration of 8 wt% samples could be the higher volume fraction of asphaltenes remaining in the supernatant and contribution of structure factor.

Bibliography

- [1] L. Barre, S. Simon, and T. Palermo. Solution properties of asphaltenes. *Langmuir*, 24, 2008.
- [2] M. P. Hoepfner, C. Vilas Bôas Fávero, N. Haji-Akbari, and H. S. Fogler. The fractal aggregation of asphaltenes. *Langmuir*, 29, 2013.